SCHOOL OF MECHANICAL

INDUSTRIAL & AERONAUTICAL

ENGINEERING

MSc(Eng) RESEARCH PROJECT

PROJECT TITLE:	EXPERIMENTAL INVESTIGATION INTO THE COMPARISON BETWEEN SHOT PEENING AND LASER SHOCK PEENING ON AA 6056-T4 ALUMINIUM ALLOY
CANDIDATE:	JOEDY RAMJITH (0408496R)
SUPERVISOR:	CLAUDIA POLESE
DATE:	21 OCTOBER 2014

THE UNIVERSITY OF THE WITWATERSRAND, JOHANNESBURG

School of Mechanical, Industrial and Aeronautical Engineering

DECLARATION

Name: Joedy Ramjith	**Student Number:** 0408496R
Course No: MECN7018	**Course Name**: MSc (Eng) Research Project
Submission Date: 20 October 2014	**Project Title**: Experimental investigation into the comparison between Shot Peening and Laser Shock Peening on AA 6056-T4 Aluminium Alloy

I hereby declare the following:

- I am aware that plagiarism (the use of someone else's work without their permission and/or without acknowledging the original source) is wrong;
- I confirm that the work submitted herewith for assessment in the course is my own unaided work except where the I have explicitly indicated otherwise;
- This task has not been submitted before, either individually or jointly, for any course requirement, examination or degree at this or any other tertiary education institution;
- I have followed the required conventions in referencing the thoughts and ideas of others;
- I understand that the University of the Witwatersrand may take disciplinary action against me if it can be shown that this task is not my own unaided work or that I have failed to acknowledge the sources of the ideas or words in my writing in this task.

Signature: …… Date: 20 October 2014

ABSTRACT

Currently, within the aviation industry there has been a large focus on enhancing the fatigue life of thin-walled aircraft structures, such as the fuselage. In the past decades, shot peening was seen to aid in accomplishing this goal. In more modern and recent times, laser shock peening techniques were said to provide a more substantial improvement to the treated material, in comparison to shot peening. Laser shock peening relies on a more focused and precise peening process, whereas shot peening utilised a multitude of shots (small spherical metal/plastic/glass beads) which are projected towards a material surface (via a high pressure), which randomly impacts the material surface to create compressive residual stresses and thus improve fatigue life.

Samples of AA6056-T4 Aluminium alloy used for integral structures, with a thickness of 3.2mm were used to represent a thin-walled component. These were used for comparative testing of material properties after Laser Shock Peening and Shot peening had been executed on the test pieces. The material properties investigated were material deflection, surface roughness, micro-hardness and residual stresses at various laser intensities and shot peening pressures. Laser shock peening had shown the best results, with higher deflections between 2.12 to 3 times higher than shot peening, a smoother surface finish (roughness values 2-2.5 times less than shot peening), deeper hardness penetration and deeper residual stress into the aluminum alloy test pieces.

ACKNOWLEDGEMENTS

A special thanks goes out to the South African Airways personnel who assisted the author in obtaining access to the Shot Peening Facility and their assistance during testing, i.e.: Denzil Pillay, Eduard Manuèl Roodt and Ryan R. Farnham.

Thanks also to: Daniel Glaser for his assistance in obtaining Laser Shock Peening samples, Rachana Bedekar and Prof João P.S.G. Nobre for their assistance in hole drill testing, and to Professor Claudia Polese, for her assistance throughout this research project.

CONTENTS

LIST OF FIGURES

LIST OF TABLES

CHAPTER ONE

1.0 Introduction

Tensile stresses are seen as one of the most common modes of material failure [2]. This mode tends to stretch and pull surface material of a structure or component, to a point of crack initiation. Thus exposing the material to environmental conditions which could lead to corrosion and to crack growth or propagation, reducing fatigue life of the structure or component and leads to an early failure of the material (i.e. to a catastrophic failure or costly repair process). Structures or components which have an induced compressive layer, were seen to slow crack growth significantly, with deeper induced compressive layers found to further reduce crack growth and extend the life of the structure or component[1],[2] . In this introductory chapter, an overview of the history and background of shot peening and laser shot peening will be highlighted as the surface enhancement methods used for inducing compressive stresses into a material.

1.1. History and Background

1.1.1 Shot Peening

Shot peening is not a new concept, as it has been around for centuries. People have long known that work hardening and pre-stressing a metal, enables it to be more durable and harder. Lockheed Aircraft in Burbank was the first to discover and patent the shot peening process (California, late 1940's). Jim Boerger, was working on an aircraft, and realized he needed stiffer wing panels, as a weight saving initiative. While working on an Almen strip, he realized that the curvature created on the strip could be induced on a wing panel. With trial and error, they found that the required curvature could be produced. Once the patent had expired, all other aircraft manufacturers adapted to using this process as the most cost effective manufacturing process for inducing curvatures in fully machined aerodynamic panels [3]. The extension of the Almen strip has been widely used thorough out industry, but aerospace being its greatest user.

Shot peen-forming has been used to induce compressive stresses on a material structure, to change its stress pattern, magnitude and depth to deliberately create a change in the in the product shape [3]. The first aircraft to use peen-forming techniques was the Constellation seen in Figure 1.1 [3].

Figure 1.1: Lockheed Constellation [4]

The shot forming process is performed at room temperature or in certain cases the substrate is warmed to obtain maximum benefit. The surface of the work piece undergoing shot peening is subjected to a pressurized blast of small round/spherical in shaped steel shots. Each shot which impacts the surface of the work piece, acts as a tiny hammer on the surface, thus producing an elastic deformation of the upper surface area. This plastic deformation creates a compressive layer of residual stresses within the work piece where shot peening had occurred. This combination of compressive residual stress and stretching/plastic deformation of the material create a compounded material with a convex curvature on the peened side of the work piece [3].

1.1.1.1 Shot peen forming: panel curvature [3]

For obtaining panel curvature, three methods were used. This includes:

- Chordwise curvature, which was obtained by peening only one side of the work piece, creating the change in shape of the work piece, with a limitation of only small curvatures can be created.
- Strain peening, where the work piece is held in a unidirectional pre-stressed state and peened on the tensile stressed surface, once released a greater curvature is created, as the compressive stress is greater in one direction than the other.
- Simultaneous peening, which was achieved on both side of the work piece, giving elongation.

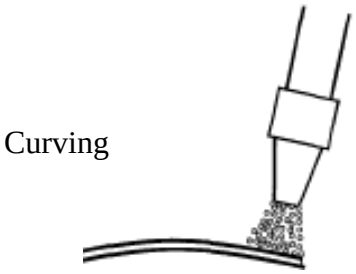

Figure 1.2: Chordwise curvature using shot peening [3]

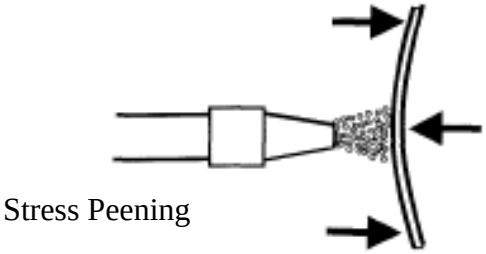

Figure 1.3: Strain peening curvature using shot peening [3]

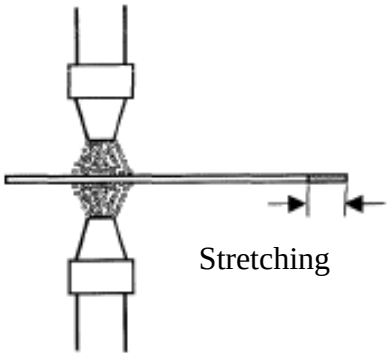

Figure 1.4: Simultaneous shot peening on both side, elongation [3]

"Peen forming methods makes them particularly suitable for aircraft components, be they fuselage, wing, or tail plane items. They are however very accurate in their shape and because peen forming is carried out cold the reproducibility of forming is very good" [3].

1.2.1 Laser

Albert Einstein described the theory of stimulated emission in 1917, which had become the basis of laser [5]. He stated that, "when the population inversion exist between upper and lower levels among atomic systems, it is possible to realize amplified stimulated emissions and the stimulated emissions has the same frequency and phase as the incident radiation" [5]. Only within the 1950s were ways discovered to use stimulated emissions within devices. American physicists Charles H. Townes and A.L. Schawlow had constructed such a device using optical light [5]. Two Soviet physicists had also proposed related ideas independently of each other. The initial laser, constructed in 1960 by Theodore H. Maiman of the United States, used a rod of ruby as a lasting medium which was stimulated using high energy of flashes of intense light [5].

This process of laser construction was later enhanced with the aid of an intense laser pulse used to produce a significant pressure on the surface of an irradiated target; this was done by the material creating a momentum impulse/pressure on the surface due to rapid evaporation, and thus creating laser shock peening [5], [6], [7]. The progression of laser development over the years can be seen in Appendix A [8].

1.2.1.1 Operations of Lasers

'Light Amplification by Stimulated Emission of Radiation' (LASER), is a device that creates and amplifies electromagnetic radiation of a specific frequency through the process of stimulated emission [10]. The radiation emitted by a laser consists of a coherent beam of photons, all in phase and with the same polarization. The laser transmits a thin, intense beam of nearly monochromatic infrared light that can travel extended distances without diffusing. Most light beams consist of many waves traveling in more or less the same direction, but the phases and polarizations of each individual wave/photon are randomly distributed. The waves are precisely in step/ in phase, with one other (and with the same polarization, such light is called coherent). All of the photons which make up the laser beam are in the same quantum state.

Coherent light formed by lasers are done through a process called stimulated emission. The laser is contained within a chamber in which atoms of a medium such as a synthetic ruby rod or a gas are excited, bringing their electrons into higher orbits with higher energy states. When one of these electrons jumps down to a lower energy state (which can happen spontaneously), it gives off the extra energy as a photon with a specific frequency. If this photon encounters another atom with an excited electron, it will stimulate that electron to jump down as well, emitting another photon with the same frequency as the first (and in phase with it). This effect cascades through the chamber, constantly stimulating other atoms to emit more coherent photons.

Mirrors at both ends of the chamber cause the light to reflect back and forth within the chamber, sweeping across the entire medium. If a sufficient number of atoms in the medium are maintained by some external source of energy (in the higher energy state, a condition called population inversion) then the emission is continuously stimulated, and a stream of coherent photons develops. One of the mirrors is partially transparent, allowing the laser beam to exit from that end of the chamber, thus the laser formation. A diagrammatic representation of the laser process can be seen in Figure 1.5.

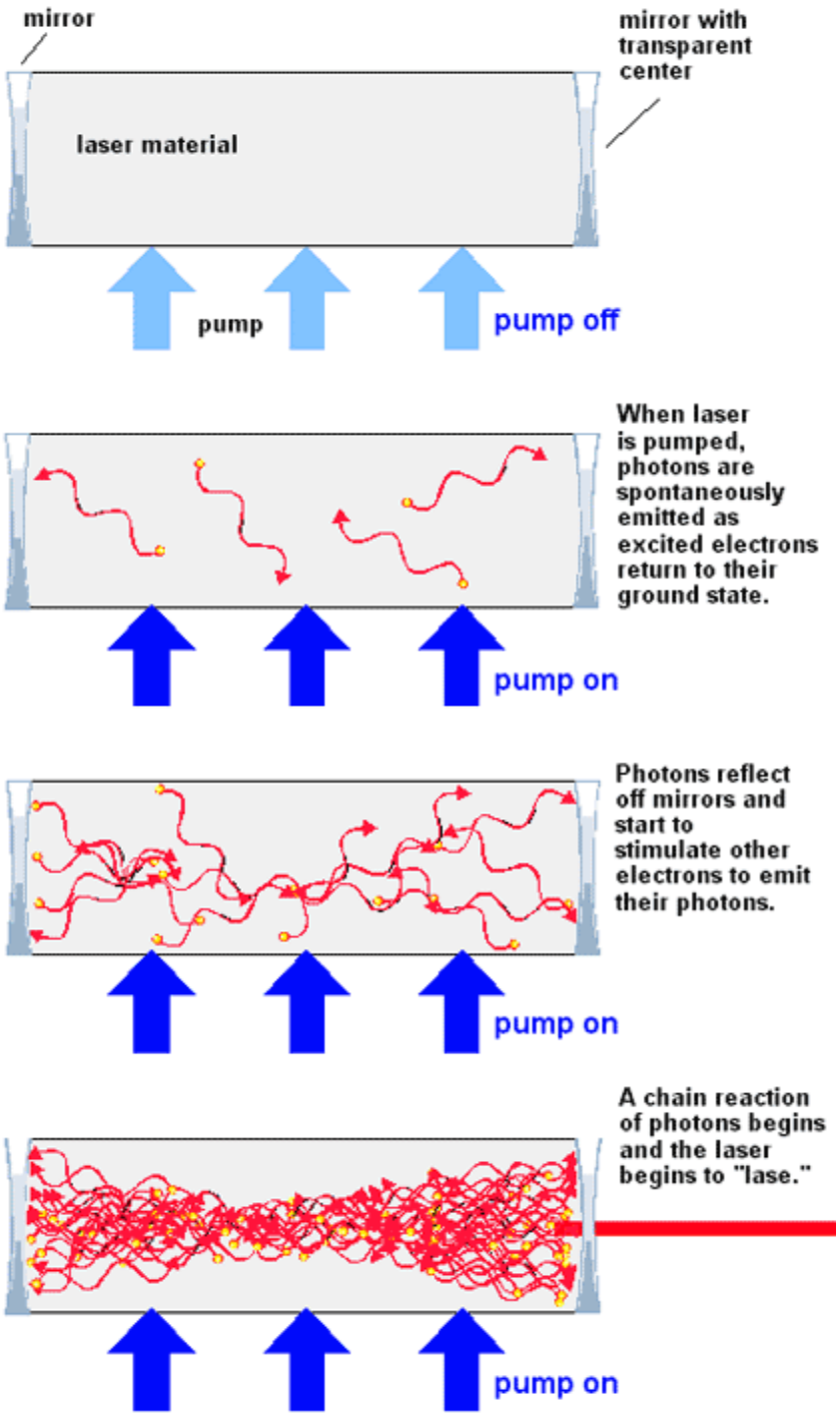

Figure 1.5: Laser Process [11]

1.2.2 Laser Shock Peening

Shot peening was one of the of the first methods of creating residual stresses within aircraft structures, but the two downfalls of this method was the shallow depth of residual stress created (around 0.25mm) and the non-uniform residual stress distribution in the material, which also leads to an uneven/rough surface with random low and high peaks. [10]

The development of laser shock peening was developed as a cold working process for the treatment of surface materials, which produced deeper residual stress within a material; a more evenly distributed residual stress and a consistent surface finish with the aid of a laser. The main advantage of inducing relatively deep compressive residual stresses into a material is the improvement of mechanical behaviors against fatigue cracking initiation and crack growth [9]. Due to the deeper residual stress created by laser shock peening, crack tips deeper than 0.25mm would be slowed down, whereas in the case of shot peening the effect of the residual stress would have little impact on slowing crack growth.

Surface finish was accomplished via the laser overlapping pattern, which solved the issue of uneven areas of non-uniform residual compressive stress distribution. Due to intensity of the laser to be varied in this process, it allows for compressive residual stress to reach up to a depth of 1mm into the material, indicating a depth of up to four times deeper than the conventional shot peening processes. Laser shock peening can be used on more complex and smaller geometries such as on rivet holes, where conventional shot peening is unable too.

1.3 Motivation

With more modern techniques being found to prolong the life of materials, more investigations are required to understand the advantages and disadvantages between the new and the old processes. In aerospace there has been an increase in interest in the use of laser shock peening over normal conventional shot peening. With the increasing number of aircraft and the importance of reducing weight and prolonging the lifespan of aircraft components, more interested has been invested into upcoming technology and processes, thus laser shock peening is seen within these lines.

Aircraft structures such as the fuselage are made up of thin walled aluminium alloy, but research has only been found for thicker materials such as Inconel, thus creating a gap in the understanding of material behavior for thinner materials such as alloys. Within South Africa there are only two facilities that are certified to conduct shot peening processes, but growing interest has been shown for material improvement methods using modern technological processes such as laser shock peening.

Thus, a direct comparison between emerging processes and the old processes need to be done i.e. laser shock peening against conventional shot peening, to analyses the pros and cons of these processes, and to analyse the material properties and compare to other existing results for materials used in the aerospace industry. As no testing results were found on AA6065-T4 aluminium alloy (a thin aerospace material currently being used within the industry) at a thickness of 3.2mm, for material properties after shot peening or laser shock peening processes had been conducted on it, thus was selected for testing for this dissertation.

1.4 Research Objectives

To evaluate the material properties between shot peening and laser shock peening specifically:

- Compressive residual stresses in AA6056-T4 of thickness 3.2mm and the depth of stress induced on the material via these peening processes.
- Test strip deflection at varying intensities, comparing the arc heights created at the different intensities.
- Surface roughness induced on the material at the various intensities.
- And Microhardness, to test the depth at which the two process affect the material and the material hardness (properties of the material).

1.5 Organisation of the Dissertation

Within the chapters to follow the comparison process between shot peening and laser shock peening will be represented for AA6056-T4. In chapter two, the literature review for the two peening processes and the material properties of AA6056-T4 are discussed. In chapter 3 the various methods used to evaluate deflection, surface roughness, microhardness and residual stress within the test material will be presented. Chapter four shows the data collected and evaluated for the different material properties. The discussion and conclusion of the evaluation of these material properties is presented chapter five.

CHAPTER TWO

2.0 Introduction

In this chapter, the literature review of shot peening and laser shock peening will be evaluated. Four features due to these peening processes, will be evaluated, i.e. curvature induced on an Almen sized test piece, surface finish, material hardness across the thickness of the material and residual stress evaluation induced into the material.

2.1 Shot Peening

When a metal has been subjected to grinding, welding, heat treatments or any other stressful production process, atoms on the surface of the worked piece would have been left with residual tensile stress. Shot peeing is a cold work process used to relieve these surface stresses and increases surface hardening of the metal component [12].

is a process of subjecting a specific component with an array of small spherical-like shots at room temperature. These shot can be metal spheres, glass beads, cut wire or ceramic beads. These shots are selected according to the type of material used or surface finish required. The residual stresses are removed by striking the metal surface with these shots at a high velocity, thus creating compressive stresses. As each shot strikes the surface of the metal, the metal is stretched beyond its yield strength, creating a convex plastic flow of the material in a spherical direction around the shot. After the shot bounces off the metal, the surface is left in residual compression [13],[53]. The depth of the depression left by the shot is within the range of 0.005-0.010 inches (0.127-0.254mm) and the metal the peened surface is left in compression. This process can be seen in Figure 2.12.1 and Figure .

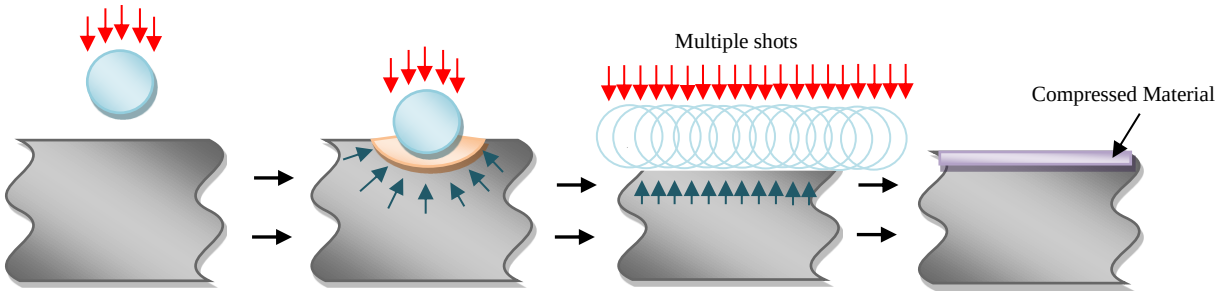

Figure 2.1: Step-by-Step shot peening process

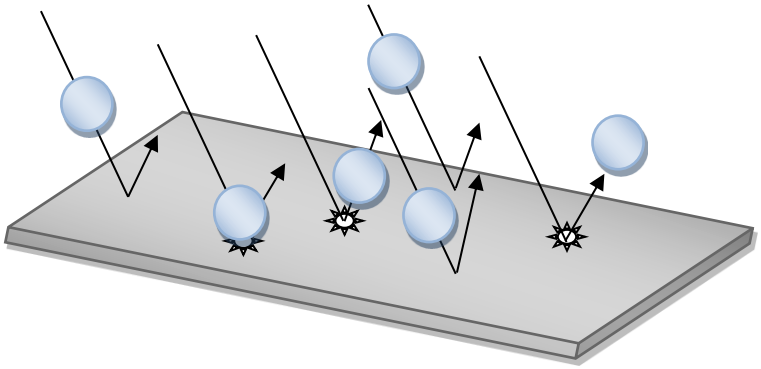

Figure 2.2: Overview of Shot Peening Process

Depending on a specific part being treated, shot peening can [14]:

- Increase fatigue strength
- Prevent cracking due to wear, hydrogen embrittlement, corrosion and stress
- Enhance lubricity by creating small pores in which lubricants can accumulate
- Prevent fretting
- Prevent galling
- Create a uniformly textured, finished surface ready for immediate use or for paint and coatings can be used to curve metal or straighten shafts without creating tensile stress. This process is known as Peen forming. This can permit the use of very hard steels by reducing brittleness
- Close up surface porosity in coatings
- Allow for the substitution of lighter materials without sacrificing strength and durability
- Increase spring life 400% to 1200%
- Increase gear life more than 75%
- Increase drive pinion life up to 400%

- Increase crankshaft life from 100% to around 1000%
- And increase the fatigue strength of damaged parts extending the wear and delaying replacement cost.

2.2. Laser Shock Peening

Laser Shock Peening, is another process of cold working a metal part, and can be regarded as a non-destructive process as no physical contact between any two metals occur[15]. This is done via the aid of a high energy pulse laser beam. This beam results in high amplitude stress waves which are induced on the material and result in creating compressive stresses on the material. This process increases the compressive residual stresses and the fatigue life of the material.

Before laser shock peening can be used, the material has to be prepared for the process. The initial surface of the material subjected to this process is covered with an opaque layer (black paint/metal foil/ tape). The opaque layer is covered with a tamping material layer, which in most cases is flowing water. When the laser strikes the material the opaque layer absorbs the pulse energy, which in turn heats up and vaporizes, thus creating high temperature plasma on the surface of the material. The opaque layer is also used to improve the creation of plasma behind the water layer and provides thermal protection to the material. "The plasma gas is trapped between the work piece surface and the transparent water layer limiting the thermal expansion of the gas. As a result the gas pressure increases to an extremely high value. The high pressure is transmitted to the work piece material producing a shock wave, which travels through the part material and generates compression stress." [16] "A peak stress the dynamic yield stress of the metal is created by the shock wave and thus the metal yields, and is "cold worked" or plastically deformed at the surface."[17]

The water in this process is not used to cool the plasma but to confine the high pressure plasma gas, and the effect of this process is not to heat or melt the material. The

compressive residual stress layer has been seen to be more than four times that of conventional shot peening. This process can be seen in Figure 2.32.3.

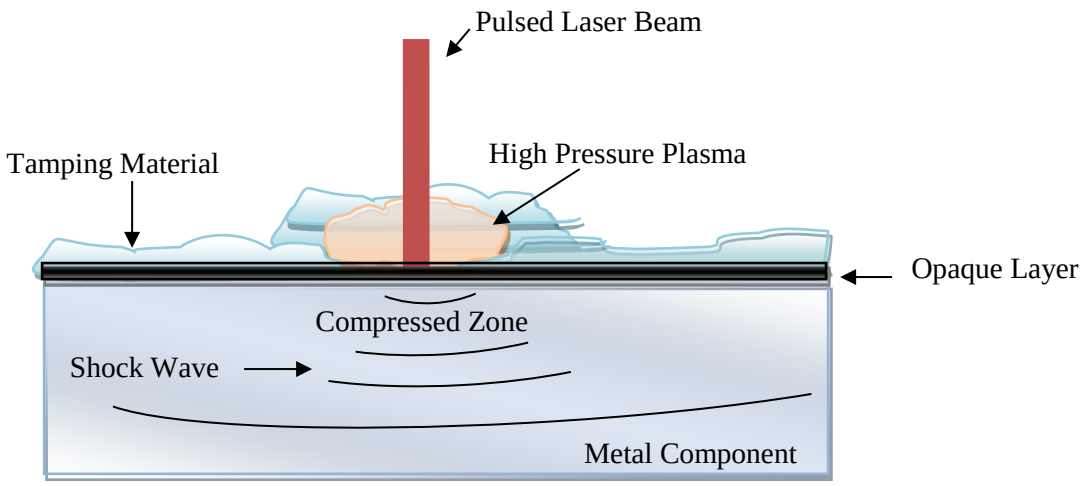

Figure 2.3**:** Laser shock Peening diagram

The initial wave sent through the material which generates the compressive stress in the material is called the elastic compressive wave, which travels at the speed of sound. The stress at the front of the wave is found to be the shock yield strength of the material, known as Hugoniot Elastic Limit (HEL) [19]. The HEL of a material is related to the dynamic yield strength ($\boldsymbol{\sigma_y}$) and Poisson Ratio (v) as seen in Equation 2.1:

$$HEL = \frac{1-v}{1-2v}\boldsymbol{\sigma_y} \qquad \text{Equation 2.1}$$

The waves which follow the initial elastic compressive wave, propagate at a slower rate and are known as the plastic compressive waves. The plastic compressive wave has higher stress values at the wave front than the elastic compressive wave. This stress is higher than the HEL of the material and will thus yield and plastically deform as the wave propagates through it, and in the process induces the residual compressive stresses in the material [18].

This deformation occurs up to the depth where the wave no longer exceeds the HEL of the material. Multiple parameters can be changed to produce the best required properties for the test piece. These parameters are spot size, spot coverage, laser beam intensity and pulse duration [19].

Spot size refers to size of the laser beam spot created on the surface of the work piece. Smaller spot sizes result in localised compressive residual stresses in the work piece, whereas spot sizes result in greater depth of residual compressive stress. Spot coverage is the number of laser impact spots per cm^2 on the work piece. Overlap is also included in this parameter, as the percentage of the next laser impact spot to cover the previous spot. The higher the overlap the greater the density of spots/cm^2. The overlap percentage can be seen in Figure 2.4.

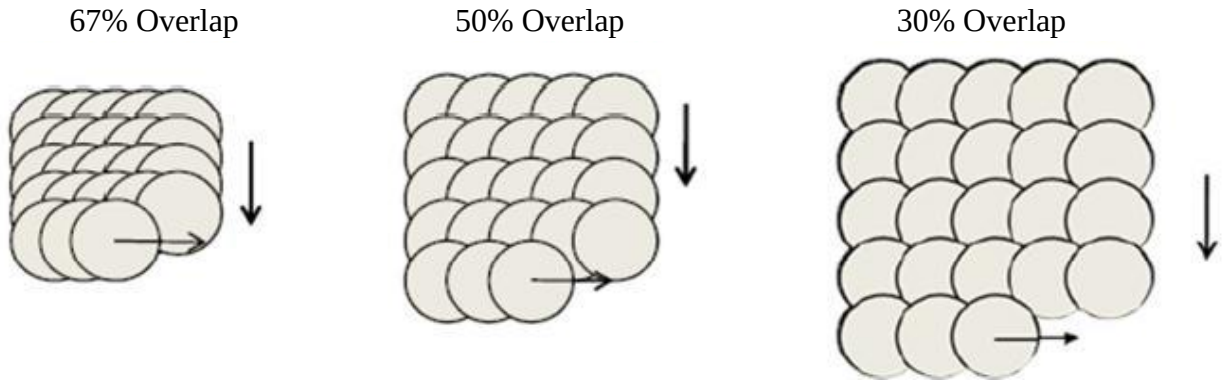

Figure 2.4: Overlap percentage of spot coverage [20]

Laser beam intensity, is the energy created by the laser beam which is projected on the work piece, which is directly related to the power supplied to the laser. Increased laser intensity leads to a deeper layer of compressed residual stress.

Pulse duration, refers to the time elapsed during laser beam projections on the work piece. The exposure time is measured in nanoseconds.

Effects of the laser beam parameters [19]:

- For deeper penetration of compressive residual stresses, higher density lasers can be used.
- Bean intensity has a direct impact on the depth of compressive residual stress achieved in the work piece.
- Higher intensity laser will be used for thicker materials and lower intensities lasers for thinner materials.
- Spot size can be altered to change the area affected by the laser peening process.
- Smaller spot sizes result in weaker shockwave propagate through the work piece and would not reach the same depth as a larger spot size.

The laser shot peening process is setup, such that the shockwave strength is larger than the pressure required to do cold work on the material. The material is plastically deformed and compressed due to the shockwave, thus inducing compressive residual stresses in the material/work piece and increasing the fatigue life of the work piece [21].

Advantages of Laser shock peening [22]:

- Deeper residual compressive stresses enabling better resistance.
- Low cycle, high stress situations (LCF)
- High cycle, low stress situations (HCF) in a deteriorating surface environment
- Erosion, strike damage, fretting and corrosion.
- Considerably less cold work enables greater retention of residual compressive stress in high load and/or thermally challenging conditions.
- Lack of shot particles using “clean” technology enables applications where contamination and/or media staining cannot be tolerated.
- Original surface finish and topography more easily maintained and controlled.
- Allows for excellent process and quality control.

“In the aerospace industry, laser shock peening can be used to treat many aerospace products, such as turbine blades and rotor components discs, gear shafts and bearing components. In particular, laser shock peening has clear advantages for treating components of complex geometry such as fastener holes in aircraft skins and refurbishing fastener holes in old aircraft, where the possible initiation of cracks may not be discernible by normal inspection.”[23]

2.3 Evaluation of Material Properties

Shot peening and laser shock peening both induce compressive stresses within a work piece, both peening processes create curvature on a material when only one side of the flat work piece is peened. This curvature can be evaluated using Almen strip sized test pieces and subjecting them to the respective peening process and measuring them with an Almen gauge. The results can be compared to an Almen strip and against each of the peening processes. The peening process also create different surface finishes, this can be evaluated via surface roughness testing. Material hardness also changes due to compressive stresses induced on the material, and can be measured using microhardness testing to evaluate the change in hardness across the thickness of the work piece. Residual stresses one of the key factors for using the peening processes can be evaluated using a residual stress testing method, this would allow for direct comparison to evaluate and compare the differ impacts on a specific material, and establish the overall best process.

2.3.1 Almen Strip Testing

Almen strips are used in industry to measure shot peening intensity. When an Almen strip is shot peened, the residual compressive stress causes the Almen strip to bend or arc toward the peened side (i.e. the side subjected to the shot peening process). The Almen strips arc height is a function of the energy of the shot stream and is very repeatable. Therefore, in order for the Almen strips to provide reliable and repeatable intensity verification, it is important that they are consistent in thickness, flatness and hardness [24]. The conventional Almen strip is made from spring tool steel with dimensions 3inches (76.2mm) by ¾ inches (19.05 mm), as seen in Figure 2.5 .

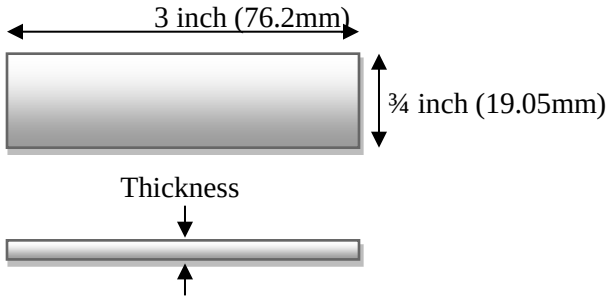

Figure 2.5: Almen Strip Dimensions

The different types of thickness of Almen Strips are:

'N' Strip = .031inches

'A' Strip = .051inches

'C' Strip = .094 inches

The 'C' strip is generally used in the motor vehicle industry (High Intensity applications), the 'N' strip is used for low intensity applications, but seldom used and the 'A' strip in the aviation sector (medium intensity applications) [23]. The strips are mounted into a Standard Hardened Block with four mounting screws to secure the Almen Strip. "The shot is prevented from impacting the reverse side of the strip in order to achieve the "Arc-

Height". The effect of the induced compressive stress on the strip results in bowing, curving or arching of the test strip. The "Arc Height" is measured with an Almen Gauge; this is done by placing the strip at the bottom end (measuring end) of the device, which is magnetised, in order to retain the metal strip to the bottom of the test fixture. In Figure the test block can be seen holding the Almen strip in place for the shot peening process and an Almen gage which is used after the process to measure arc height. In Figure , the shot peening process and deflection measurement is demonstrated.

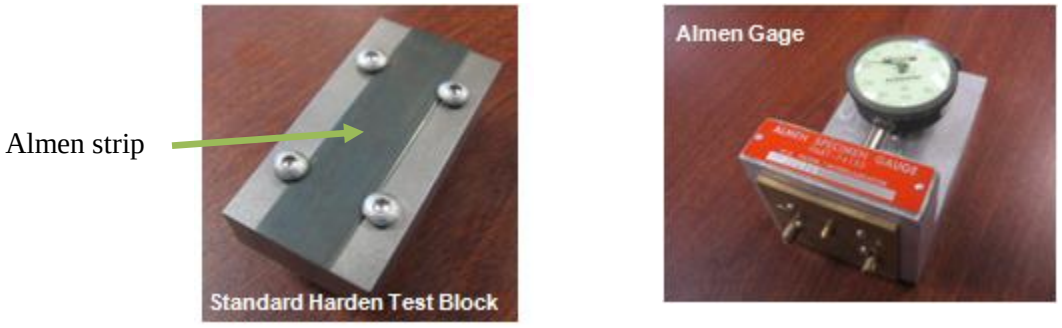

Figure 2.6: Standard Hardened Test Block holding an Almen Strip and an Almen gage [26]

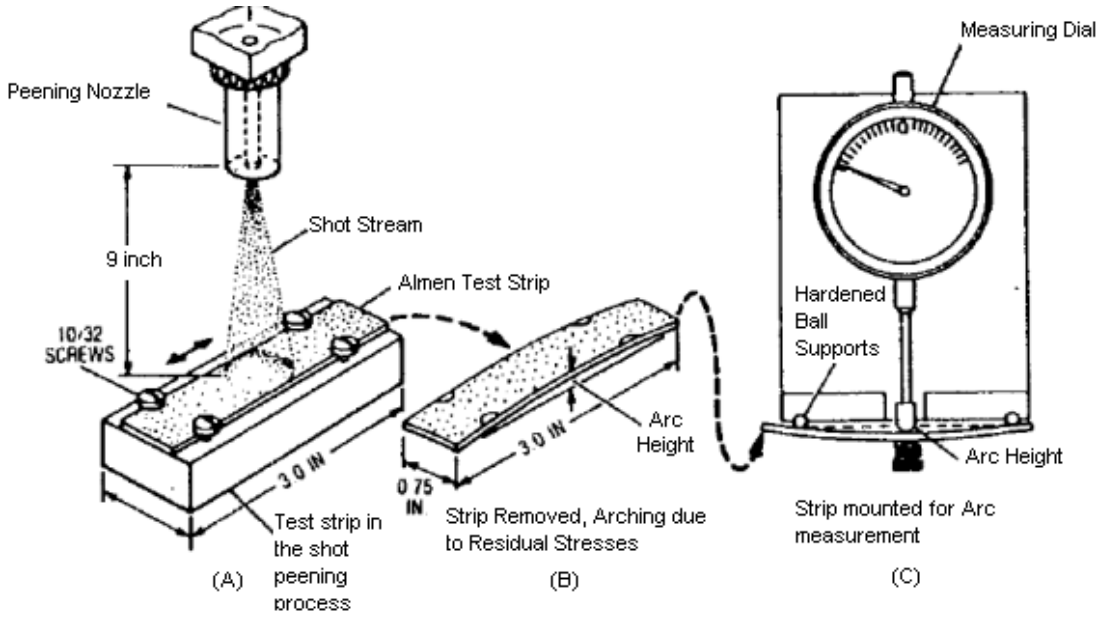

Figure 2.7: Shot Peening Process and Arc Measurement [27]

2.3.2 Surface Roughness

Surface roughness or surface finish, is the surface irregularities left behind after a machining process, such as finely spaced micro irregularities left behind by a cutting tool. A close approximation of the roughness height can be calculated from the profile chart of the surface. This is done by dragging a measurement stylus across the testing surface, but the stylus has to be run perpendicularly to the surface. In Figure , the stylus can be seen to be dragging over the surface creating the profile chart of the testing area.

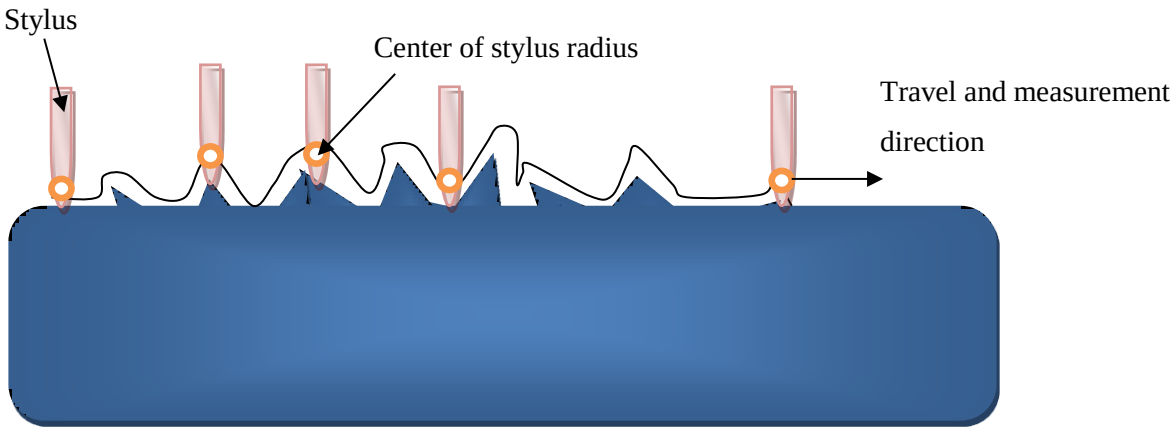

Figure 2.8: Stylus dragged across surface to create profile chart of surface area.

2.3.2.1 Arithmetical Mean Roughness (Ra) [28]

"Ra" is the most common parameter used to measure surface roughness. It is calculated across a sampling length which measures the average length between peaks and valleys on the material surface, and the deviation from the mean line within this sampling length. This calculation averages all peaks and valleys so that the extreme peaks in the sample length are neutralised and have no significant impact on the result. An example of the sample length can be seen in Figure .

The equation used to measure "Ra" is:

$$\boldsymbol{Ra = \frac{1}{l}\int_0^l |f(x)|dx} \qquad \text{Equation 2.2}$$

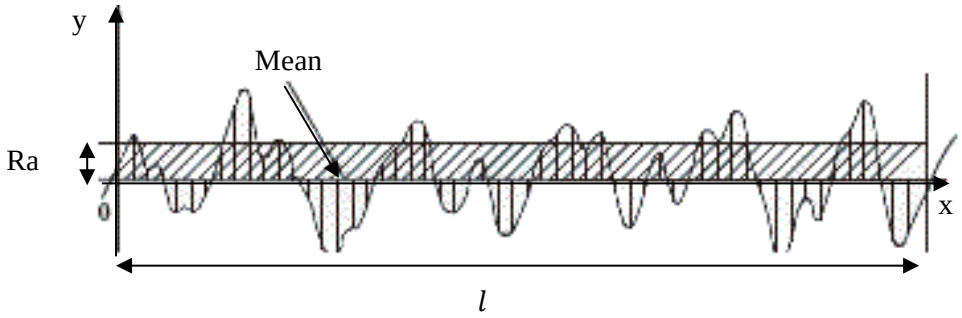

Figure 2.9: Sample Length for calculating "Ra", Arithmetical Mean Roughness

2.3.2.2 Mean Roughness Depth (Rz) [28]

"Rz" is calculated by measuring the vertical diatance of the highest peak to the lowest vally within 5 sampling lenghts, and then the average of these lenghts. Only the 5 highest peaks and the 5 lowest vallys are used in this calculation. The extream peaks would make a significant difference in the results. The equation and diagram representing the calculation of "Rz" can be seen in Figure 2.10 .

$$\boldsymbol{Rz} = \frac{|\boldsymbol{Yp1}+\boldsymbol{Yp2}+\boldsymbol{Yp3}+\boldsymbol{Yp4}+\boldsymbol{Yp5}|+|\boldsymbol{Yv1}+\boldsymbol{Yv2}+\boldsymbol{Yv3}+\boldsymbol{Yv4}+\boldsymbol{Yv5}|}{\mathbf{5}} \qquad \text{Equation 2.3}$$

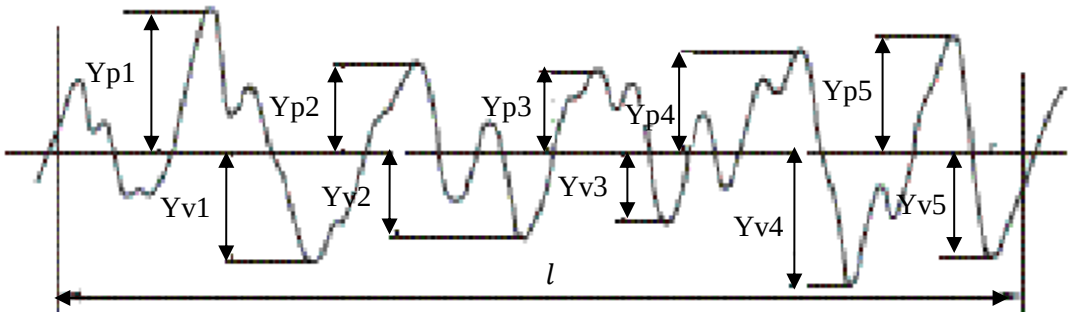

Figure 2.10: Diagrammatic representation of how peaks and valleys are measured for Rz.

$\boldsymbol{Yp(i)|_{i=1}^{5}}$: Height of the top 5 peaks within the sampling length.

$\boldsymbol{Yv(i)|_{i=1}^{5}}$: Height of the lowest 5 valleys within the sampling length

2.3.3 Hardness Measurement

Hardness is not a fundamentally physical property but the characteristic of the material [29]. It is the property of the material to resist plastic deformation and the resistance of the material to be indented/penetrated, which is determined by measuring the permanent depth of an indentation created by a force/load and an indenter. The term could also relate to stiffness/temper or the resistance to scratching, abrasion or cutting [30].

Within material science, four different type of hardness testing methods are which are mainly used are (shown with their applicable loads) [30]:

- Vickers Microhardness Test: 10gf (grams of force)–100kgf (kilograms of force)
- Knoop hardness Test: 10gf-1kgf
- Brinell Hardness Test: 1kgf-3000kgf
- Rockwell Hardness Test: 15kgf-150kgf

2.3.3.1 Vickers Microhardness Test

The Vickers Microhardness (HV) is determined by measuring the diagonal lengths of an indent left on the test material, via a diamond indenter with a given load [31]. The diamond used in the indentation process is pyramidal in shape, with an angle of 136˚ (22˚ from the horizontal) between the opposite faces of the diamond (which is set on a square unpeened), as seen in Figure [32].

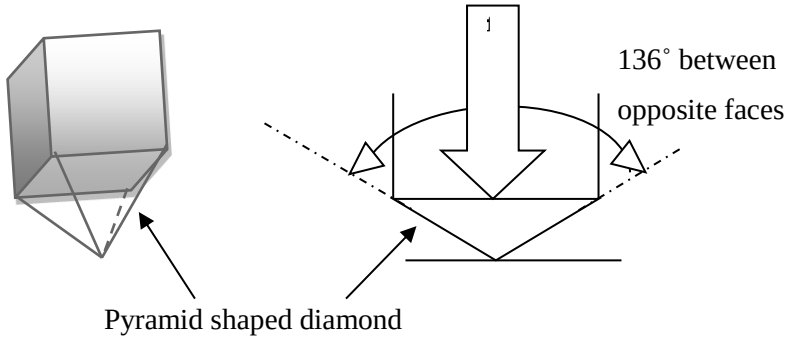

Figure 2.11: Diamond indenter

A force is applied to the diamond indenter as it makes contact with the material, for a dwell time of between 10 to 15 seconds. When the force is released and the indenter removed, an indentation is seen in the shape of a diamond. This indentation is measured across the diagonals of the diamond shape (seen in Figure) and the sloping surface of the diamond.

In the case of indentation, the smaller the indentation created on the test area, the harder the material. This test is mostly used for small parts and thin chapters. ASTM E-384 is the microhardness test procedure, which specifies the range of light loads using a diamond indenter to make the indentation, which is measured and calculated to yield the hardness value. This process can be tested on almost any material.

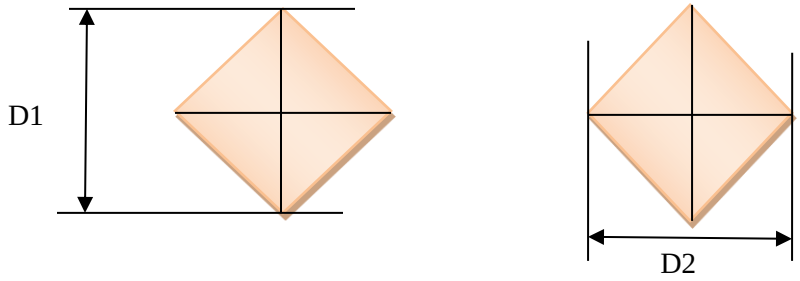

Figure 2.12: Vickers Microhardness measurement, dimensions of diamond formed on material surface after the indentation process.

The dimensions of the diamond are averaged (or the area of the diamond used) and the area of the sloping surface calculated and substituted into the equation seen. The dimensions are measured in millimeters and the force in kgf.

$$\boldsymbol{Vickers\ Hardness\ (HV)} = \frac{\boldsymbol{2.Force.Sin\left(\frac{136^{\circ}}{2}\right)}}{\boldsymbol{\left(\frac{D1+D2}{2}\right)^{2}}}$$

$$\cong \boldsymbol{1.8544\frac{Force}{\left(\frac{D1+D2}{2}\right)^{2}}\left[\frac{kgf}{mm^{2}}\right]} \qquad \text{Equation 2.4}$$

Or

$$\boldsymbol{Vickers\ Hardness\ (HV)} = \frac{\boldsymbol{2.Force.Sin\left(\frac{136^{\circ}}{2}\right)}}{\boldsymbol{(D1.D2)}}$$

$$\cong \boldsymbol{1.8544\frac{Force}{(D1.D2)}\left[\frac{kgf}{mm^2}\right]} \qquad \text{Equation 2.5}$$

The Vickers Microhardness number is represented by 'HV', and is written in the form (Calculated Hardness Value).HV.(Force used)/dwell time, i.e. for a calculated value of 100kgf/mm2 at a force of 300 grams for a dwell time of 10 seconds will be written as follows: 100HV300/10 or HV 0.3 representing just the force used [32].

2.3.3.2 Knoop Hardness Testing

This test was developed as an alternative to the Vickers Microhardness Testing, to overcome cracking in brittle materials and to test thin layers. The diamond in this test are not symmetrical but elongated. The Knoop hardness (HK) is calculated by measuring the long diagonals lengths created through indentation [31]. The dent is seen as an elongated diamond shape. In Figure , the hardness process and equation can be seen.

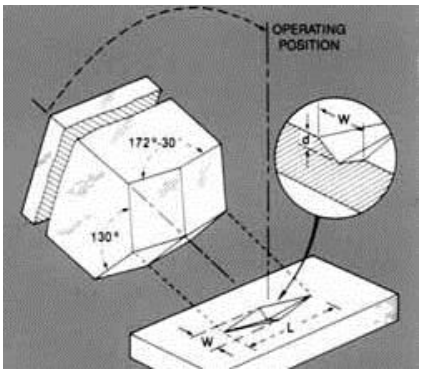

Figure 2.13: Knoop Hardness Testing [33]

$$(Knoop\ Hardness\ Number)HK = \frac{P}{0.07028L^2}\ \text{kgf/mm}^2 \qquad \text{Equation 2.6}$$

2.3.3.3 Brinell Hardness Testing

This test uses tungsten carbide/steel balls of 1, 2.5, 5 and 10mm in diameter, to press into the test material and measure the impressed diameter left behind. This test is done for larger samples with a coarse or inhomogeneous structure, such as casting or forging [31]. The Brinell hardness testing process and equation can be seen in Figure 2.14 and Equation 2.7.

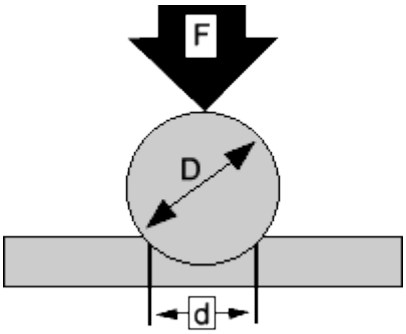

Figure 2.14: Brinell hardness testing [34]

$$(Brinell\ Hardness\ Number)BHN = \frac{F}{\frac{\pi}{2}D\left(D - \sqrt{D^2 - d^2}\right)} \qquad Equation\ 2.7$$

2.3.3.4 Rockwell Hardness Testing

This test differs from the other test, by only measuring the depth of the indent left behind by the indenter. The larger the depth the softer the material.

Principles of the Rockwell Hardness Test [35]

- The indenter is positioned on the surface of the test piece
- A minor load is applied and a zero reference position is established
- A major load is applied for a specified time period (dwell time) beyond zero
- The major load is released leaving the minor load applied

Figure 6 shows the Rockwell hardness process.

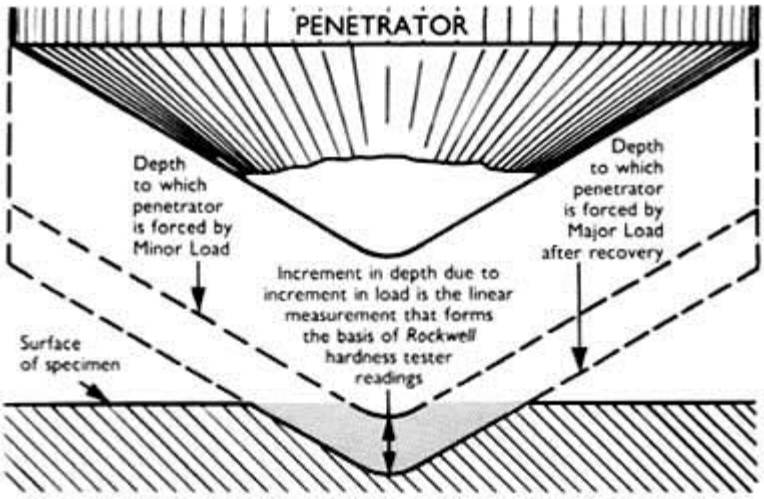

Figure 6: Rockwell Hardness Testing [36]

"The resulting Rockwell number represents the difference in depth from the zero reference position as a result of the application of the major load" [35].

For testing conducted on the thin aluminium alloy, micro testing was selected to determine the non-linear behavior of hardness created across the thickness of the material due to the peening processes. Due to non-brittle material being used, the Vickers Microhardness test was selected.

2.3.4 Residual Stress

After a solid material had been subjected to any external force which induces plastic deformation or temperature gradients or material phase transformation (structural change), the stresses which remain behind and upon material equilibrium are known as residual stresses [37]. These stresses can be beneficial or non-beneficial to the material. Non-beneficial stress is undesired and uncontrolled. These occur when there is an initial crack formation. When an external tensile force is applied to the material, an increase in localised tensile stress occurs, thus causing the crack to propagate and leading to fracture and material failure. Compressive residual stresses are seen as a beneficial stresses, as an external tensile stress would need to be larger than the compressive stresses formed in the

material before a crack can propagate. This type of stress is used on turbine engine fan blades, and to toughen glass displays used on cellular phones. Laser shock peening and shot peening are seen to induce compressive residual stresses within a material. The breakdown of the residual stress testing methods can be seen in Table 2.1 .

Table 2.1: Residual Stress Testing methods [38]

Technique	Restrictions to Materials	Penetration	Spatial Resolution	Accuracy	Comments
X-Ray Diffraction	Crystalline	5µm (Ti), 50µm (Al)	20µm depth, 1mm Lateral	±20 MPa	Combined often with layer removal for greater depth
Synchrotron Diffraction (Hard X-rays)	Crystalline	>500µm, 100µm for Al	20µm lateral to incident beam, 1mm parallel to beam	± $10x10^{-6}$ strain	Triaxial stress, access difficulties
Neutron Diffraction	Crystalline	4mm (Ti), 25mm (Fe), 200mm (Al)	500µm	± $50x10^{-6}$ strain	Triaxial, low data acquisition rate, access difficulties
Curvature/Layer Removal	None	0,1-0,5 of thickness	0,05 of thickness		Stress field not uniquely determined
Hole Drilling	None	~1,2xhole Diameter	50µm Depth	±50 MPa	Flat surface needed (for strain gauges) semi-destructive
Slitting (crack compliance)	None	N/A	1mm Depth		Flat surface needed, destructive
Surface contour	None	N/A			Simple and cheap, suits well for welds, destructive
Ultrasonic	Metals, Ceramic	>10cm	5mm	10%	0,5-10 MHz
Magnetic	Magnetic	10mm	1mm	10%	Microstructure sensitive
Raman/ Fluorescence/ Birefringence	Ceramics, Polymers	<1µm	<1µm approximately	50 MPa	Not applicable directly for metals(Feasible by using proper coating)

Residual stress testing methods consist of destructive methods and some without detrimental alteration of the component being tested. Material restrictions and spatial resolution can be seen to differ from the different testing methods. According to the research required across the thickness of the material and the non-linear residual stress distribution expected, only two sets of equipment could be used, i.e. Neutron diffraction

method and hole drill testing. With the Neutron diffraction equipment being located in other parts of the world and limited access granted (at the time of this research project none of these facilities were available in South Africa), hole drilling residual testing machine was selected for testing purposes in this dissertation, as it was also a new purchase at the University of the Witwatersrand and allowed for ease of access in comparison to other testing methods.

2.3.4.1 Hole Drilling Residual Stress Testing [39]

The most modern procedure for measuring residual stress is the hole-drilling strain gauge method. A special three or six element strain gauge rosette is mounted on the test piece at the location point, where residual stress is to be determined. Wires are connected from the connection points on the strain gauge rosette, to a multichannel static strain indicator. A milling guide/monocular is part of the apparatus used to accurately center the drilling target on the rosette. As demonstrated in Figure 76.

Figure 76: Example of hole drilling alignment through a monocular

After zero-balancing the gauge circuits, a small, shallow hole is drilled through the geometric center (drilling point) of the rosette. Readings are taken of the relaxed strains, corresponding to the initial residual stress. Using special data-reduction relationships, the principal residual stresses and their angular orientation are calculated from the measured strains.

2.3.5 Material Specifications

Aluminium alloys are widely used in industry, with a large amount being used in the aviation/aerospace sector. The properties of aluminum alloys provide for a lighter material in comparison to steel and other metals and have a high material strength. These are key factors for aircraft manufactures, as aircraft design is dependent on a lighter aircraft or weight reduction, which enables increased efficiency and less fuel used. Pure Aluminium on its own is a very ductile material, with a low melting point of 660 ºC.

The introduction of alloys into pure aluminum enhances its material properties to suit its desired use, and unlike most composite material aluminum alloys can be recycled. The material selected to be used in these test were of AA6056-T4 Aluminium alloy. It is a 6xxx series Aluminium alloy.

This type of series is known to have high strength, good formability and good weld-ability. Its high silicon percentage helps to increase the alloys strength, high magnesium to allow for the control, recovery, recrystallization and grain growth of the strengthened precipitate. Copper is one of the elements which contribute to the enhanced hardness and refinement of the microstructure. T4 in the name of the alloy indicates that it had been thermally treated, quenched and naturally aged at room temperature [40]. The properties and material strength can be seen in Table 2.2 . This material has been tested to have an ultimate tensile strength of 405 MPa and a yield strength of 230 MPa.

Table 2.2: Chemical composition of the AA6056-T4 (wt %) [41]

	Si	Mg	Cu	Mn	Fe	Zu	Zr
AA6065	0.70-1.30	0.60-1.20	0.50-1.10	0.40-1.00	<0.50	0.10-0.70	0.07-0.20

2.3.6 Previous Findings for Shot peening vs. Laser Shock peening

Previous research done compared the residual stresses within a material after it had been shot peened and laser shock peened. Testing found through research, were conducted mainly for thick materials, and for thinner material could not be located.

In

Figure 8, Figure 9 and Figure 10 , the tested data for residual stress analysis of Inconel 718, Aluminium 7375-T7351, Ti-6Al-4V and Ti-6Al-2Sn-4Zr-2Mo can be seen respectively.

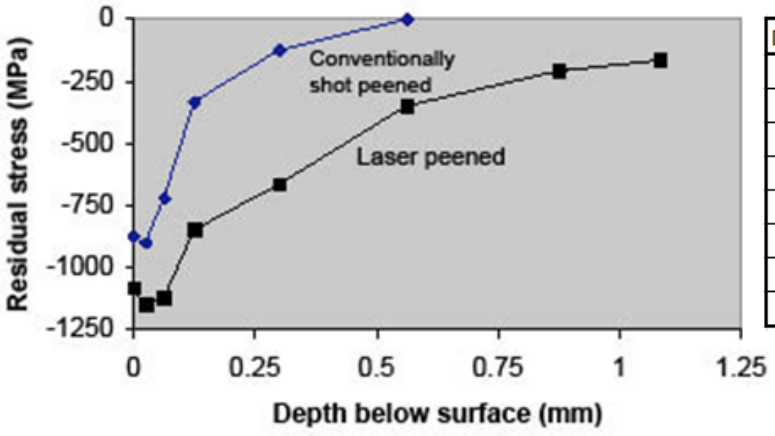

DEPTH	Shot Peened	Laser Shot Peened
0	-875	-1083
0.025	-900	-1150
0.0625	-720	-1125
0.125	-334	-850
0.3	-125	-667
0.5825	0	-350
0.875		-208
1.083		-167

Figure 817: Residual Stress Results of Inconel 718 [42]

In Figure 2.17, The laser shot peening data is seen to have a higher compressive residual stress (i.e. up to 5 times higher than shot peening) and seen to penetrate deeper into the material when compared to normal shot peening (seen to be more than 2 times the material penetration).

In Figure 9.18 , the residual stress of Aluminium 7075-T7351, for laser shock peening is also seen to penetrate deeper into the material, where after 0.2mm into the material depth, shot peening residual stress results reached back to material normalization i.e. 0MPa, indicating no stresses act within the material from this point.. Whereas the residual stress

is seen to penetrate past 0.8mm and further into the material i.e. more than 4 times the penetration of shot peening.

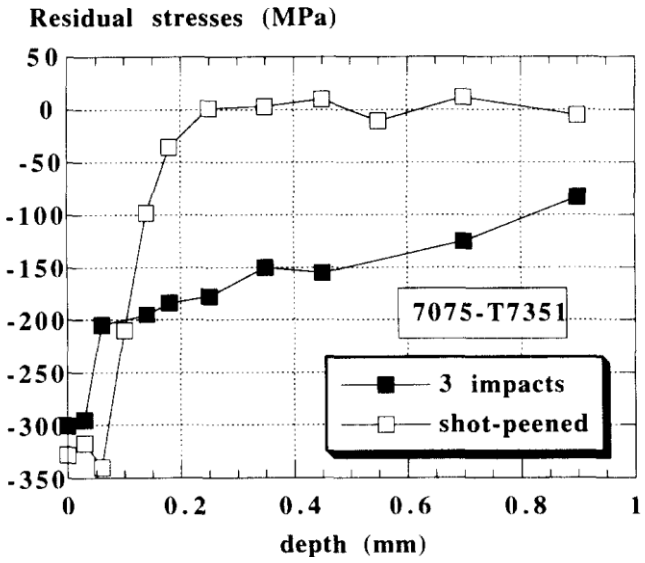

Figure 9.18: Residual Stress Results of 7075-T7351 [43]

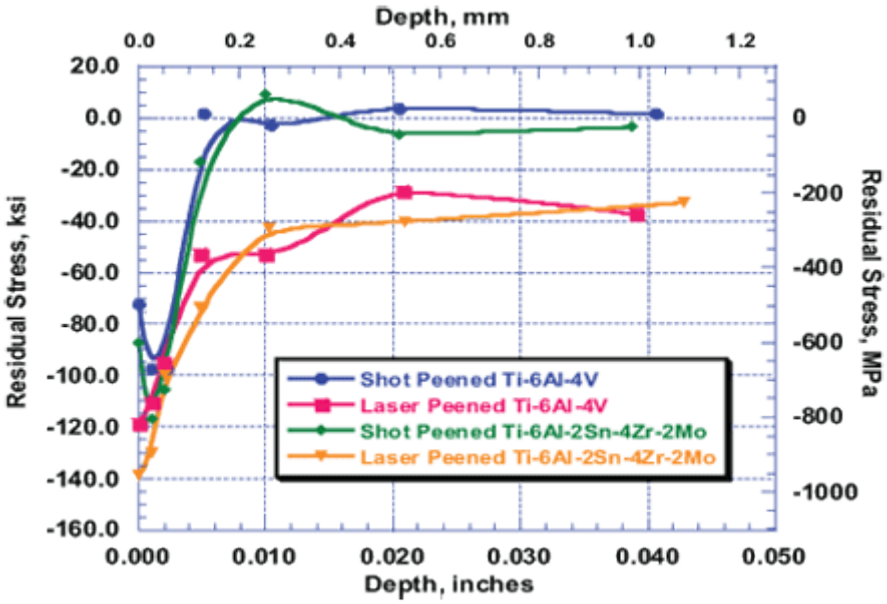

Figure 10: Residual Stress Results of Ti-6Al-4V and Ti-6Al-2Sn-4Zr-2Mo [44]

In Figure 10 , the residual stress of graph of Ti-6Al-4V and Ti-6Al-2Sn-4Zr-2Mo shows residual stresses for both Ti-6Al-4V and Ti-6Al-2Sn-4Zr-2Mo similar residual stress curves for both shot peening and laser shock peening. Laser shock peening is still seen to penetrate deeper into then shot peening but up to 5 times, as the residual stress results of shot peening reaches material normalisation at around 0.2mm into the depth of the material, and laser shock peening continues past 1 mm into the material depth. From these observations compressive residual stresses subjected into the work piece are expected to penetrate much deeper into a work piece for laser shock peening in comparison to shot peening.

Microhardness testing was also done in previous research, comparing shot peening results to laser shock peening for Aluminium alloy AA6082-T651, 7075-T7351 and A356-T6. From the results seen in Figure 11.20, Laser shock peening is seen to have a higher microhardness value in comparison to shot peening, and is also seen to penetrate deeper into the material.

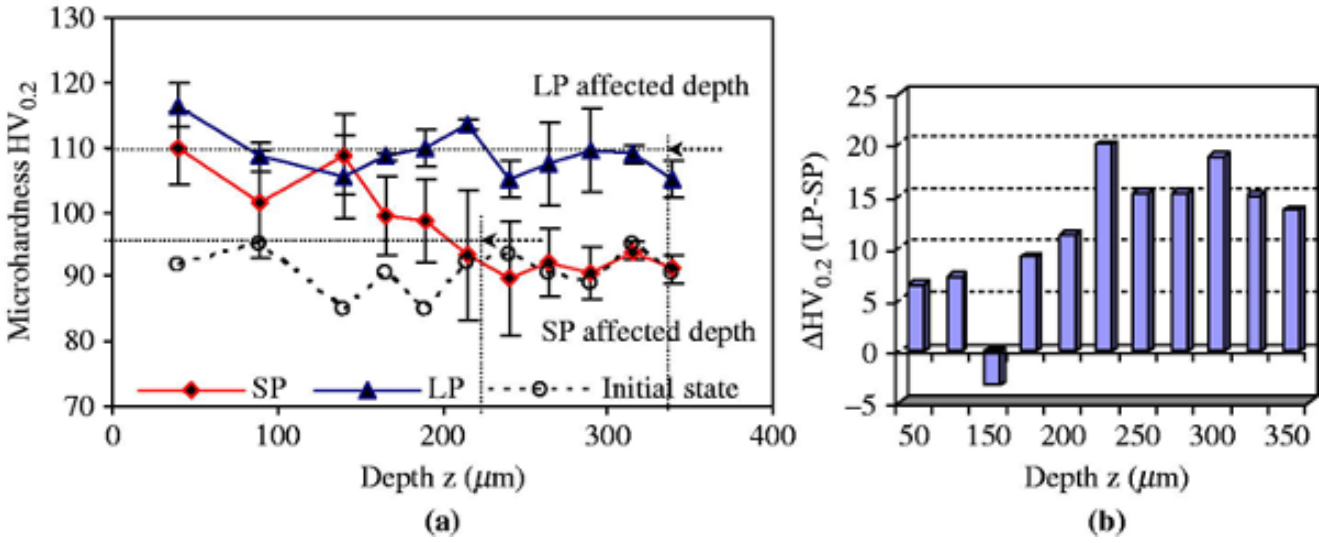

Figure 11.20: Microhardness results of precipitation-hardened aluminum alloy AA6082-T651 [45

In Figure 1221, shot peening result of both 7075-T7351 and A356-T6, show a higher hardness value, whereas laser shock peening results show minor changes in hardness

within the material. This could indicate material hardness differs within different material for the two peening processes.

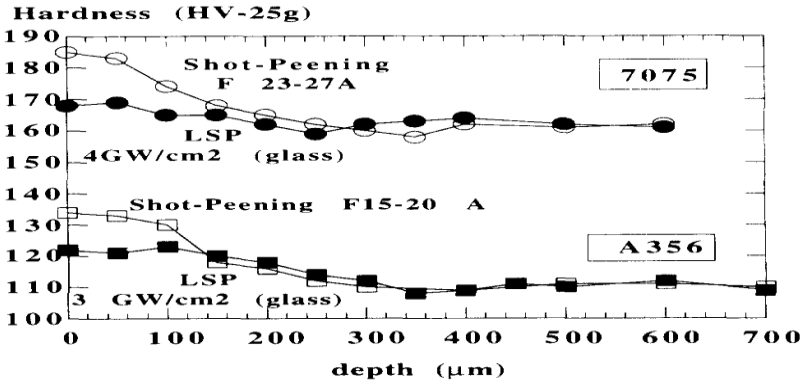

Figure 12: Hardness testing of 7075-T7351 and A356-T6 [46]

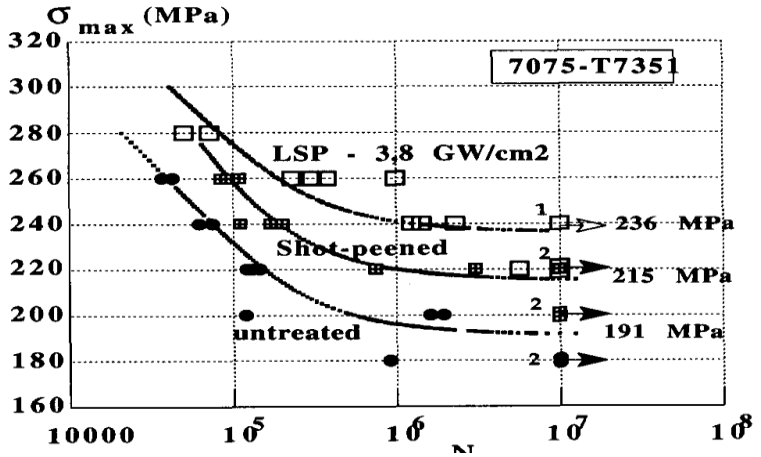

Figure 13: Max Stress Curve of 7075-T735 [46]

In Figure 13 the maximum stress curves are seen before and after the material of Aluminium Alloy 7075-T7351 is subjected to shot peening and laser shock peening. Both peening processes increase the maximum stress of the material, but laser shock peening is seen to give a higher maximum stress.

CHAPTER THREE

3.0 Introduction

Shot peening and Laser shock peening both serve to improve the fatigue life of materials by inducing compressive residual stresses. These processes in addition, change the material surface roughness, and introduce a deflection/curvature to a test piece. The curvature differs at the various intensities used during each process. In this chapter the study method and design can be seen, thereafter the following properties will be evaluated and data captured through experimentation for both shot peening and laser shock peening processes:

- Compressive residual stresses in AA6056-T4 of thickness 3.2 mm
- Deflection
- Microhardness
- Surface roughness.

3.1 Apparatus

3.1.1 Shot Peening

The approximate blasting area used by South African Airways Technical (SAAT) for its shot peening process, consist of an inside peening area of 10 feet (≈ 3.048m) wide by 12 feet (≈ 3.657m) long and 14 feet (≈ 4.267m) high. These shot peening room facilities are used for large work pieces. Compressed air was the moving force which was responsible for the functioning of the system. The room consists of one door, a viewing window and two arm holes (i.e. manual operating process).

All internal walls are rubber coated. Within the Chamber was a rotating table with a maximum turn table speed of 10 revolutions per minute for ease of peening larger parts. This table had extendible arms to increase the diameter of the table up to 9 inches (≈

228.6mm) to allow for larger components to be shot peened. Blast generators are used to deliver shots at a controlled feed rate under the required pressure through the blast nozzle.

Each blast generator contains its own shot pressure chamber, where the shots are contained and maintained under a pressure from a separate supply of compressed air. The blast generators contain the shot feed valve, to monitor the amount of shot from the shot pressure tank, into the blast hose and to the nozzle. There was a reclaiming system that separates the unusable shots and dust from the remains, which was recycled back to be used by the system. The system used separators with vibrating screens to sort out the required shots size being used. These are sent to a storage hopper, and stored there until the blast generator was ready for it. Figure shows a schematic of the layout seen at SAAT.

3.1.1.1 Shot peening Equipment details:

Manufactured by: Vacu-Blast Corporation 600N. Washington Abilene, Kansas

Manufacturers Serial Number: 8-9626-R2

Year Built: 1980

Efficiency: 70%

Max Allowable pressure: 125 psi

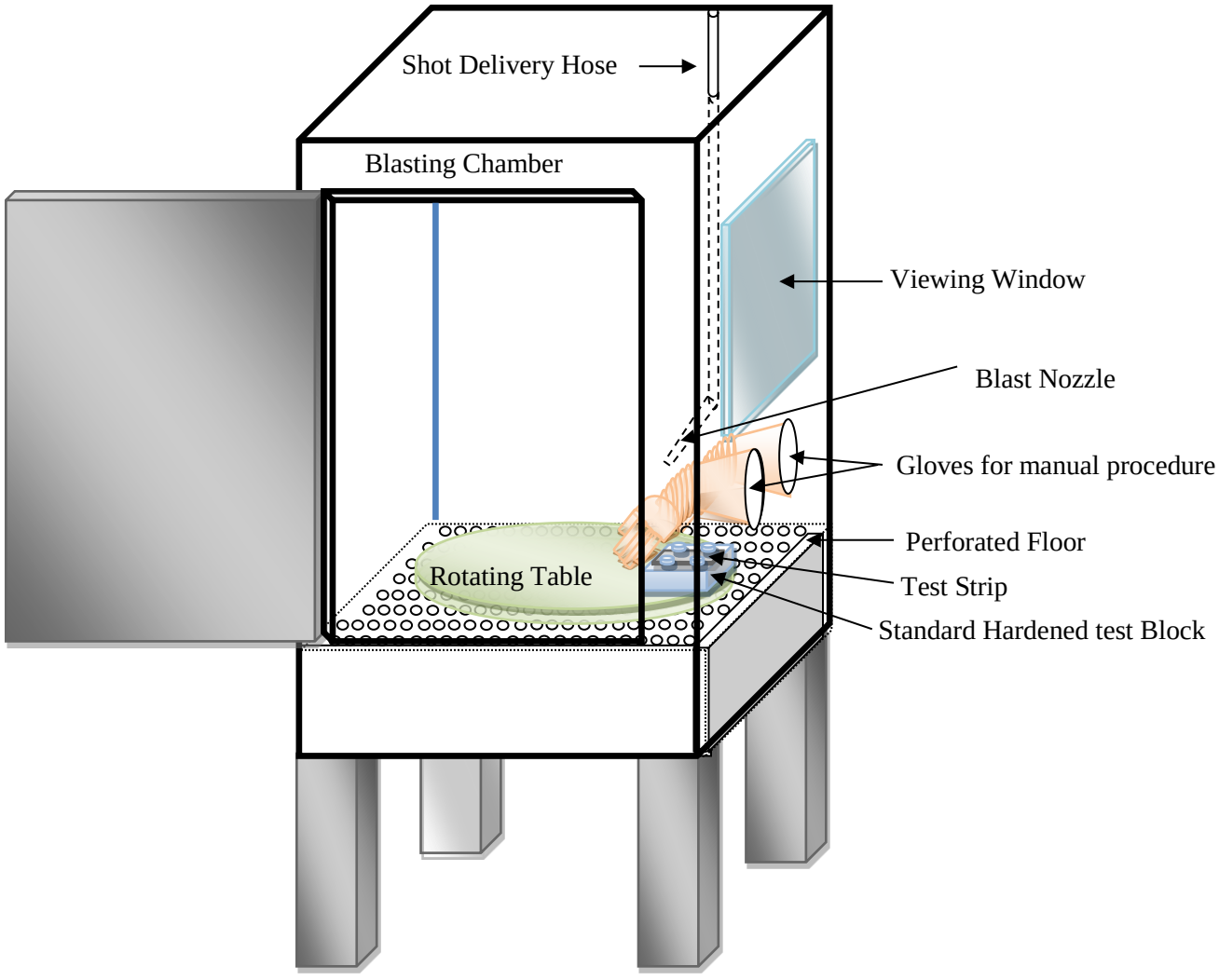

Figure 3.1: Schematic of Shot peening setup used at SAAT

South African Airways Technical currently use this facility to shot peen wheel hubs of all the aircrafts they maintain and various other components.

Turbine blades used at the “Eskom” power stations are also brought into these facilities and placed in a larger room to be shot peened. Each blade is shot peened in a predetermined shot peening process, to enable that even shot distribution is established and all blades obtain similar compressive stresses are induced. This is seen to increase the fatigue life of the blades.

Recoil springs used in heavy artillery vehicles were also brought into the facility to induce compressive stresses on the spring to increase its life cycle and fatigue life. Shot peening was seen as an easy, fast and cheaper method to increasing a components fatigue life. All these components return within a certain time period, back to the facility for the process to be repeated and the fatigue life increased once again.

Precautions are taken for the shot peening process, all components are only shot peened after any heat process/treatment was carried out if needed, as any excessive heat on the peened component would release the compressive stresses induced on the component after shot peening had occurred. The shot peening facility is also used to remove paint from certain components, each component has a dedicated peening process, which had been developed over the years.

3.1.2 Laser Shock Peening

"The Nd: YAG (neodymium-doped yttrium aluminum garnet; Nd:Y3Al5O12) is a crystal substance that is used as a lasing medium for solid-state lasers. The dopant, triply ionized neodymium, Nd(III), typically replaces a small fraction of the yttrium ions in the host crystal structure of the yttrium aluminum garnet (YAG), since the two ions are of similar size. It is the neodymium ion which provides the lasing activity in the crystal, in the same fashion as red chromium ion in ruby lasers. Generally the crystalline YAG host is doped with around 1% neodymium by atomic percent". [47]

The Nd:YAG lasers are typically used in Q-switching mode which uses an optical switch to control pulse operation. Another method of laser shock peening, where a test piece was operated on without an opaque layer (known as, Laser Peening without coating (LPwC)), i.e. where only water was utilised to confine the high pressure plasma produced by the laser. This was seen as the most practical approach as is done by, Toshiba and MIC (Metal Improvement Company). Thermal effects such as local melting could be controlled by the intensity of the laser energy used.

The beam being utilized was circular and created difficulty in creating a square beam shape via beam shaping, thus the overlapping technique was utilised to reduce the effects of surface wave focusing. The laser had fixed parameters i.e. pulse width, pulse profile and repetition rate. From investigation, it was found that Power Density (GW/cm2) and coverage ratio (spot overlay) were to be the key parameters used in this research project.

The laser shock peening equipment layout found at the "CSIR" facility can be seen in Figure 14 (This lay out was setup by other Wits Researchers in a collaborative effort for research with Laser Shock Peening). The laser is part of the "Rental Pod Program" by the National Laser Centre (NAC), which is a state of the art facility fully equipped laser facility. The laser assigned by the NLC was the Spectra Quanta-Ray PRO270 Q Switch Pulse ND: YAG Laser.

A beam was sent from the ND: YAG Laser to mirror 1 where it was reflected to mirror 2 onto mirror 3 and through the lens, where it was concentrated onto the test strip. The laser beam firstly moved through the transparent overlay (water layer which flows over the test strip) and there after hits the surface of the test piece, where it vaporizes, and as a result forms plasma.

This plasma was confined between the test piece and the water layer (transparent overlay) and thus creating a shockwave, which propagates through the material and enhances the material properties, increasing compressive residual stresses within the material. The laser beam was localised to one spot (i.e. does not move), as the mounting plate holding the test strip moved with every pulse of the laser (laser in a pulsating mode).

This was done with a mechanical system (2 degrees of freedom, vertical(Y) and lateral motion(X)), specially developed for this process and controlled via a specialized computer program (developed by Mastercut, a privately owned company, for this process) and the CNC Mach 3 controller software.

With every pulse the specimen was moved in the required sequence, to obtain coverage over the test area (i.e.in the Y (stepping direction) and X (travel direction) direction). The laser peening directions can be seen in Figure 3.2. Travel direction is along the length of the test piece.

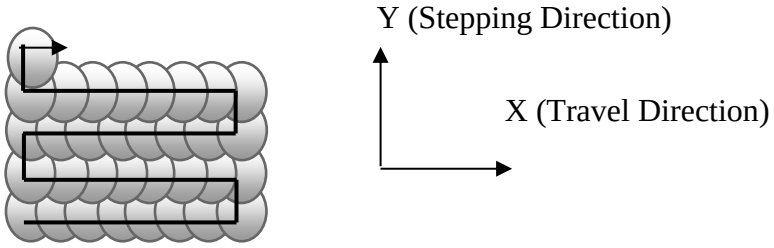

Figure 3.2: Stepping and travel direction of the Laser Shock Peening process.

The laser was pulsed in a range of 1-50 ns of high power intensity to create the required shock wave on the test piece, in order to create compressive residual stresses to occur within the test piece. The Laser shock peening data can be seen in Table 3 .

3.1.2.1 Laser Shock Peening Equipment Details:

Table 3.1: Q-switch pulse ND: YAG (yttrium aluminum garnet) Laser Specifications

Model	Spectra-Physics Quanta-Ray Pro 270	
Dimensions [cm]	117.25 x 50.81 x 30.58	
Max Beam Diameter [mm]	10	
Max Beam Divergence [mrad]	0.5	
Spatial & Temporal Beam Profile	Gaussian	
Repetition Rate [Hz]	10	
Wavelength [nm] :	Energy [mJ/Pulse]	Pulse Width [ns]
1064	1750	8 to 10
532	900	6 to 8
355	475	5 to 7
266	160	4 to 6

For this experimentation a wavelength of 1064nm was chosen. The coverage selected was 100, 250, 500, 1000 and 2000 spots/cm^2.

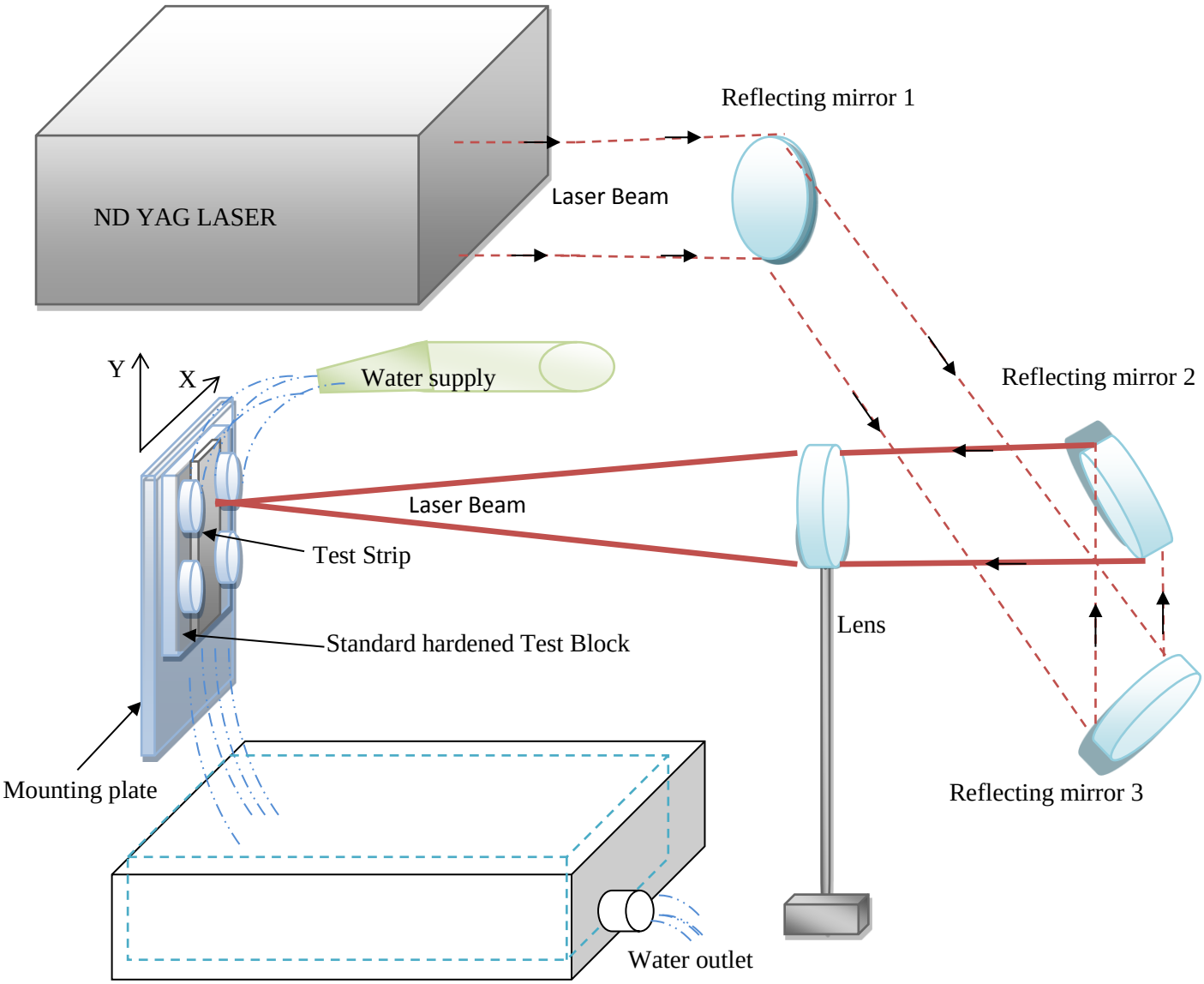

Figure 14: Setup of Laser Shock Peening equipment at “CSIR”

3.2 Test Piece Setup

This process was done with test strips within the same dimensions as normal Almen test strips, but with a thickness of 3.2mm as shown in Figure .4 . This sized test piece was made of AA6056-T4 aluminium alloy. This strip was used for both shot peening and laser shock peening, for the purposes of deflection, surface roughness and micro-hardness testing.

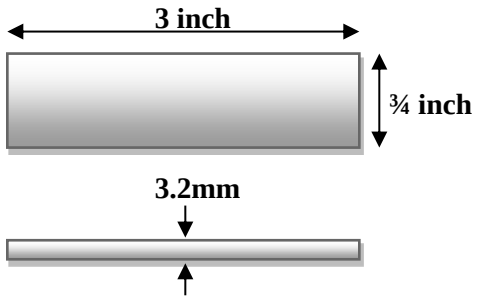

Figure 3.4: AA6050-T4 Test Strip dimensions

Three larger test pieces were also shot peened (i.e. 195mm by 45mm, with a 3.2mm thickness). Two areas of 21mm by 21 mm were subjected to the shot peening process (similar test pieces and test areas were also used for laser shock peening process) as can be seen in Figure 15 .

Thick layers of tape were used to cover the non-tested areas on the larger test piece, for the shot peening process (This was done as the shot peening process was not a concentrated process, i.e. the blast impact area form the nozzle was not constant.) as only a certain area was required to be peened, whereas the laser shock peening process was more precise and no added measures were required.

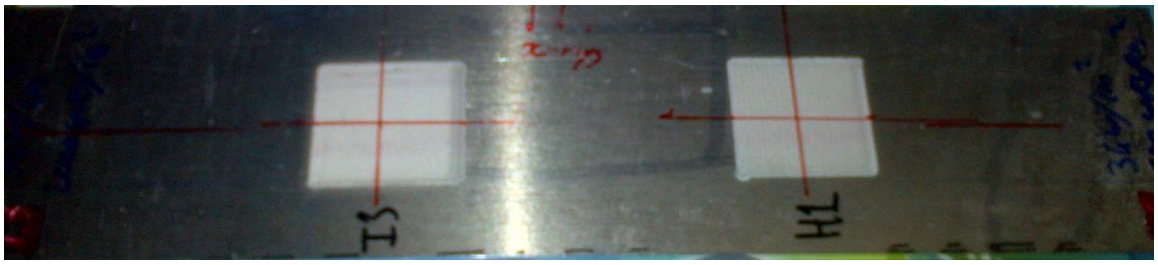

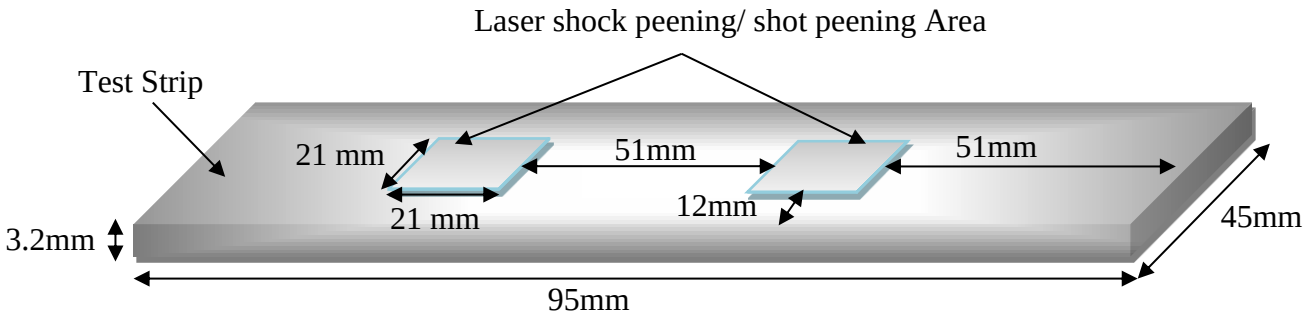

Figure 15: Actual Larger test piece, and dimensioned test piece.

The peened area was located 51mm from either end of the test strip and 51mm between each peened area, and 12mm from either side of the test strip.

As the larger test pieces were too large to be mounted on the standard hardened test block, they were held by hand in position and shot peened, whereas the laser shock peening process had specialized equipment to keep it in place. These larger test pieces were only used for residual stress testing, as the laser shock peening required a more controlled area to be tested and compared.

3.3 Shot Peening Process

The test was done at pressures of 60psi (≈0.413 MPa), 80 psi (≈0.551 MPa) and 100psi (≈0.689 MPa) and a shot size of 280 (largest diameter shot size available at SAAT). This was a manual process. Each test piece was first checked on the Almen gauge to have a zero deflection, before it was to be mounted on the standard hardened test block. It was then placed in the shot peening chamber as seen in Figure 1.15 (Chapter 5.1). The system was set to the required pressure and "cut wire" shots were used to shot peen each test piece. As this was a manual process, coverage was determined by the number of times the test piece was passed over by the shot peening blast nozzle system. Saturation was determined at 100% coverage, as this was within a 10% difference to the 200% coverage samples.

Five samples were taken at each pressure setting
i.e.:

- 25% coverage (test piece passed over's 2, times with the shot blasting nozzle).
- 50% coverage (test piece passed over's 4, times with the shot blasting nozzle).
- 75% coverage (test piece passed over's 6, times with the shot blasting nozzle).
- 100% coverage (test piece passed over's 8, times with the shot blasting nozzle).
- 200% coverage (test piece passed over's 16, times with the shot blasting nozzle).

3.4 Laser Shock Peening Process

This process was also done with the two types of test pieces used in the shot peening process (excluding the uses of Almen 'A' strips). The laser shot peening process was carried out by an overlap pattern defined by travel direction(Y) and stepping direction(X) (i.e. the mounting equipment, which was controlled via the specially developed program for this process). In

Figure 16 , a picture of the laser shock peening process can be seen. An air hose was used to prevent water splashing onto the optics during experimentation, as this was seen to cause errors during experimentation, as well as a side plate which was used to prevent diffracting laser beams from hurting anyone as aluminum is known to be 80% reflective according to literature. Before any experimentation, safety equipment such as tinted glasses and ear muffs were worn, as the laser was used at around eye level and the loud noise created via the laser shock peening process. A more in-depth look at the process and setup of the equipment used can be seen in the dissertation of "*Daniel Glaser*" [48], this dissertation is under a private international patent [52].

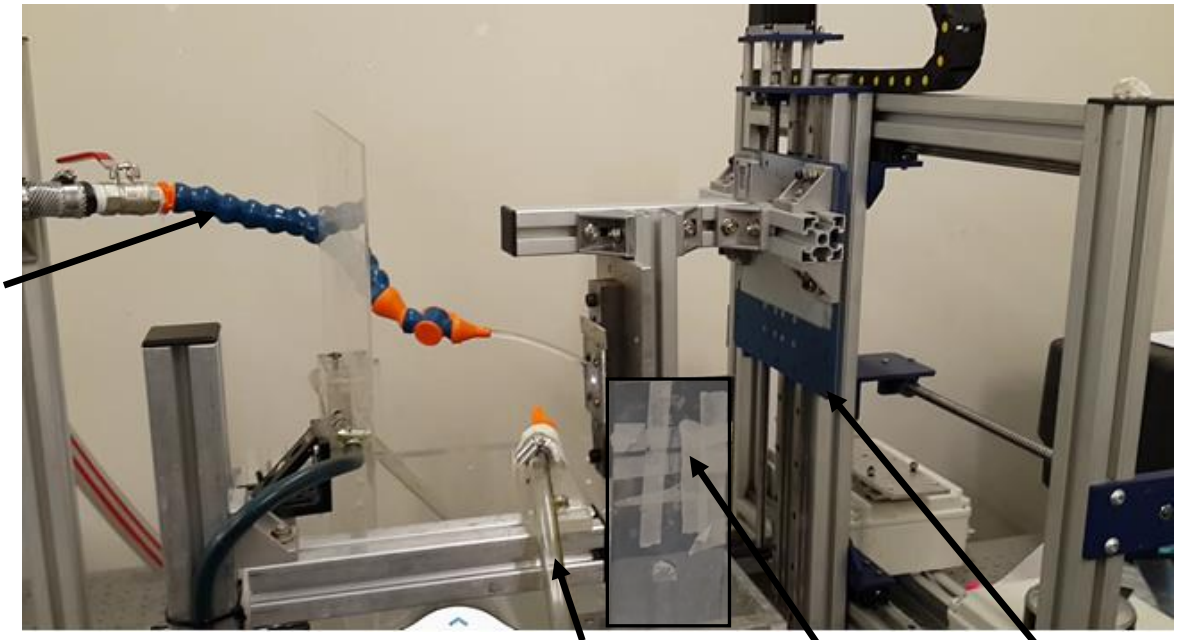

Figure 16: Actual Laser Shock peening test setup at CSIR.

3.5 Deflection/Arc Curvature

Each tested piece processed via shot peening and laser shock peening were measured with an Almen gage as shown in Figure 6 (i.e. the Almen strip sized test pieces).

The curvature was measured across the length of the material, as the highest residual stress occurs along the stepping direction (X) of the material, thus a higher deflection is expected along this length and a smaller deflection in the travel direction (Y) of the laser shock peened results, according to research obtained from "*Daniel Glaser*" [48][52].

Due to AA6056-T4 being non-magnetic, each of the test pieces were held at the hardened balled support to obtain the correct deflection as seen in Figure 3.7 (this did not compromise any of the results as the curvature had not changed via any excessive force on the test pieces).

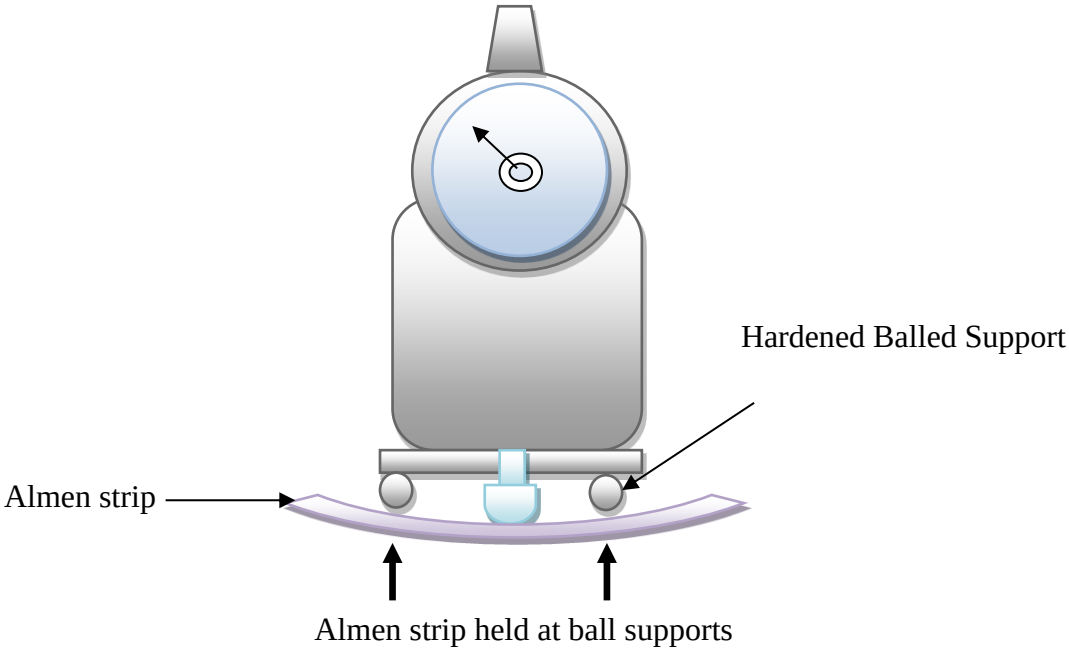

Figure 3.7: Almen Strip measured on Almen Gauge

3.6 Surface Roughness

Each of the Almen sized test pieces was tested with the Hommel Tester 1000. Before testing, the machine was calibrated by running the stylist over a tested block supplied by the manufacturer.

- Each test piece was secured to the table and there after the stylist was placed on the material surface (similar to Figure 17.8)
- A test was run on each specimen, by pressing the start button (i.e. for shot peening and laser shot peening, Almen sized test pieces)
- The stylus was run across the material and a profile chart created and the Ra and Rz values were outputted on the screen
- Each value was collected and tabulated.

Figure 17: Hommel Tester 1000

3.6.1 Surface Roughness Equipment Details:

In Table 4, the Hommel tester 1000 data can be seen.

Table 3.2: Hommel Tester Data

Hommel Tester 1000	
Art Nr:	240851
Serial Number:	82823
D-78056 VS-Schwenningen HOMMEL-ETAMIC Gmbh Austerwertegerat T1000B Alte Tuttlinger straβe 20	

3.7 Microhardness Test sample preparation

For hardness testing: all specimens used, underwent a specific surface preparation process. Each test pieces used in the deflection testing were cut to obtain a new test piece of 10mm x ¾ Inch (19.05 mm) (i.e. the Almen sized test pieces were cut 10mm from its far end, i.e. last area affected by the peening process).

These pieces were cut with a band saw. Each test piece was set in a thermoplastic mold (made from a material called ClaroFast, a molding acrylic resin for transparent embedding of metallographic specimens), which was used to hold the material for testing as seen in Figure 3.9.

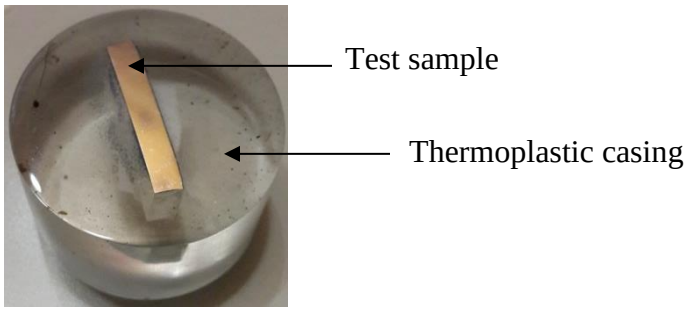

Figure 18: Microhardness test piece encased in a thermoplastic mold

After the thermoplastic casing process, each test piece underwent a grinding and polishing procedure. The grinding of each test piece was done with MD-Piano 240, MD-Piano 500 and MD-Piano 1000 grit silicon carbide paper. These silicon carbide papers were circular and set on a rotating plate, with a constant flow of water. The samples were held with the test surface in direct contact with the silicon carbide paper and rotated in the opposing direction of the rotating table (ensuring not too much pressure was applied on the test piece to ensure an even surface was obtained).

Each test piece was rotated 90˚ with each new grinding paper used. This was done to cancel the previous grinding marks subjected onto the test samples during the grinding process. The MD-Piano 1000 grit silicon carbide paper was the finest grinding application thus giving the smoothest finish, but it had also induced scratches on the surface of the sample. Thereafter a polishing process was followed using the polishing disk MD-Largo (9µm), MD-Mol (3µm) and MD-Chem (0.05µm).

A similar process to the grinding procedure was followed (but instead of water), a thin film of 9 Micron Leco Ultra Diamond Suspension was lightly prayed onto the center of the disk and evenly distributed around the disk. Thereafter the test piece was held on the polishing disk and rotated in the opposing direction of the rotating plate.

After each polishing process (i.e. after each polishing disk used), the test piece was washed under water and wiped with ethanol to remove any of the residue left due to the polishing process.

This process was followed for the 9µm, 3µm and 005µm, until a mirror finish was accomplished for each sample. The mirror finish was important, as this enabled the researcher to evaluate the indentations on the surface of the test piece with more visibility. The machine used for this testing was the FutureTech Fm-700 Vickers Microhardness Machine as seen in Figure 3.10.

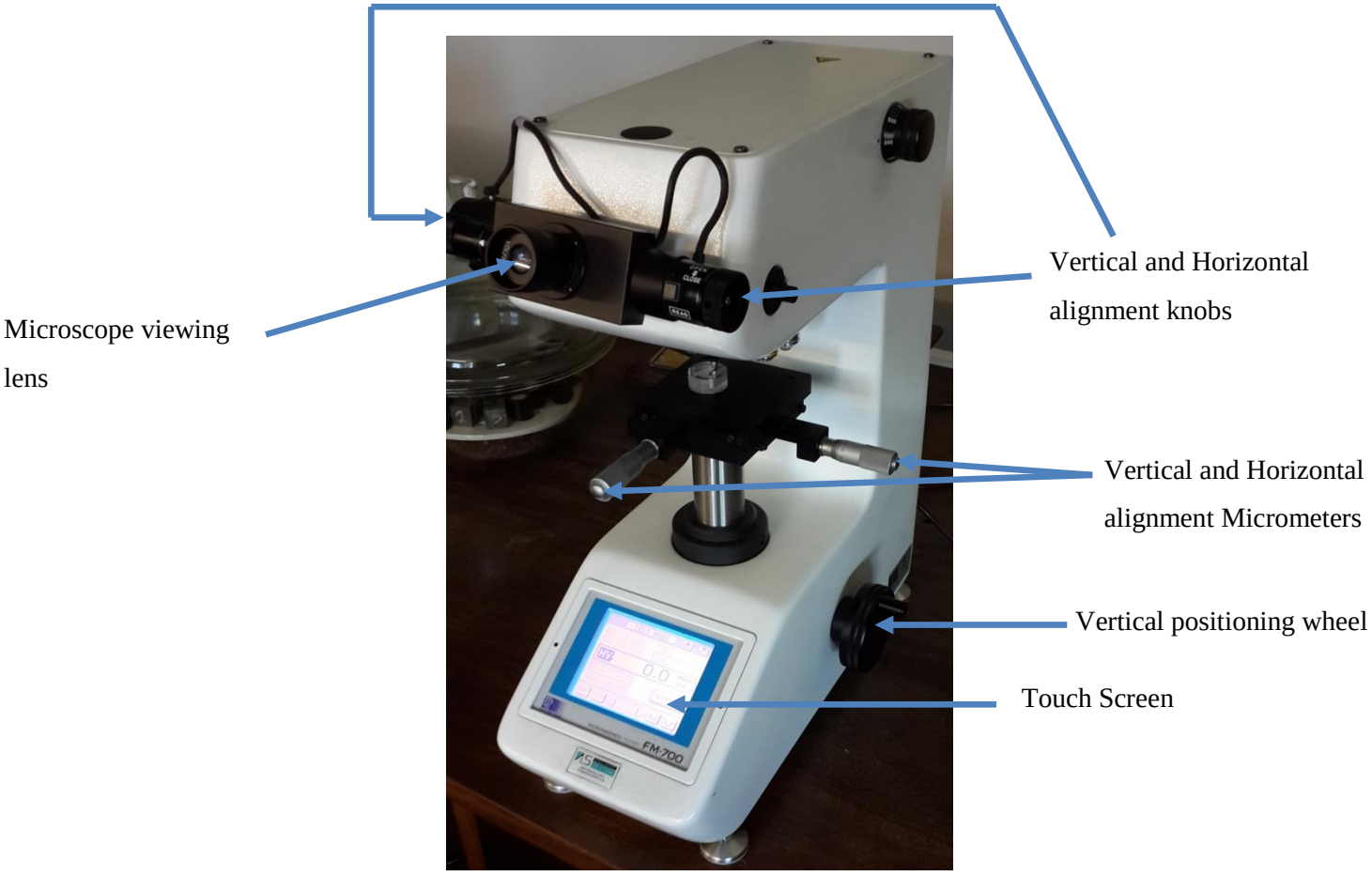

Figure 19.10: FutureTech FM-700 Vickers Microhardness Machine

3.7.1 Microhardness test procedure

This test was done along the height/dept (the 3.2mm thickness side) of each test piece. Each test piece had undergone the following process:

- It was placed on the machines testing surface, and the M10 Lens was used to view the test piece and the vertical positioning wheel was used to bring the test piece into focus.
- Each test piece was rotated till it was parallel to the vertical lines seen through the microscope.
- Using the micrometers and parallel lines found within the microscope viewing lens, the test piece were aligned at its tested side (i.e. the peened edge).
- The M30 lens was then selected to magnify the view and position the test piece to its 1st indentation location.
- A force of 100g was used with the diamond indenter on the test piece for a dwell time of 10 seconds. This can be seen in Figure 20.11 .

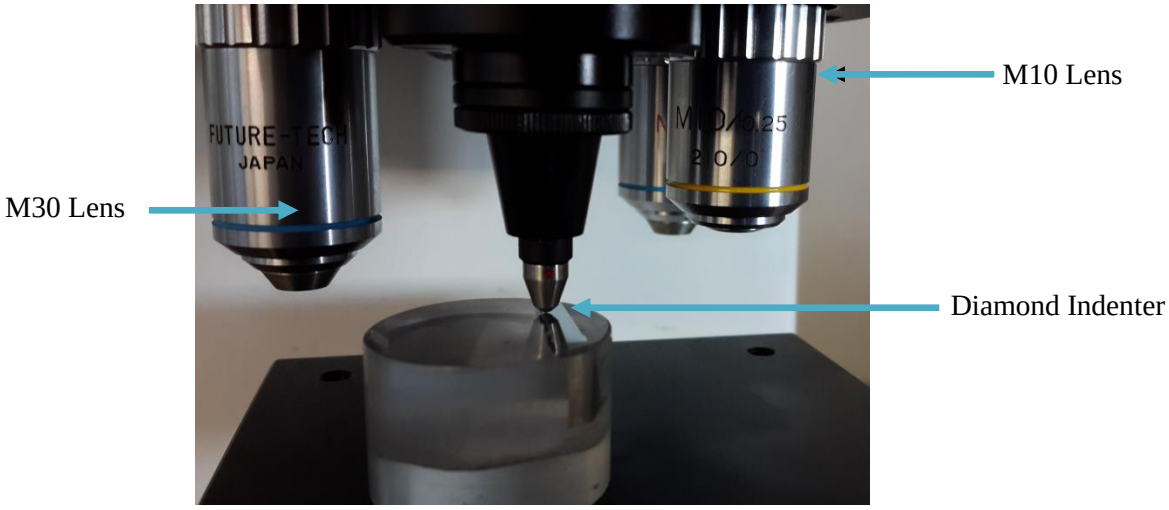

Figure 20.11: Diamond indenter creating an indent on the test specimen

- No results were found, indicating that a higher force was to be used; thereafter the force was increased by 100g at a time, till a measurable indent was found. This was found to be at 300g of Force and thus used for the remaining test pieces.
- After the indent, using the M30 lens and vertical micrometer the test piece was moved to the next indent position (this was in the direction towards the middle of the test piece, and moved to a point where the previous test piece was just out view of the microscope). This was done to prevent any material deformation or material change which might have occurred to affect the next indent results.
- This process was repeated till the line of indentations reached the end of the test material. The line of indentations seen through the M10 lens can be seen in Figure 21 .

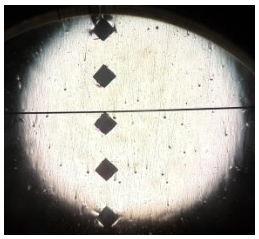

Figure 21: Line of Indentations seen from the M10 lens

- After the indentation process was complete, the distance from the end of the test piece to the middle of the indentation was recorded. This was done by 1st aligning the parallel lines found in the microscope lens into one line (overlap). And pressing the reset tab on the touch screen, thus zeroing the data values. As seen in Figure . Using the vertical and horizontal alignment knobs place the lines in the required positions and record the measurement displayed on the touch screen.

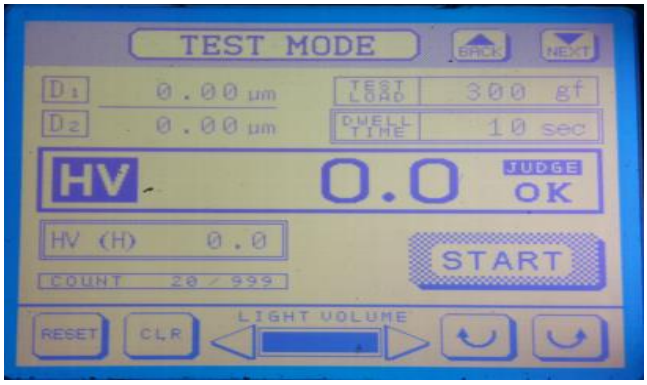

Figure 3.13: Touch Screen on Hardness machine, after being zeroed

- The measurements of D1 and D2 were also recorded using the same process as . This can be seen in Figure .

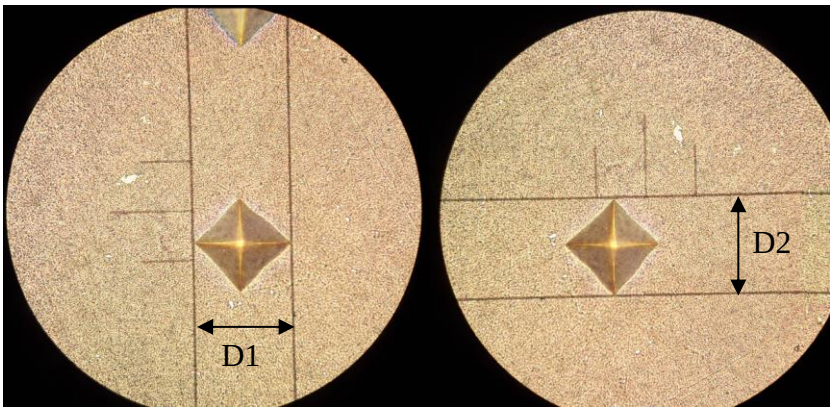

Figure 3.14: Measurement of D1 and D2, seen through the microscope

- The distances between the centers of the diamonds were also recorded using the process, until the end of the test piece was reached. This can be seen in Figure3.15

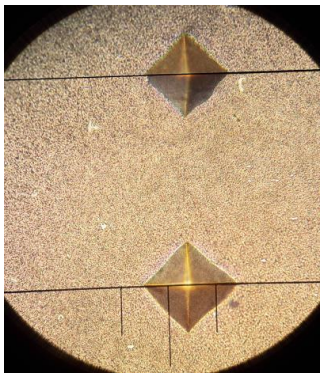

Figure3.15: Measurement between the centers of two indentations, seen through the microscope

3.8 Compressive Residual Stress

This process was done via the Hole Drilling strain gauge method. The larger test pieces which were mentioned in chapter 3, were used in this method of testing. The test areas were mounted with a stress-strain rosette and a small hole drilled through the middle of the strain gauge and into the material. Relieved surface strains were recorded and allowed for reverse calculations were utilised to calculate the residual stressed via the program supplied with the hole drill testing machine.

3.8.1 Strain Gauge Test setup

Each area that underwent a peening process was cleaned thoroughly before the stress-strain gauge rosette was mounted on the test surface.

- This was done by wiping the surface with several white cotton swabs and acetone (each cotton swab was only used once over the area and there after a new swab used, until no residue was found i.e. until the last cotton swab remained clean after wiping the surface).
- Tweezers were cleaned with acetone and a cotton swab (ensuring that no contamination via body contact occurs, as fatty residue from fingers could interfere with the strain gauges result output).

- A small glass pane was cleaned with acetone and cotton swabs, to ensure a clean surface to place the strain gauge.
- With the tweezers, the strain gauge was removed from its packaging and place on the glass pane.
- The strain gauge was orientated in the required direction and a strip of tape was placed over the strain gauge (this was done to prevent contamination to the strain gauge when placing it in position on the test specimen).
- The strain gauge was placed on the test specimen in the required orientation (in the center of the drilling area, and orientated with the number 1 gauge (see figure) parallel to the side of the test piece).
- The tape was peeled back, to a position where the bottom of the strain gauge was off the test surface (this was done to keep the position and orientation of the strain gauge when gluing, seen in Figure). The strain gauge data can be viewed in Figure3.16.

GAGE PATTERN AND DESIGNATION Insert Desired S-T-C No. in Spaces Marked XX. See Note 1		RES. IN OHMS	DIMENSIONS					
			GAGE LENGTH	GRID CTR'LINE DIA.	TYPICAL HOLE DIA.		MATRIX	
					Min.	Max	Length	Width
EA-XX-031RE-120 EA-XX-031RE-120/SE		120 ± 0.2% 120 ± 0.4%	0.031	0.101	0.03	0.04	0.29	0.29
			0.79	2.56	0.8	1.0	7.4	7.04
			Due to small pattern size, measurement error can be magnified by slight mislocation of drill hole. Pattern not recommended for general-purpose applications.					

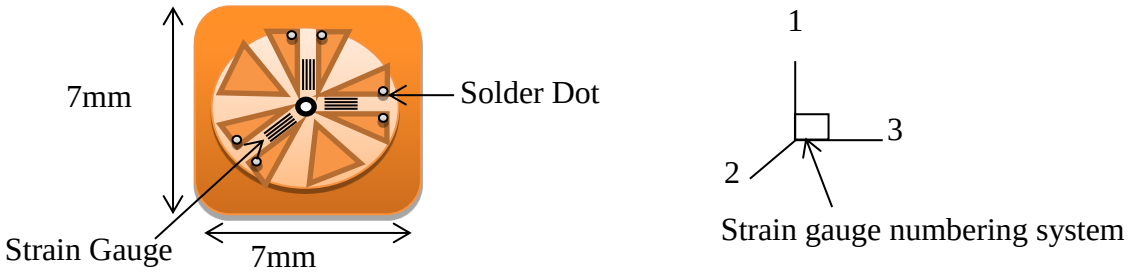

Figure 3.16: Strain gauge data and orientation information.

- A drop of special strain gauge glue (Z70 Schnellklebstoff) was used on the surface of the test specimen (where the strain gauge was to make contact).

- Using a piece of Teflon, the tape containing the strain gauge was pressed down onto the surface of the test piece (allowing the glue to spread under the strain gauge), pressure was applied over the strain gauge using the thumb, for 3 minutes (this was done to secure the strain gauge in position, the Teflon was also used to prevent the glue from making contact with the experimenter). The preparation process using the tape can be seen in Figure .

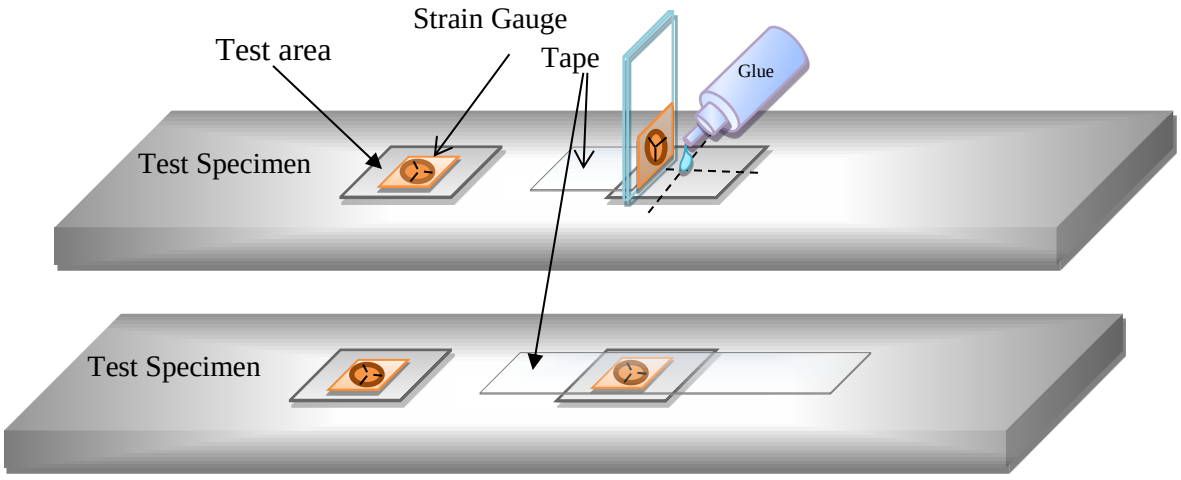

Figure 3.17: Shot / Laser Shock Peened Area with strain gauge preparation process

3.8.2 Hole Drilling Test Setup

- After 3 hours had past, the tape was removed and the strain gauge was soldered at each solder dot, and connected to its respective contact points via a wire. (This process was prolonged, due to the size of the solder dots on the strain gauge being so small and hard to solder).
- Before and after soldering, each strain gauge was tested with a voltmeter, for the resistance across each strain gauge to be 120Ω. This ensured the strain gauges were still valid to be used for testing purposes.

- Each of the solder dots with their respective soldered connections were coated with a coat of Lacquer to ensure that no connection was lost and to prevent shorting to occurs due to aluminum chips being dispersed during testing (due to the pressurised hole drilling process).
- Each of the contact points which were connected to each strain gauge solder dot, were soldered to a wire on one contact and two wires on the next contact to create a half bridge connection as depicted in the Figure .
- Each of these wire were connected to a special wire board created for this process, each containing wires for strain gauges 1,2 and 3.
- This board was connected to the digital strain gauge amplifier (spider 8).
- Pressure was supplied through a pressure regulator and into the electronic control system; from here it was supplied to the hole drilling machine (the pressure was monitored via the electronic control system as the machine is only operable between pressures of 3.5bar to 4.5 bar).

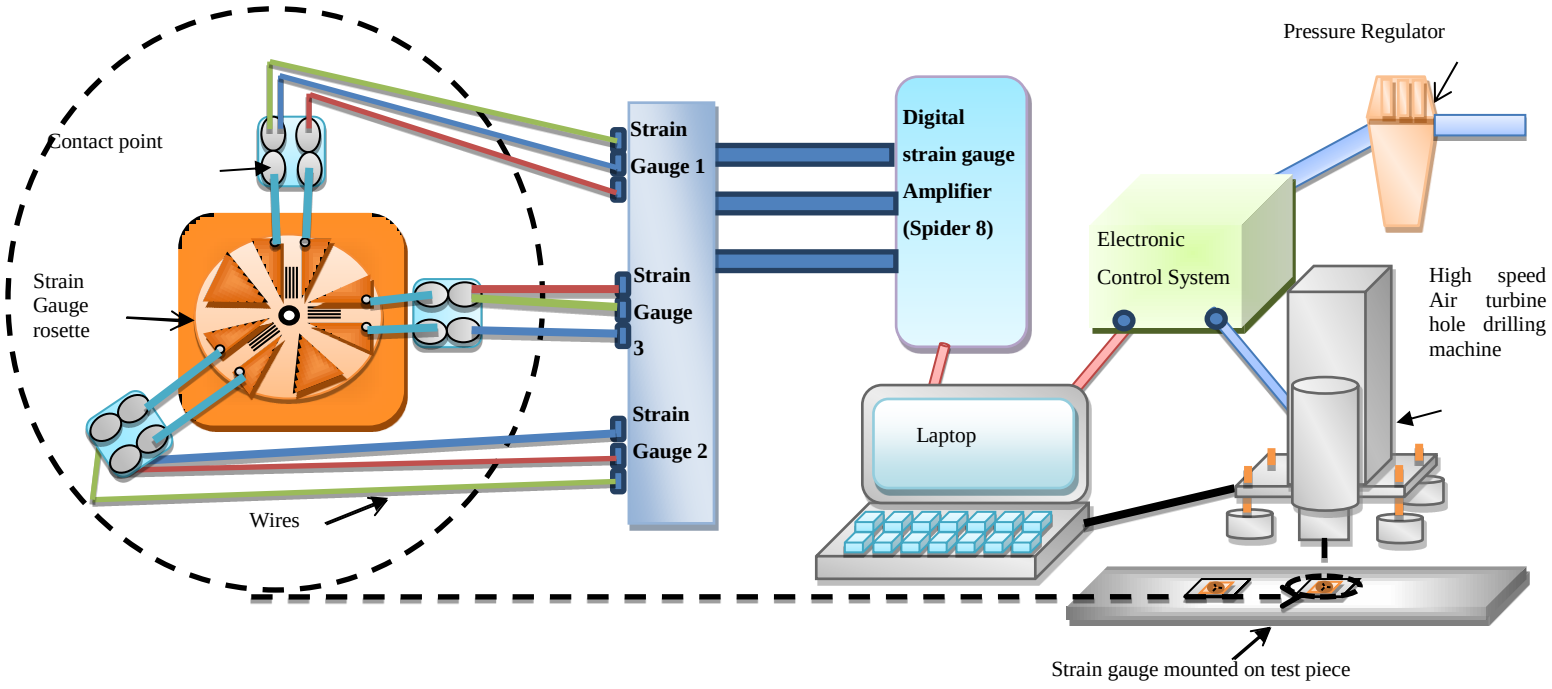

Figure 3.18: Strain gauge and Hole Drilling System Setup

3.8.3 High Speed Air Turbine Hole Drilling Machine setup

In Figure to Figure depicted , the setup of the hole drilling process can be seen step by step. (All data and machine specifications can be seen in Appendix A). The machine selected to be used was the MTS3000-RESTAN.

1. The air turbine chamber was opened by pushing the tab down and moving it to the side of the machine.
2. With a star screw driver, the center screw located on top of the air turbine was removed.
3. A drill bit was selected and placed within a drill chuck.
4. An Allen key was inserted into the back of the drill chuck (drill bit assembly) and positioned over the opening (now seen where the screw was removed).
5. A special “U” wrench was placed in the slot (located in the front of the machine the tab) of the machine, and the drill and drill chuck assembly were inserted into the opening and tightened with the Allen key wrench. (It was ensured, not to over or under torque the drill bit and drill chuck into the machine, as this could damage the air turbine).
6. The screw was replaced and tightened. And thereafter closing the air turbine chamber.
7. The test piece was secured to the workbench by using super glue (this prevented the test piece from moving during the experiment).
8. The hole drilling machine was then placed over the test piece, and the air turbine chamber opened. With the vertical alignment turning wheel, monocular and the cross hairs (lines located in the monocular), the accurate position of the center of the strain gauge was located and centered. The machine was secured to the metal work table by magnetic feet (these were connected to a threaded bold and a ball and socked joint to allow for any uneven surface to be used, i.e. to level the machine for testing).
9. Once the material and alignment was correct, the air turbine was closed to its original position and alligator clips placed on the machine and test piece.

10. Using the program provided, clicking the “Positioning Endmill on surface” tab, allowed the drill to make contact with the surface and stop, and thus assuming the zero position on the test piece. (Ensuring the alligator clips were in position when doing this, as this creates an electric contact point for the machine to stop on the surface of the material without damaging it, this is called ‘touch-off’).
11. The program was setup with all the required data and thereafter the test was run. At the end of each test a new drill bit was required, thus repeating the steps. 1 and 2. Then unscrewing the chuck and drill bit with the “U” wrench and Allen key wrench and then repeating steps 3-11 again.

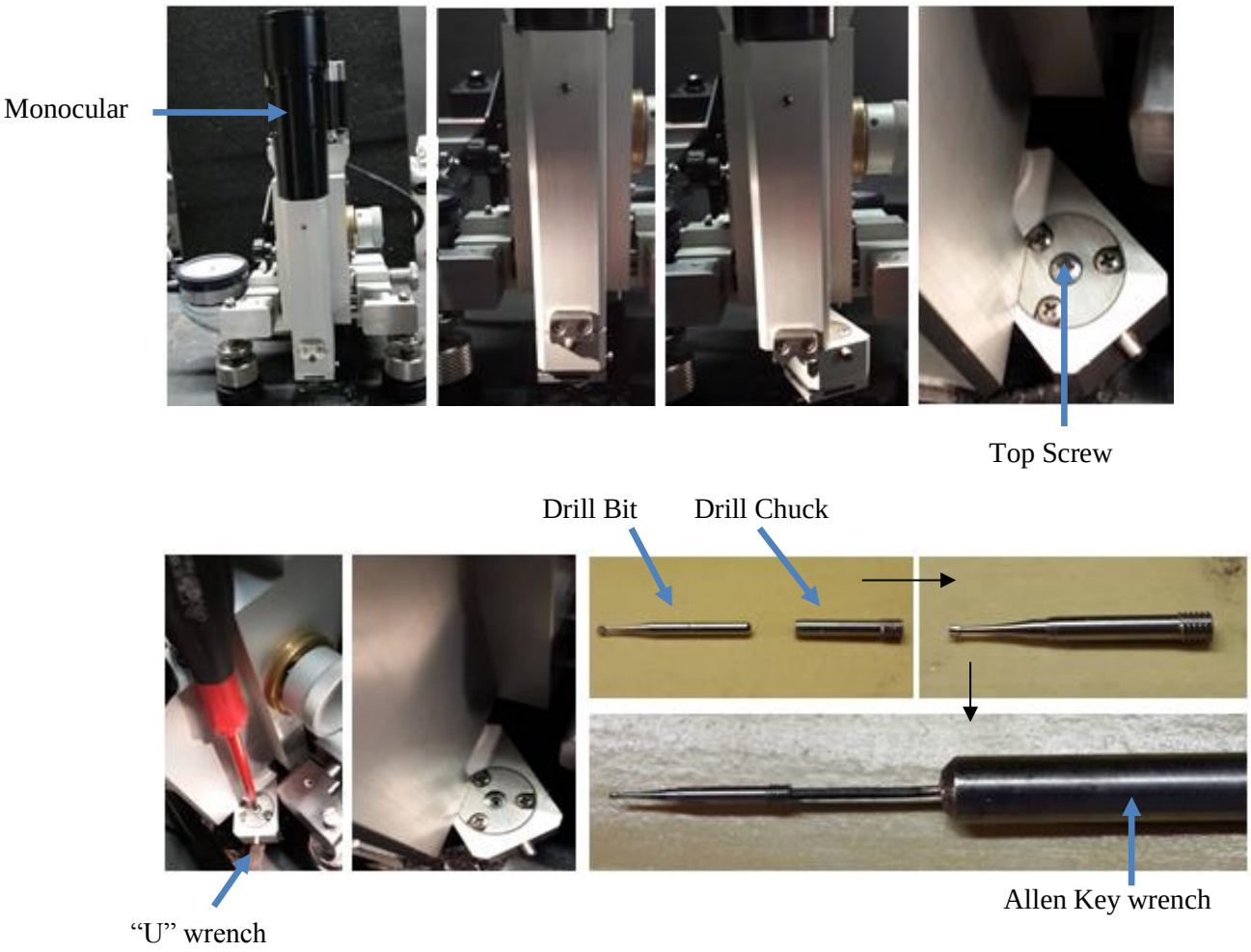

Figure 3.19: (a) High Speed Air Turbine step by step pictorial Setup

Figure 3.20: (b) High Speed Air Turbine step by step pictorial Setup

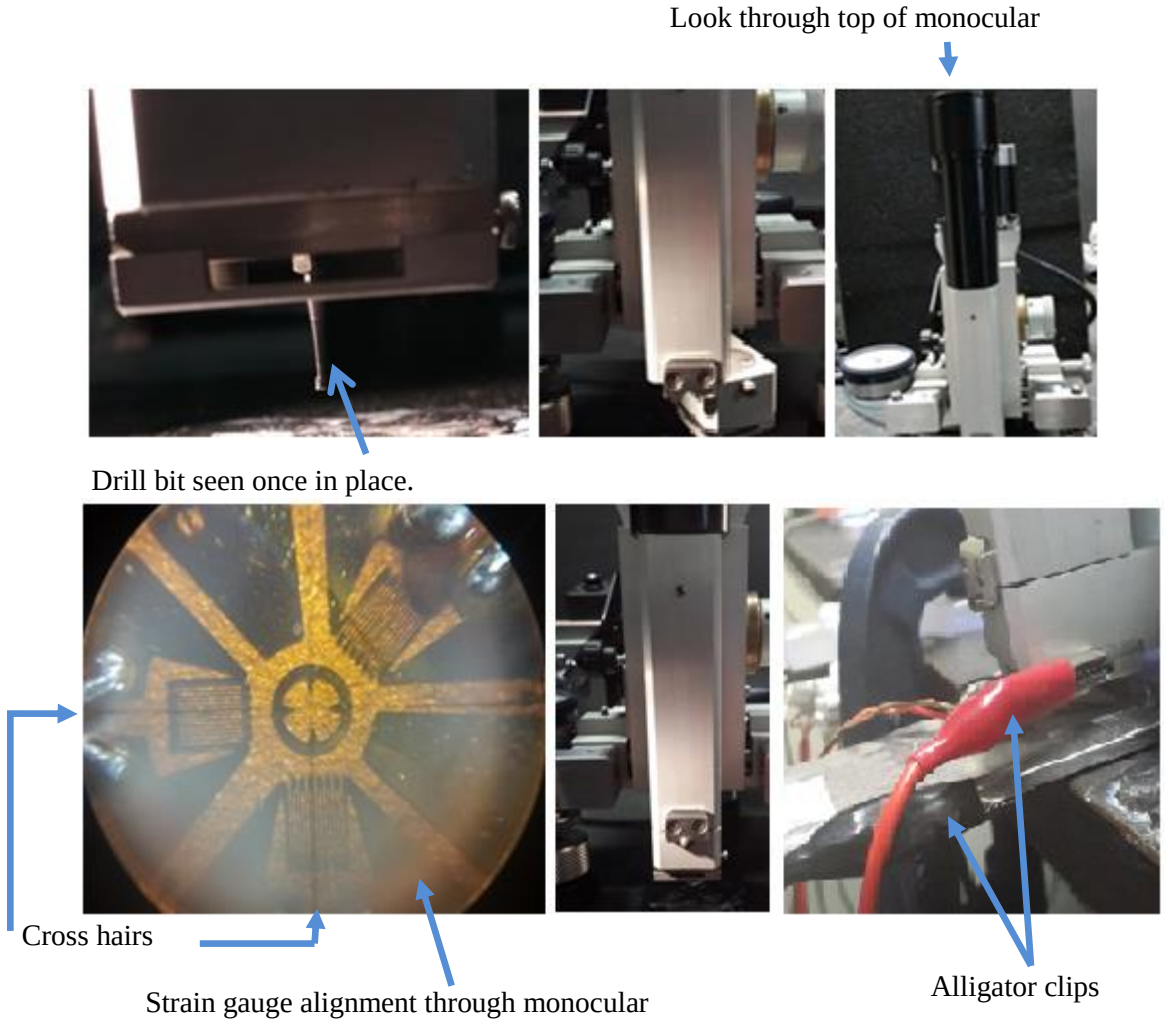

Figure 3.21: Stain gauge alignment, drill bit placement and alligator setup.

3.8.4 Hole Drill Test: Machine Software Setup

The main program used in the Hole drilling software was called “SINT_RSM.EXE”, also known as the residual stress analyzer (MTS3000-RESTAN) software. When the program ran, the three main tabs utilised on the main screen were:

- Test Setup
- Position Control
- And Test Manager.

3.8.4.1 Test Setup Tab

In this tab, the material information was entered and the instrument selection was done (this allowed for all the strain gauge information to be provided to the system, i.e. type of strain gauge and the gage factors of each grid). There after the Step setting was set, thus was the nominal hole diameter, total number of steps , step distribution (Linear), hole depth and step depth.

3.8.4.2 Position Control Tab

In this tab, the drill speed was set and the tab “Positioning Endmill on Surface” was used to position the drill bit in direct contact with the surface. This was done with the alligator clips placed on the test piece and the hole drilling machine. When the drill bit made contact with the test piece, an electric circuit is complete and the drill bit (z-axis) stopped. This position was assumed as the zero position.

3.8.4.3 Test Manager

In this tab, the strain gauge values were balanced closest to a zero value (using the tab “Tae Balance”) and thereafter the drilling process initiated.

3.8.3.4 Eccentricity

This box pops up on screen, after the drilling process has been completed. The dimensions X+, X- , Y+ and Y-, coinciding with the hole dimension (the hole that has been drilled in the test piece) are entered. This was done by opening the air turbine chamber and using the monocular and cross hairs. The vertical and horizontal dial gauges located on the sides of the machine were used to obtain these values, by turning the dials, the machine moved in the 'X' and 'Y' direction.

Data was captured by the program, and analysed using another program called "RESTAN Eval" (Evaluation program). In this program the various different methods for residual stress calculation can be utilised to output the required residual stress curve and data.

3.9 Summary

In this chapter, the equipment used for inducing shot peening and laser shock peening for the AA6056-T4 test pieces from SAAT and CSIR NLC can be seen respectively in chapters 3.1.1.1 and 3.1.2.1. The process for each method used for capturing data for deflection, surface hardness, microhardness and residual stresses within the material was also seen.

CHAPTER FOUR

4.0 Introduction

From the 7 sets of AA6056-T4 Aluminum alloy (Almen sized test pieces) samples, 4 sets were sent for laser shock peening , 3 sets sent for shot peening and 3 sets of Almen "A" strips also sent for shot peening. Each set was made up of 5 test pieces, tested in a range of surface coverage from 25% to 200%. In the following chapter the test data and results for deflection, surface roughness, microhardness and residual stress can be seen.

4.1 Deflection Data and Results

In this chapter the deflection data obtained from using the Almen gauge size test pieces of the AA6056-T4, after shot peening and laser shock peening, as well as the Almen "A" test pieces which were also shot peened were captured and can be seen in Table 4.14.1 to Table 4.8.

In Table 4.14.4, Table 4.5 and Table 4.6, the point of saturation is determined as the point (200% value) where the value of deflection is within 10% of the previous deflection value (100% value). This is confirmed as seen in the Tables, thus confirming the theory established for this process. The deflections are also seen to increase as the nozzle blast pressure is increased and as coverage is increased for the shot peening results, for both the Almen "A" test pieces and the AA6056-T4 test pieces.

In Table to Table , the results also show deflection values increase as the intensity of the laser is increased, and as the coverage is increased from 100 spots/cm^2 to 2000 spots/cm^2. The coverage percentages are used to help compare results of shot peening to laser shock peening.

Table 4.1: Deflection Results of Shot Peening Data 60psi (≈0.413 MPa)

	Pressure: 60psi (≈ 0.413 MPa)		Deflection (0.0005inches)		Percentage of deflection to determine Saturation
Passes	Time [s]	Coverage	3.2mm 6056	Almen "A" strip	
2	2.5	25%	4.3	14.3	
4	5	50%	4.6	15.6	
6	7.5	75%	4.8	17	
8	10	100%	5	19.2	
16	20	200%	5.1	20.4	6.25%

Table 4.2: Deflection Results of Shot Peening Data 80 psi (≈0.551 MPa)

	Pressure: 80 psi (≈0.551 MPa)		Deflection (0.0005inches)		Percentage of deflection to determine Saturation
Passes	Time [s]	Coverage	3.2mm 6056	Almen "A" strip	
2	2.5	25%	5.1	17.8	
4	5	50%	5.5	19.2	
6	7.5	75%	5.8	20	
8	10	100%	5.9	22.8	
16	20	200%	6.1	23.6	3.51%

Table 4.3: Deflection Results of Shot Peening Data 100psi (≈0.689 MPa)

	Pressure: 100psi (≈0.689 MPa)		Deflection (0.0005inches)		Percentage of deflection to determine Saturation
Passes	Time [s]	Coverage	3.2mm 6056	Almen "A" strip	
2	2.5	25%	5.5	19.6	
4	5	50%	5.9	21.3	
6	7.5	75%	6	22.5	
8	10	100%	6.5	25.1	
16	20	200%	7.4	27.6	9.96%

The results obtained in Tables 4.1, 4.2 and 4.3 were used to compare the deflections results between shot peening data for the AA6056-T4 test pieces and the Almen "A" test pieces, to establish a relationship between them. In Figure , the two sets of shot peening results were plotted.

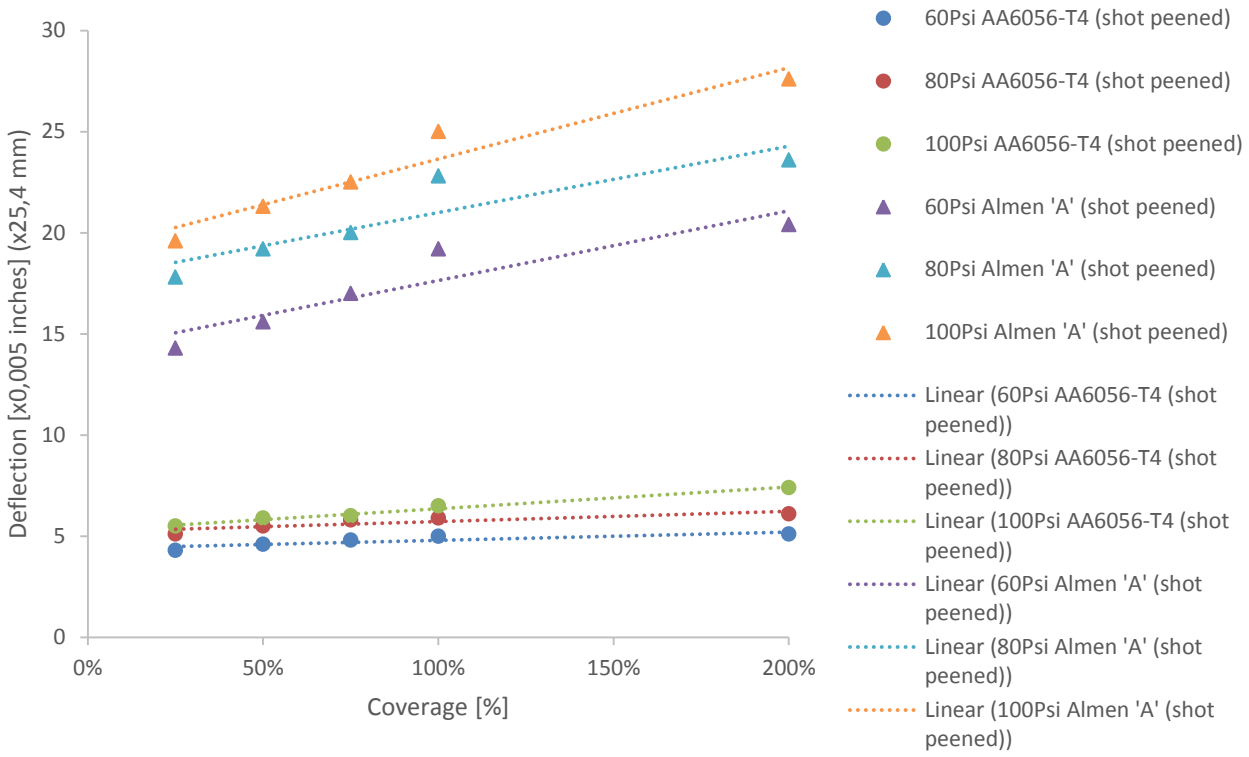

Figure 4.1: Shot Peened deflection data of AA6056-T4 and Almen "A' test pieces against surface coverage.

From the Figure , the Almen "A" data results are seen to incur a higher deflection when compared to the data of the AA6056-T4 results. The higher deflection of the Almen "A" (made of spring steel) test pieces could be due to this test strip being around 1.3mm in thickness, compared to the 3.2mm thickness of the AA6056-T4 material. For the three pressures used in the shot peening process, AA6056-T4 test results were seen to be between the values of 6.3 to 7.4 (x 0.005 inches) and the Almen "A" test pieces 14.3 - 27.6 (x 0.005 inches). The deflection of the AA6056-T4 test strips are seen to change

very little in terms of deflection for the different pressures, whereas the Almen "A" strip displays significant increases in deflection as the pressure is increased.

Using the data results used to create Figure , a table was created to find the difference in values between the Almen "A" and the AA6056-T4 test results for their respective shot peening pressures. This can be seen in Table .

Table 4.4: Difference in deflection results for the Almen "A" and AA6056-T4 test results

	Difference in deflection [(Almen "A")-(AA6056-T4)] x (0.005 inches)				
Coverage	60psi (≈0.413 MPa)	80 psi (≈0.551 MPa)	100psi (≈0.689 MPa)	80 psi-60psi	100psi - 60psi
25%	10	12.7	14.1	2.7	4.1
50%	11	13.7	15.4	2.7	4.4
75%	12.2	14.2	16.5	2	4.3
100%	14.2	16.9	18.5	2.7	4.3
200%	15.3	17.5	20.2	2.2	4.9
			Average =	2.46	4.4

In Table , it can be seen that the difference in deflection between the two material increases as coverage increases. In the right two columns of the table, the data of the 60psi (≈0.413 MPa) difference in deflection is used as a datum and deducted from the 80 psi (≈0.551 MPa) and 100psi (≈0.689 MPa) values respectively. In these columns it can be seen that the 80 psi (≈0.551 MPa) values are within an average range of 2.46 (x 0.0005) inches and the 100psi (≈0.689 MPa) within an average on 4.4 (x 0.0005) inches from the 60psi (≈0.413 MPa) data results. From this we can deduce a similar pattern could occur at higher pressure values in relation to these or at lower pressures.

Table 4.5: Deflection Results of Laser Shock Peening Data 1 GW/cm^2

Calculated power intensity (GW/cm^2)	Intended [GW/cm^2]	[Spots/cm^2]	Distance of test piece to lens [mm]	Spot size	Coverage	Arc height deflection (0.0005) inch
0.81	1	100	303	1.5	10%	1.6
0.81	1	250	303	1.5	25%	2.9
0.81	1	500	303	1.5	50%	4.2
0.81	1	1000	303	1.5	100%	5.8
0.81	1	2000	303	1.5	200%	7.4

Table 4.6: Deflection Results of Laser Shock Peening Data 3 GW/cm^2

Calculated power intensity (GW/cm^2)	Intended [GW/cm^2]	[Spots/cm^2]	Distance of test piece to lens [mm]	Spot size	Coverage	Arc height deflection (0.0005) inch
2.77	3	100	547	1.5	10%	4.9
2.77	3	250	547	1.5	25%	8
2.77	3	500	547	1.5	50%	10.7
2.77	3	1000	547	1.5	100%	13.1
2.77	3	2000	547	1.5	200%	15.4

Table 4.7: Deflection Results of Laser Shock Peening Data 5 GW/cm^2

Calculated power intensity (GW/cm^2)	Intended [GW/cm^2]	[Spots/cm^2]	Distance of test piece to lens [mm]	Spot size	Coverage	Arc height deflection (0.0005) inch
4.60	5	100	534	1.5	10%	7.2
4.60	5	250	534	1.5	25%	11.4
4.60	5	500	534	1.5	50%	14
4.60	5	1000	534	1.5	100%	15
4.60	5	2000	534	1.5	200%	15.2

Table 4.8: Deflection Results of Laser Shock Peening Data 7 GW/cm^2

Calculated power intensity (GW/cm^2)	Intended [GW/cm^2]	[Spots/cm^2]	Distance of test piece to lens [mm]	Spot size	Coverage	Arc height deflection (0.0005) inch
6.29	7	100	524	1.5	10%	7.5
6.29	7	250	524	1.5	25%	11.5
6.29	7	500	524	1.5	50%	13.2
6.29	7	1000	524	1.5	100%	14.4
6.29	7	2000	524	1.5	200%	16

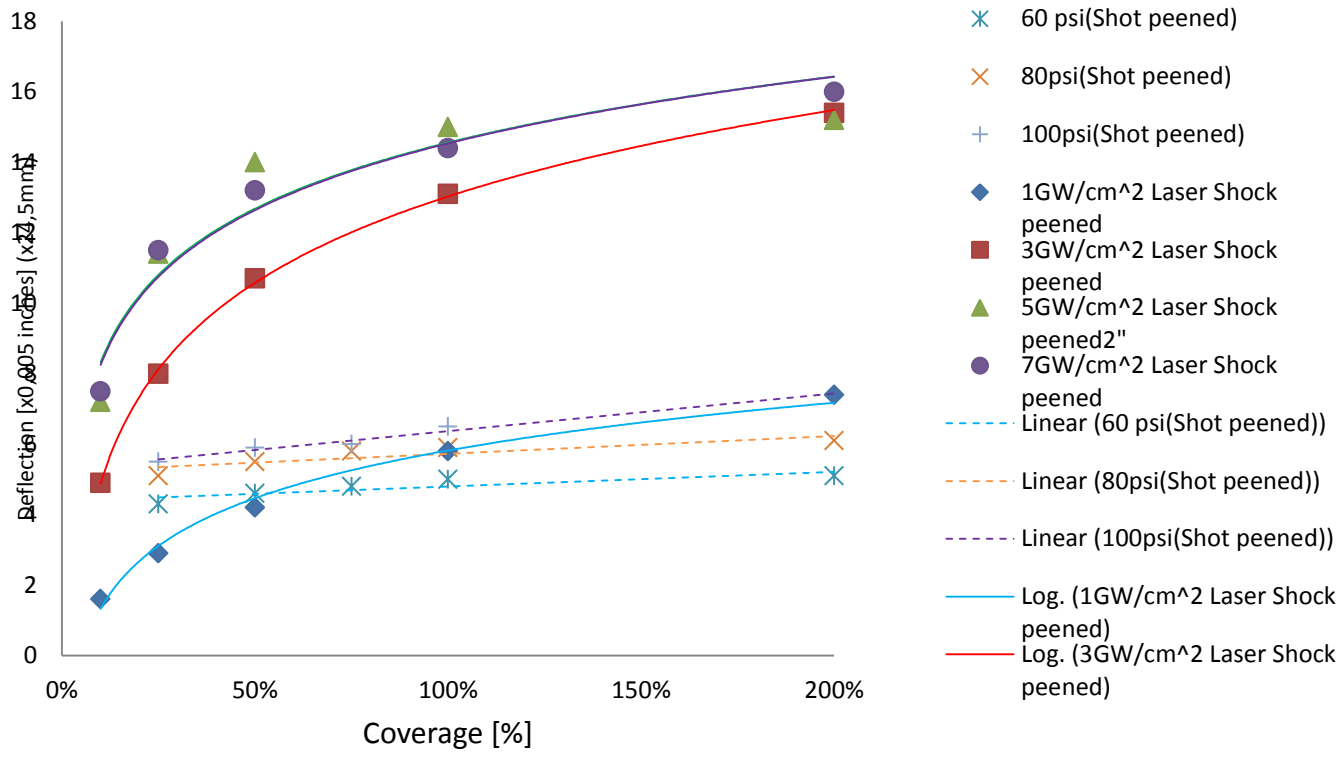

Figure 4.2: Shot Peened and Laser Shock Peened deflection data of AA6056-T4 test pieces against surface coverage

In Figure , the shot peening and laser shot peening results for AA6056-T4 Aluminum alloy were plotted from the data captured in Tables 4.1-4.8. From the figure it can be seen that laser shot peening had a significantly higher deflection/arching in comparison to the shot peening results. The 1 GW/cm^2 (Laser shot peening) data is seen to correspond to data points across the various pressure changes for the shot peening results. At saturation the 100psi (≈0.689 MPa) and 1GW/cm2 data points are seen in close approximation to each other. The Laser shock peening results is also seen to induce deflections that are between 2.12 to 3 times more than that of the shot peening results. This could indicate a higher force or energy is transferred into the test pieces during the laser shock peening process. Laser shock peening deflection is also seen to follow a logarithmic scale of deflection as coverage increases. The 5 GW/cm^2 and 7GW/cm^2 trend lines are seen to overlap thus indicating a form of saturation, this would require further research to evaluate this outcome.

4.2 Surface Roughness Data and Results

Surface roughness data was obtained from the laser shock peened and shot peened test pieces. These were the Almen strip sized test pieces of AA6056-T4. Five AA6056-T4 pieces were shot peened and five laser shot peened, and five Almen "A" test strips were shot peened. The results from the surface roughness test can be seen in Table to Table , and the images of the AA6056-T4 test pieces after their respective peening process can be seen in Figures 4.3- Figure 4.10. All surface roughness tests were performed along the stepping direction over a sample area of 50mm.

In Table , Table and Table , the "Ra" and "Rz" values for the shot peening results both show increase in surface roughness as the pressure from the blast nozzle increases and as coverage increases. AA6056-T4 is seen to have a much higher surface roughness in comparison to the Almen "A" test strip. Thus indicating, a much rougher surface finish as the nozzle blast pressure and coverage increases. The "Ra" values are seen to range from 8.34 to 13.39 mμ for AA6056-T4 test pieces and 3.694 to 5.989 mμ for the Almen "A" test pieces.

In Table to Table 4.15, the "Ra" and "Rz" values show a decrease in surface roughness for the laser intensity of 1 GW/cm^2 and 3 GW/cm^2, and the 5 GW/cm^2 and 7 GW/cm^2 show an increase in surface roughness as the intensity goes higher. All these values are within a close range to each other i.e. the "Ra" values are between 1.76 mμ and 2.76 mμ.

Table 4.9: Surface Roughness Data of Shot Peening 60psi (≈0.413 MPa)

	Pressure: 60psi (≈0.413 MPa)		Surface Roughness			
			3.2mm 6056		Almen Strip A	
Passes	Time [s]	Coverage	Ra	Rz	Ra	Rz
2	2.5	25%	8.34	40.6	3.694	18.48
4	5	50%	9.66	51.9	3.508	20.22
6	7.5	75%	11.02	55.5	4.491	22.71
8	10	100%	10.51	51.8	4.261	20.78
16	20	200%	11.55	56.6	4.25	20.89

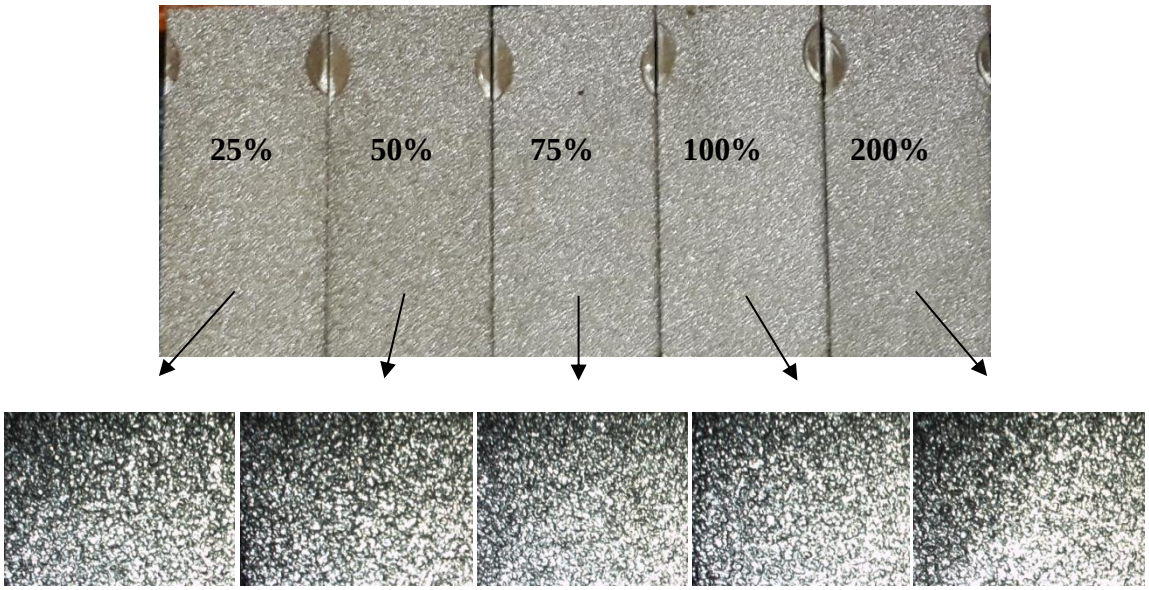

Figure 22: AA6056-T4 Shot peened surface Area at 60psi (≈0.413 MPa), and magnified area.

Table 4.10: Surface Roughness Data of Shot Peening 80 psi (≈0.551 MPa)

	Pressure: 80 psi (≈0.551 MPa)		Surface Roughness			
			3.2mm 6056		Almen Strip A	
Passes	Time [s]	Coverage	Ra	Rz	Ra	Rz
2	2.5	25%	13.12	62	4.537	23.45
4	5	50%	12.36	64.6	5.072	27.34
6	7.5	75%	12.34	58.4	5.47	28.88
8	10	100%	14.73	66.8	5.721	24.76
16	20	200%	12.37	54.5	4.956	24.47

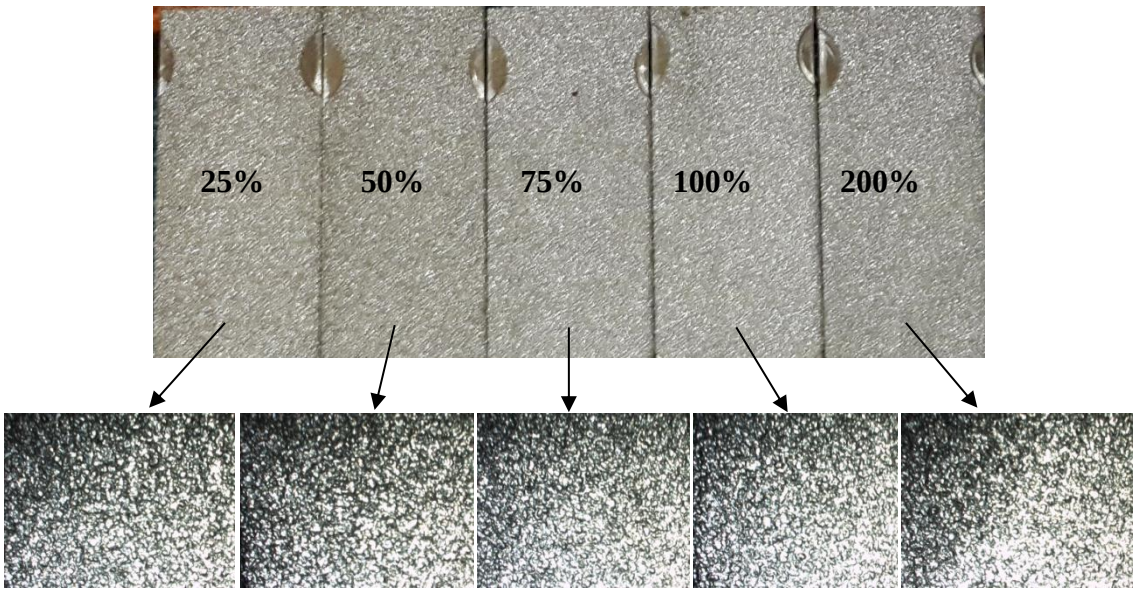

Figure 4.4: AA6056-T4 Shot peened surface Area at 80 psi (≈0.551 MPa), and magnified area.

Table 4.11: Surface Roughness Data of Shot Peening 100psi (≈0.689 MPa)

	Pressure: 100psi (≈0.689 MPa)		Surface Roughness			
			3.2mm 6056		Almen Strip A	
Passes	Time [s]	Coverage	Ra	Rz	Ra	Rz
2	2.5	25%	12.35	60	5.637	28.19
4	5	50%	11.75	55.9	5.734	27.52
6	7.5	75%	13.5	62.7	5.312	28.56
8	10	100%	13.97	67.4	5.592	27.02
16	20	200%	13.39	65.8	5.989	31.9

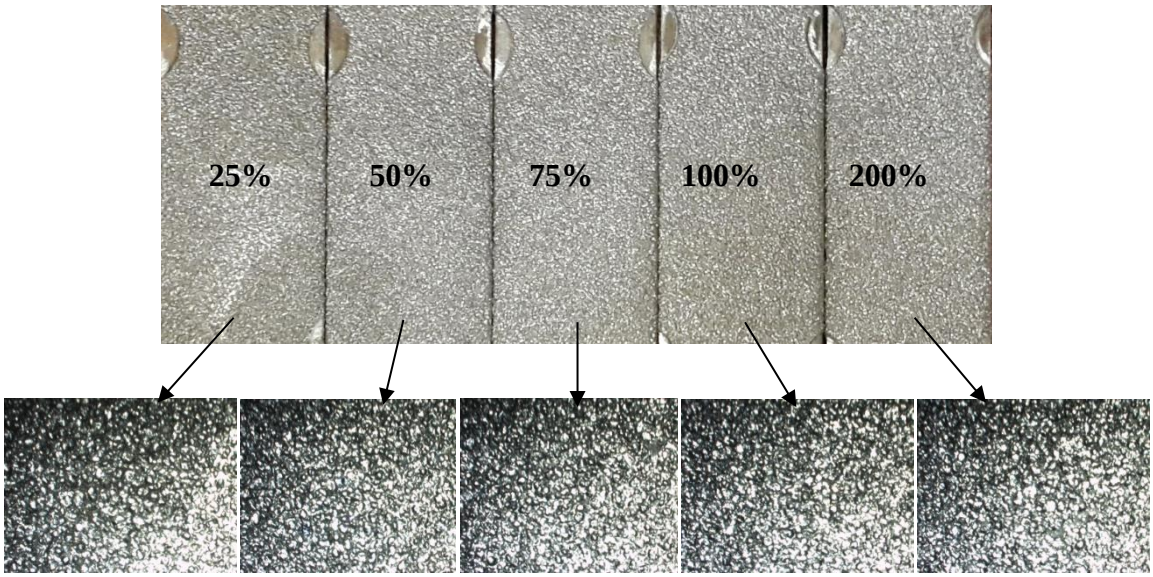

Figure 4.5:AA6056-T4 Shot peened surface Area at 100psi (≈0.689 MPa), and magnified area.

Table 4.12: Surface Roughness Data of Laser Shock Peening 1 GW/cm^2

Calculated power intensity (GW/cm^2)	Intended [GW/cm^2]	[Spots/cm^2]	Distance of test piece to lens [mm]	Spot size	Surface Roughness	
					Ra[mμ]	Rz[mμ]
0.81	1	100	303	1.5	2.35	16.61
0.81	1	250	303	1.5	2.14	13.60
0.81	1	500	303	1.5	2.15	13.21
0.81	1	1000	303	1.5	1.73	12.33
0.81	1	2000	303	1.5	1.75	12.13

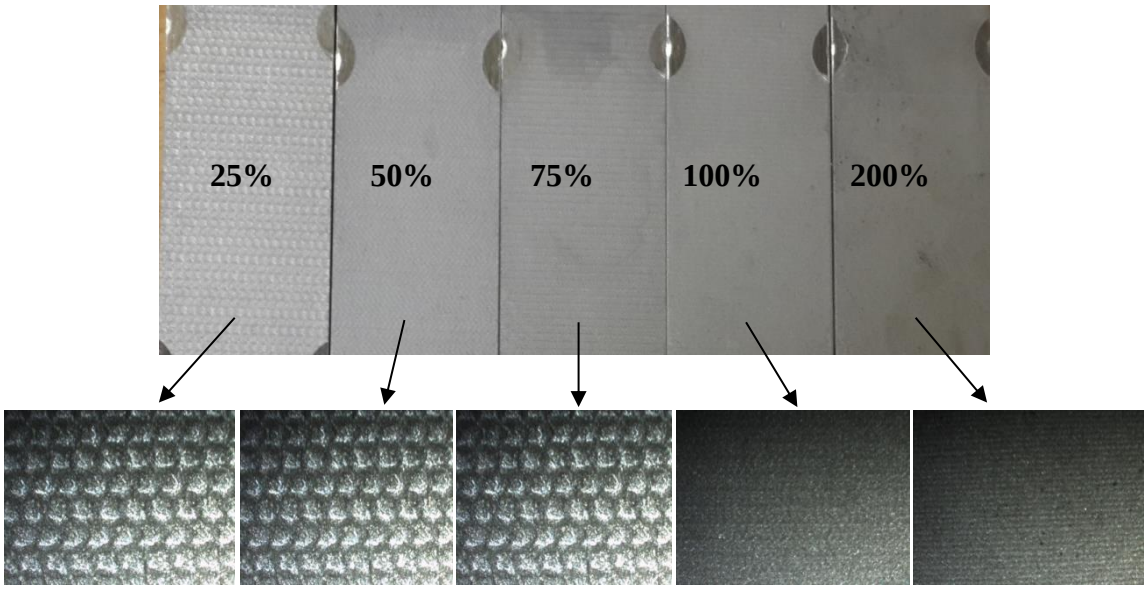

Figure 4.6: AA6056-T4 Laser Shock peened surface area at 1 GW/cm2, and magnified area

Table 4.13: Surface Roughness Data of Laser Shock Peening 3 GW/cm^2

Calculated power intensity (GW/cm^2)	Intended [GW/cm^2]	[Spots/cm^2]	Distance of test piece to lens [mm]	Spot size	Surface Roughness	
					Ra[mμ]	Rz[mμ]
2.77	3	100	547	1.5	1.81	14.13
2.77	3	250	547	1.5	2.82	13.26
2.77	3	500	547	1.5	1.66	11.62
2.77	3	1000	547	1.5	2.21	12.42
2.77	3	2000	547	1.5	1.97	12.43

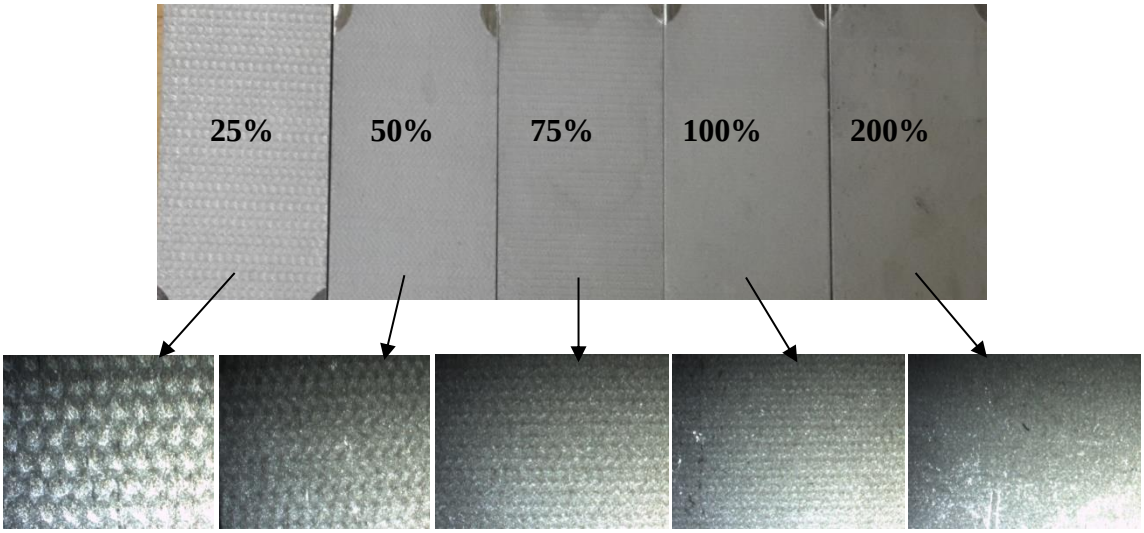

Figure 4.7: AA6056-T4 Laser Shock peened surface area at 3 GW/cm2, and magnified area

Table 4.14: Surface Roughness Data of Laser Shock Peening 5 GW/cm^2

Calculated power intensity (GW/cm^2)	Intended [GW/cm^2]	[Spots/cm^2]	Distance of test piece to lens [mm]	Spot size	Surface Roughness	
					Ra[mμ]	Rz[mμ]
4.60	5	100	534	1.5	2.16	14.99
4.60	5	250	534	1.5	2.00	12.75
4.60	5	500	534	1.5	2.07	13.46
4.60	5	1000	534	1.5	2.72	15.97
4.60	5	2000	534	1.5	2.46	15.28

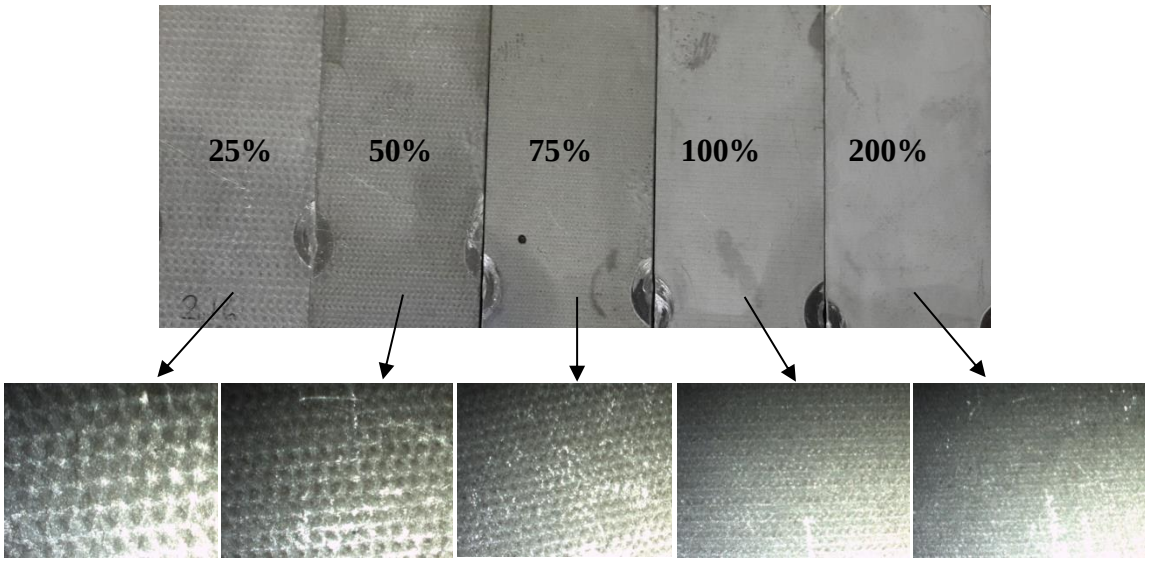

Figure 4.8: AA6056-T4 Laser Shock peened surface area at 5 GW/cm2, and magnified area

Table 4.15: Surface Roughness Data of Laser Shock Peening 7 GW/cm^2

Calculated power intensity (GW/cm^2)	Intended [GW/cm^2]	[Spots/cm^2]	Distance of test piece to lens [mm]	Spot size	Surface Roughness	
					Ra[mμ]	Rz[mμ]
6.29	7	100	524	1.5	1.97	12.64
6.29	7	250	524	1.5	2.10	13.19
6.29	7	500	524	1.5	2.07	12.69
6.29	7	1000	524	1.5	2.27	12.79
6.29	7	2000	524	1.5	2.34	14.33

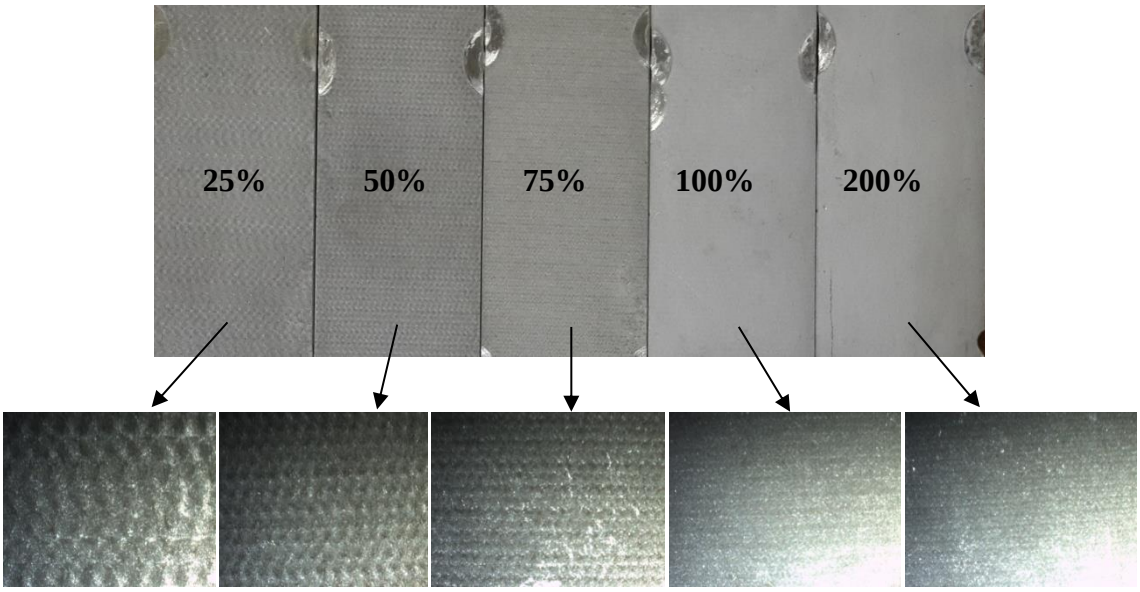

Figure 4.9:AA6056-T4 Laser Shock peened surface area at 7 GW/cm2, and magnified area

Surface roughness curves comparing the shot peening data for the AA6056-T4 test pieces and the Almen "A" test pieces, using the data captures in Tables 4.9-4.11 can be seen in Figure .

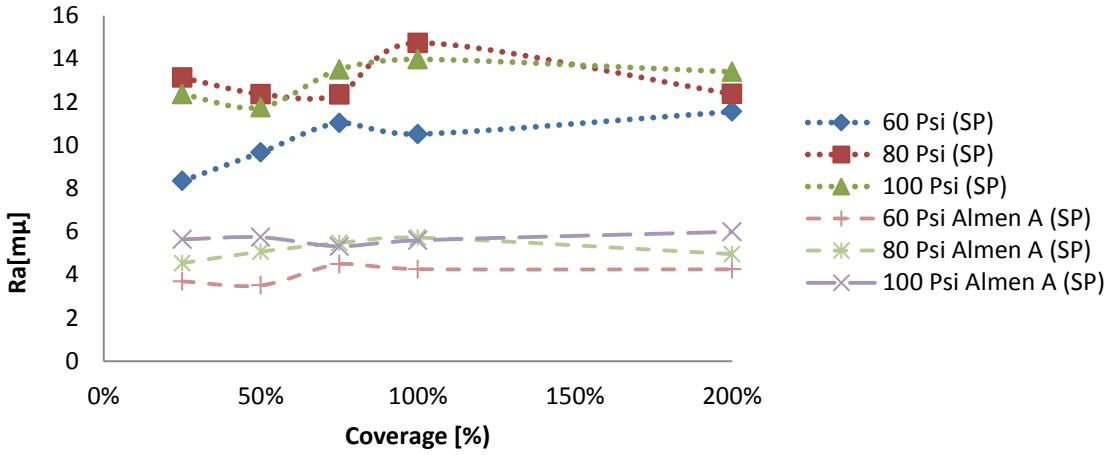

Figure 4.10: Surface Roughness (Ra) against surface coverage

From Figure for surface roughness, the AA6056-T4 aluminum alloy is seen to have a significantly higher surface roughness value 2 to 2.5 times higher in comparison to the Almen "A" test pieces. This indicates that the AA6056-T4 material is a softer alloys in comparison to the Almen "A" test pieces which was expected, as the Almen "A" test piece is made of spring steel. From the graph there are some fluctuations in the results of all the test pieces in the 50% to 100% coverage region. Further investigation might be required to understand the reasons behind this (beyond the scope of this project). From the data is can be stated that the AA6056-T4 aluminum Alloy with shot peening results at 200% coverage for the nozzle blast pressure of 100psi (≈0.689 MPa), has the highest surface roughness and the laser shot peening result at 7 GW/cm^2 at 200% coverage has a lower surface roughness (i.e. smoothest finish) in comparison. The laser shock peening results are 2.3("Ra") (and 2.56 for "Rz") times lower than those obtained with the shot peening process (when comparing the maximum constraints i.e. at 200%). From Figure 223 to Figure , the images show surface roughness of the laser shot peened specimens

became smoother as the coverage increased, and the shot peened results are seen to become rougher.

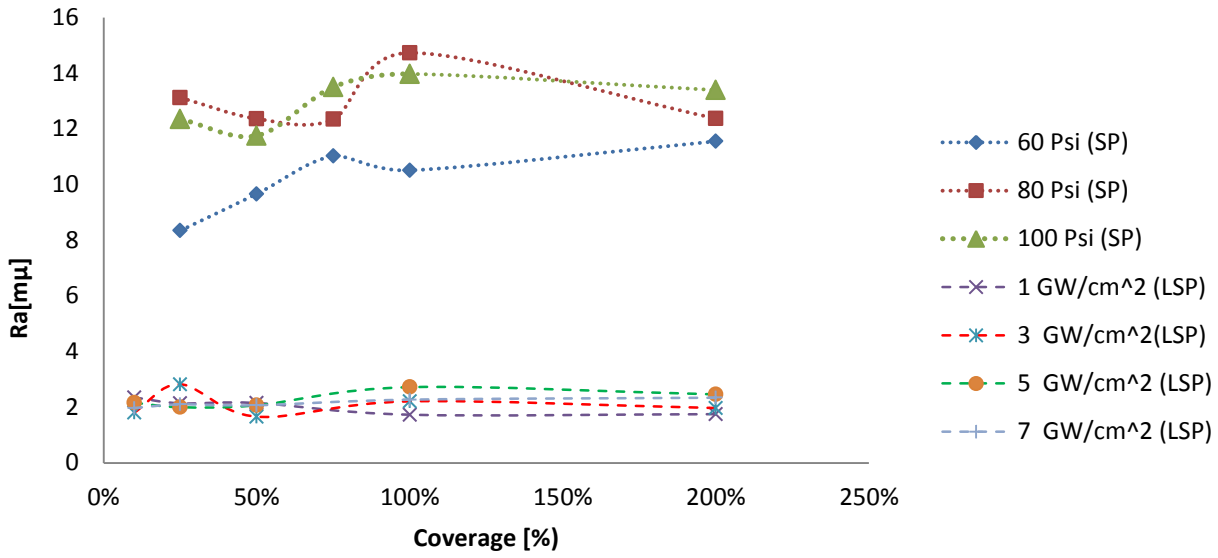

Figure 4.11: Laser Shot Peening and Shot Peening roughness results of AA6056-T4 against Surface coverage.

In Figure , the surface finish results for shot peening and laser shock peening of AA6056-T4 Aluminum alloy were plotted, from the data captured in Table to Table . In the figure, laser shot peening results are seen to be in close proximity of each other, thus creating similar surface finishes. The shot peening results are seen to fluctuate and give a higher surface roughness value in comparison to laser shock peening. The results of the laser shot peening process is seen to reach a steady state curve the 100% mark. The results of shot peening is seen to be around 5.7 times higher than the surface roughness of laser shot peening. The surface areas of the shot peening test piece can visually be seen to have a rougher surface and can be felt using the finger nail test (i.e. dragging the back of one of the finger nails across the surface of the test piece).

4.3 Microhardness Testing Data and Results

Vickers Microhardness data obtained from using the test pieces of AA6056-T4 aluminum alloy after shot peening and laser shock peening had been done, and can be seen in Table to Table . The initial state of the sample can be seen in Table . It can be seen that the Vickers Microhardness readings range from 93.8 HV to 105.3HV for this state of the material.

Table 4.16: Initial state of AA6056-T4 Aluminium Alloy [49]

Distance from peened surface [µm]	D1 [µm]	D2[µm]	HV
200	74.71	74.21	100.3
400	72.72	74.25	103
600	77.38	73.74	97.4
800	72.72	76.94	99.4
1000	76.68	74.85	96.9
1200	73.8	76.48	98.5
1400	75.78	72.96	100.6
1600	73.19	75.51	100.6
1800	77.74	74.94	95.5
2000	77.03	77.03	93.8
2200	76.02	76.32	95.9
2400	74.71	74.21	100.3
2600	75.74	76.46	96.1
2800	73.07	73.57	103.5
3000	74.92	75.66	98.1

In Table , the Vickers microhardness data for the shot peening results at 60psi (≈0.413 MPa), can be seen. It can be seen that the Vickers Microhardness readings range from 108.2 HV to 130.9 HV.

Table 4.17: Microhardness Testing Data of Shot Peening 60psi (≈0.413 MPa)

Distance from peened surface [µm]	D1 [µm]	D2[µm]	HV
163.48	68.09	66.24	123.3
311.95	70.56	71.62	110.1
448.63	7058	70.58	112.2
597.6	70.96	72.43	108.2
760.48	73.06	69.54	109.3
898.36	69.94	71.14	111.8
1061.12	70.22	70.19	112.9
1224.59	66.9	69.85	119
1398.39	69.2	69.2	113.7
1550.41	68.02	72.5	112.7
1712.84	67.52	69.14	119.2
1869.32	67.28	69.39	119.1
2039.59	68.94	68.47	117.9
2167.71	68.93	70.09	115.1
2331.19	71.97	68.25	113.2
2496.48	70.02	72.75	109.2
2638.82	69.44	69.44	115.6
2812.62	69.59	71.43	111.9
2952.32	65.92	64.44	130.9

In Table , the Vickers Microhardness data for the shot peening results at 80 psi (≈0.551 MPa), can be seen. It can be seen that the Vickers Microhardness readings range from 98.2 HV to 130.2 HV.

Table 4.18: Microhardness Testing Data of Shot Peening 80 psi (≈0.551 MPa)

Distance from peened surface [µm]	D1 [µm]	D2[µm]	HV
167.02	65.09	65.64	130.2
317.95	68.99	68.99	115.3
474.72	68.62	66.18	122.5
624.27	70.08	67.08	118.3
777.15	70.24	67.47	117.3
935.93	71.71	67.83	114.3
1090.1	70.68	68.73	114.5
1242.23	70.46	70.46	110.8
1394.75	72.84	70.81	106.4
1551.1	72.41	70.25	109.3
1704.17	73.63	72.04	104.9
1860.14	79.96	71.37	111.4
2009.1	73.75	71.1	106.1
2163.49	69.88	71.07	112
2315.69	72.61	70.88	108.1
2472.72	67.17	69.41	119.3
2615.48	74.26	75.8	98.8
2763.59	75.03	75.47	98.2
2910.18	73.91	74.68	100.8
3061.97	73.11	74.55	102.1

In Table , the Vickers Microhardness data for the shot peening results at 100psi (≈0.689 MPa), can be seen. It can be seen that the Vickers Microhardness readings range from 97 HV to 130.8 HV.

Table 4.19: Microhardness Testing Data of Shot Peening 100psi (≈0.689 MPa)

Distance from peened surface [µm]	D1 [µm]	D2[µm]	HV
168.41	65.18	65.24	130.8
374.51	69.28	72.1	111.3
644.47	74.88	74.88	101.1
846.07	72.93	72.98	104.5
1051.53	72.5	74.69	102.7
1257.33	73.41	76.61	98.9
1463.29	73.46	75.81	99.9
1666.74	74.44	74.91	99.8
1872.04	74.01	73.9	101.7
2083.25	72.36	73.63	104.4
2292.1	75.15	76.29	97
2501.35	72.71	74.91	102.1
2711.84	73.88	74.56	101
2925.9	74.5	73.7	101.3

In Table , the Vickers micro hardness data for the laser shock peening results at 1 GW/cm^2, can be seen. It can be seen that the Vickers Microhardness readings range from 105.7 HV to 119.5 HV.

Table 4.20: Microhardness Testing Data of Laser Shock Peening 1 GW/cm^2

Distance from peened surface [µm]	D1 [µm]	D2[µm]	HV
86.42	68.42	69.75	116.6
204.83	68.88	67.6	119.5
357.55	70.91	68.35	114.7
502.74	68.71	70.52	114.8
652.27	69.9	70.01	113.7
804.24	70.06	69.62	114.1
953.19	70.18	69.63	113.8
1105.3	71.43	71.43	107.5
1261.06	72.63	71.15	107.6
1414.87	72.69	71.22	107.4
1565.52	72.91	73.54	103.8
1724.54	72.36	71.89	106.9
1886.44	69.41	71.47	112.1
2042.79	71.61	73.29	106
2202.77	71.15	73.3	106.6
2363.97	71.05	71.53	109.5
2520.56	71.57	73.5	105.7
2687.05	72.63	71.09	107.7
2845.14	71.08	67.79	115.4
3005.11	70.63	70.81	111.2

In Table , the Vickers micro hardness data for the laser shock peening results at 3 GW/cm^2, can be seen. It can be seen that the Vickers Microhardness readings range from 105.3 HV to 127 HV.

Table 4.21: Microhardness Testing Data of Laser Shock Peening 3 GW/cm^2

Distance from peened surface [µm]	D1 [µm]	D2[µm]	HV
72	67.65	67.65	121.559
216.4	66.87	65.9	126.2
365.11	66.22	66.17	127
513.56	70.64	67.1	117.3
659.03	68.24	68.24	114.7
808.91	69.48	69.54	115.1
958.94	70.52	69.16	114.1
1108.23	70.49	71.2	110.8
1258.96	68.1	69.84	117
1409.93	71.4	72.13	108
1560.4	74.52	70.85	105.3
1711.03	72.57	71.04	107.9
1863.92	72.5	71.92	106.7
2015.48	69.81	70.31	113.3
2170.64	70.86	71.19	110.3
2325.24	71.34	71.11	109.7
2477.48	72.57	70.77	108.3
2632.25	73.01	71.27	106.9
2785.62	71.82	70.12	110.5
2940.07	72.48	69.43	110.5

In Table , the Vickers Microhardness data for the laser shock peening results at 5 GW/cm^2, can be seen. It can be seen that the Vickers Microhardness readings range from 97.4 HV to 125.8 HV.

Table 4.22: Microhardness Testing Data of Laser Shock Peening 5 GW/cm^2

Distance from peened surface [µm]	D1 [µm]	D2[µm]	HV
134.94	66.19	66.79	125.8
322.4	67.73	65.78	124.8
502.04	68.76	68.06	118.9
684.3	67.63	68.85	119.5
866.46	66.08	67.9	124
1032.1	71.75	72.4	107.1
1216.66	70.38	70.75	117
1391.91	69.88	72.21	110.2
1571.07	73.25	75.11	101.1
1744.03	72.65	72.54	105.6
1919.09	72.81	71.55	106.8
2112.07	72.19	71.88	107.2
2296.78	75.21	71.75	103
2487.22	71.75	71.55	108.1
2680.42	74.3	73.48	101.9
2849.85	73.49	71.86	105.3
3029.19	73.1	71.55	106.4

In Table , the Vickers Microhardness data for the laser shock peening results at 7 GW/cm^2, can be seen. It can be seen that the Vickers Microhardness readings range from 100.4 HV to 124.7 HV.

Table 4.23: Microhardness Testing Data of Laser Shock Peening 7 GW/cm^2

Distance from peened surface [µm]	D1 [µm]	D2[µm]	HV
143.41	67.99	65.58	124.7
326.81	66.78	66.64	125
485.52	68.31	67.21	121.2
645.25	70.14	67.05	118.2
804.84	68.83	68.14	118.6
970.08	69.14	70.55	114
1123.12	68.81	71	113.8
1290.71	69.69	71.41	111.8
1459.42	71.03	71.01	110.3
1620.36	73.38	71.29	106.3
1792.87	72.98	73.59	103.6
1974.03	72.16	71.54	107.8
2140.92	75.31	72.34	102.1
2304.87	75.73	73.11	100.4
2476.11	74.93	72.2	102.8
2696.11	72.34	69.74	110.2
2909.17	70.65	69.51	113.3

In Figure , data captured in Table 4.16- Table 4.19 for microhardness can be seen for the shot peening results at saturation (i.e. 100% coverage).. The microhardness was tested from the top surface (the peened area) to 3000µm (3mm) into the material. In the figure, the unpeened line is the initial state of the material before any testing was done on it, and this is used as the point of reference.

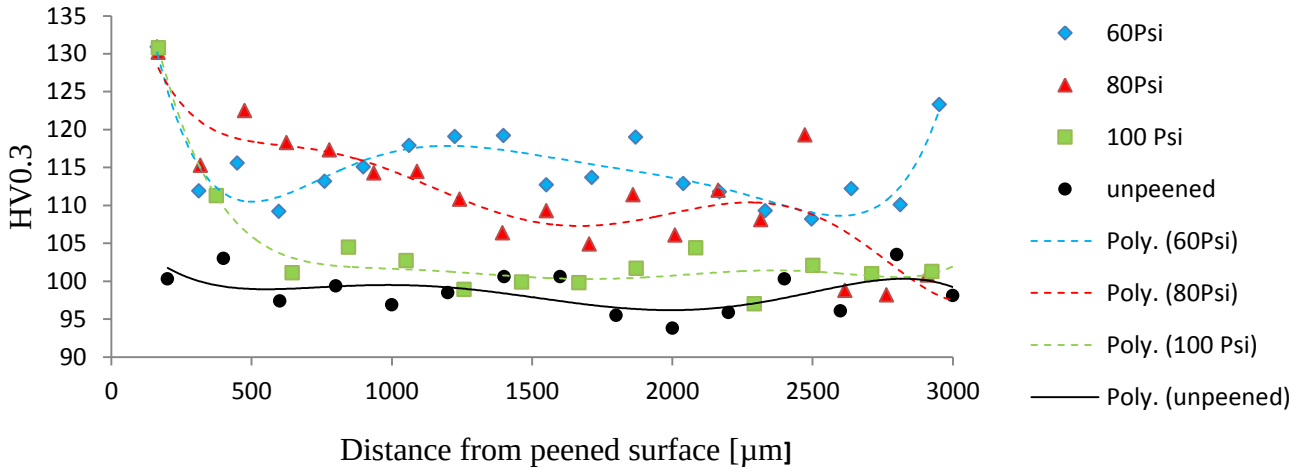

Figure 4.12: Vickers Microhardness test measurements for shot peening test pieces against distance from peened surface

From Figure , the 60psi (≈0.413 MPa) test piece is seen to have a higher Vickers Microhardness value which is seen to propagate through the thickness of the material. The 80 psi (≈0.551 MPa) test piece is also seen to propagate through the material up to around 2600µm into the thickness of the material. The 100psi (≈0.689 MPa) test piece is seen to have very little propagation into the material as it is seen to follow the unpeened line from around 640µm. Thus from these results it was seen that, the lower the pressure, the higher the Vickers Microhardness propagation through the material thickness. From the linear trend lines, both the 80Psi and 100Psi hardness values are seen to propagate towards the unpeened line, whereas the 60Psi trend line is seen to seen to propagate straight through the material. In comparison to higher pressures, it can be stated that this would be an unlikely event and leads to the conclusion that these results at 60Psi would need to be further investigated to validate this result.

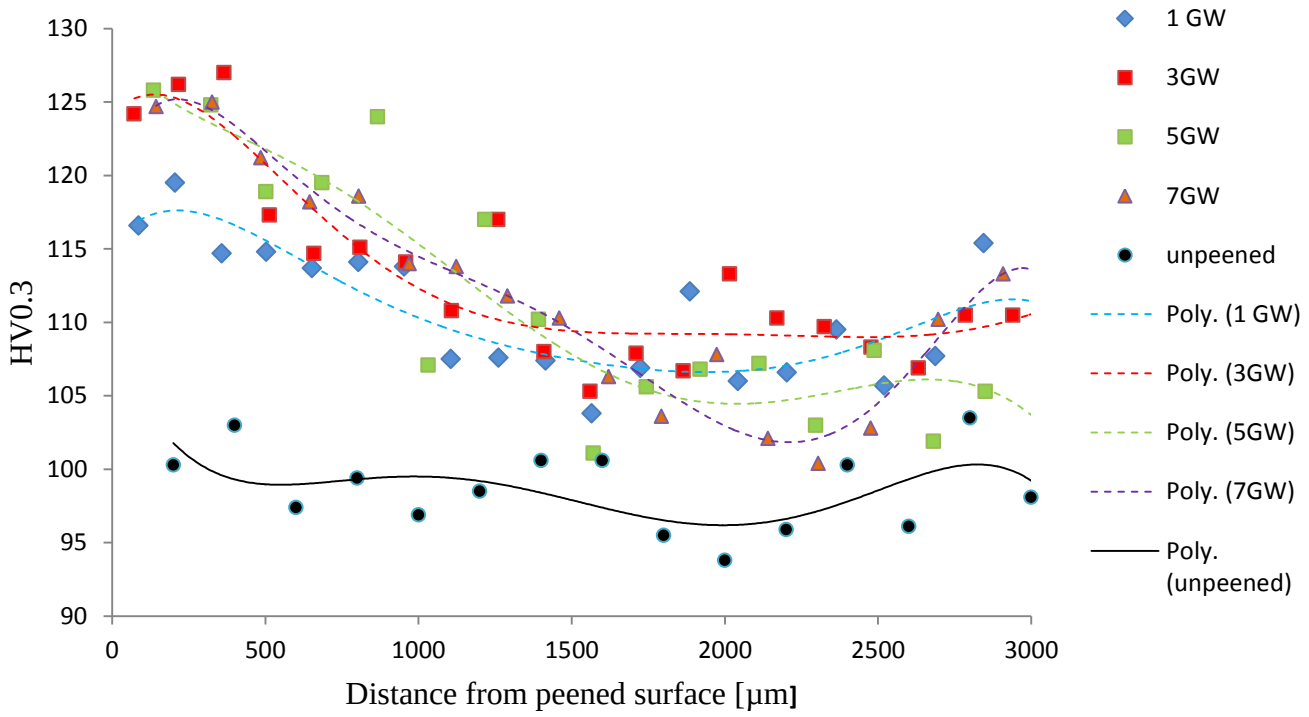

Figure 4.13: Vickers Microhardness test measurements for Laser Shock peening test pieces against distance from peened surface

In Figure , the Vickers Microhardness test results were plotted for the laser shock peening test results, obtained from the data captured in Tables 4.16 and Tables 4.20-4.23, for laser intensities at 200% coverage. From the figure, it can be seen that the Vickers Microhardness values are within close proximity between all the laser intensities. They are also seen to propagate through the thickness of the material and within a similar pattern to each other. The 7GW/cm2 result is seen to follow the unpeened curve at around 2300µm, and there after increase in hardness. All trend lines show a decrease in hardness as results go deeper into the material. The lower intensities are seen to create a higher hardness value in comparison to the higher intensities. Further investigation into this could give a better understanding to this outcome.

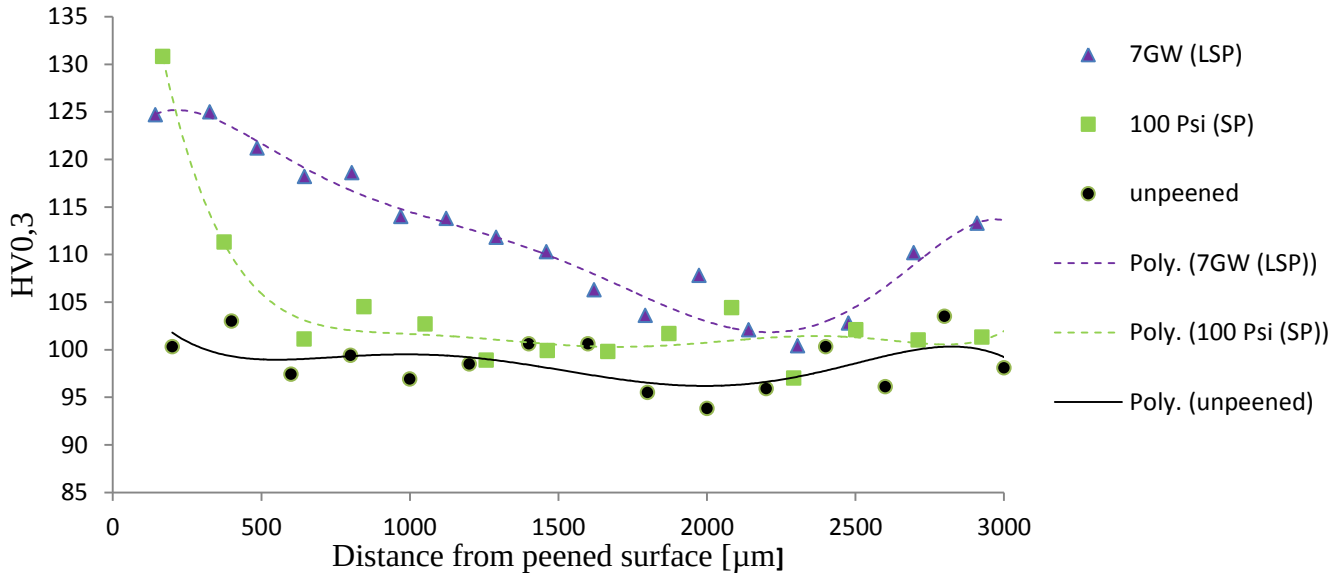

Figure 4.14: Vickers Microhardness test measurements for Laser Shock peening and Shot peening test piece against distance from peened surface

In Figure the highest laser intensity and highest shot peening pressure (nozzle blasting pressure) was plotted for Vickers Microhardness test results along the thickness of the material, from the data obtained from Tables 4.16, 4.20 and 4.23. From the figure, it can be seen that the laser shot peening results are much higher than that of shot peening and it is seen to propagate much further into the material. From this result we can see that laser shock peening penetrates deeper into the material by up to 3.8 times. This is seen to correspond to expected behavior between the two processes. This behavior was seen within the literature review for other materials which underwent similar testing (Figure 2.21 and Figure 2.22).

4.4 Residual Stress Data and Results

Successful residual testing data, from hole drill testing can be seen in , and this calculation method can be seen in the ASTM E837-08 for non-uniform stress distribution. ASTM E837-08 is the regulations for hole drill testing and can be seen in Appendix C.

Table to Table . Only one set of data from shot peening results captured, showed viable results and four sets of results captured for the laser shock peening test. The β Angle is the angle between the maximum and minimum stress. The maximum and minimum stresses are the principle stresses calculated via the residual stress program, this is the angle where the shear stress becomes zero [51]., and this calculation method can be seen in the ASTM E837-08 for non-uniform stress distribution. ASTM E837-08 is the regulations for hole drill testing and can be seen in Appendix C.

Table 4.24: Residual Stress Data for Shot peening, 60Psi (0.413 MPa) at 200% coverage

Depth [mm]	Strain (1) [1E 10^{-6}]	Strain (2) [1E 10^{-6}]	Strain (3) [1E 10^{-6}]	β Angle [°]	σ_{min} [N/mm^2]	σ_{max} [N/mm^2]
0,012	18,319	54,096	57,346	-19,904	-380,89	-133,929
0,037	70,805	111,289	119,579	29,492	-337,037	-307,168
0,062	128,357	167,643	185,42	41,029	-320,581	-256,394
0,087	184,144	221,685	251,324	37,059	-276,638	-210,238
0,112	241,205	276,992	318,661	35,398	-261,878	-203,785
0,137	302,307	335,099	387,366	39,74	-268,37	-220,108
0,162	366,973	394,288	454,875	51,006	-279,957	-234,666
0,187	432,192	451,099	517,487	62,346	-281,807	-224,03
0,212	494,368	502,405	572,216	68,444	-257,372	-190,022
0,237	551,023	546,85	618,034	72,219	-232,625	-158,412
0,262	601,553	585,194	656,098	75,451	-192,328	-119,232
0,287	646,973	619,652	689,048	79,03	-176,823	-111,413
0,312	688,983	652,698	719,803	83,632	-184,736	-130,922
0,337	728,868	685,862	750,362	89,985	-214,962	-174,014
0,362	766,708	719,013	781,059	-81,773	-254,265	-225,021
0,387	801,215	750,375	810,528	-75,349	-260,506	-240,194
0,412	830,229	777,246	836,349	-68,366	-215,94	-205,833

0,437	851,683	797,148	856,133	-21,705	-110,576	-108,661
0,462	864,646	808,953	868,638	13,607	69,349	79,951
0,487	870,005	813,558	874,477	12,662	246,306	264,072

Table 4.25: Residual Stress data for Laser Shock Peening, 1GW/cm^2 at 75% coverage

Depth [mm]	Strain (1) [1E 10^{-6}]	Strain (2) [1E 10^{-6}]	Strain (3) [1E 10^{-6}]	β Angle [°]	σ_{min} [N/mm^2]	σ_{max} [N/mm^2]
0,013	-15,655	-14,441	-10,84	13,186	83,496	111,804
0,038	-11,859	-9,105	-5,757	-38,529	-55,234	-44,205
0,062	6,566	9,513	12,399	-73,567	-135,098	-129,198
0,088	31,43	32,922	35,326	78,571	-152,459	-140,068
0,113	56,739	55,737	57,48	75,962	-133,954	-116,829
0,138	79,53	75,914	77,028	74,935	-104,437	-88,779
0,163	98,863	93,294	94,198	69,715	-77,238	-67,9
0,187	114,738	108,287	109,647	35,273	-61,475	-57,729
0,213	127,449	121,208	123,678	4,819	-51,566	-41,858
0,237	137,367	132,168	136,189	-0,148	-46,062	-30,987
0,263	144,938	141,234	146,966	-1,927	-34,558	-17,679
0,288	150,701	148,593	155,981	-2,717	-24,142	-7,761
0,312	155,242	154,589	163,483	-2,352	-17,666	-3,328
0,338	159,07	159,638	169,895	-0,622	-16,192	-4,345
0,363	162,499	164,083	175,608	1,992	-19,367	-8,803
0,388	165,6	168,098	180,819	2,794	-23,902	-13,559
0,413	168,258	171,68	185,509	0,61	-24,364	-13,679
0,437	170,316	174,756	189,558	-4,292	-21,013	-9,256
0,463	171,74	177,308	192,934	-9,444	-9,041	3,858
0,488	172,694	179,452	195,812	-11,26	-1,428	12,787

Table 4.26: Residual stress data for Laser Shock Peening, 3GW/cm^2 at 75% coverage

Depth [mm]	Strain (1) [1E 10^{-6}]	Strain (2) [1E 10^{-6}]	Strain (3) [1E 10^{-6}]	β Angle [°]	σ_{min} [N/mm^2]	σ_{max} [N/mm^2]
0,013	32,905	11,72	-4,738	86,421	-222,559	-4,276
0,038	97,538	44,501	1,828	87,324	-391,317	-110,743
0,062	180,688	91,253	16,082	88,724	-442,622	-156,387
0,088	266,18	141,272	33,784	89,083	-396,359	-154,43
0,113	345,908	188,591	51,928	88,791	-321,578	-133,877
0,138	418,678	232,383	68,868	89,535	-262,367	-111,269
0,163	486,241	274,36	84,025	-87,023	-232,384	-96,204
0,187	550,272	316,134	97,523	-82,137	-228,387	-89,841
0,213	611,282	357,895	109,834	-78,261	-228,617	-85,447
0,237	668,887	398,476	121,465	-76,949	-237,504	-94,687
0,263	722,534	436,252	132,711	-78,167	-223,092	-95,442
0,288	771,953	470,092	143,537	-82,447	-217,075	-103,803
0,312	817,153	499,836	153,63	-87,402	-212,046	-106,961
0,338	858,17	526,137	162,597	-89,487	-205,871	-108,041
0,363	894,88	549,884	170,209	-86,696	-201,135	-105,882
0,388	927,103	571,631	176,557	-80,446	-186,35	-95,257
0,413	954,893	591,373	181,999	-74,652	-169,569	-83,506
0,437	978,765	608,781	186,921	-72,621	-162,186	-87,684
0,463	999,597	623,682	191,439	-77,234	-150,296	-90,549
0,488	1018,222	636,403	195,303	-84,565	-163,949	-104,21

Table 4.27: Residual stress data for Laser Shock Peening, 5GW/cm^2 at 75% coverage

Depth [mm]	Strain (1) [1E 10^{-6}]	Strain (2) [1E 10^{-6}]	Strain (3) [1E 10^{-6}]	β Angle [°]	σ_{min} [N/mm^2]	σ_{max} [N/mm^2]
0,013	10,766	6,08	-2,775	-81,445	-71,495	8,409
0,038	40,135	22,58	-1,633	-88,01	-177,269	-39,747
0,062	86,749	53,687	6,593	-84,356	-259,322	-92,206
0,088	149,004	98,96	20,48	-80,882	-324,886	-125,003
0,113	223,236	154,264	37,177	-79,658	-366,53	-138,564
0,138	304,888	214,421	54,539	-80,301	-385,386	-141,87
0,163	389,706	275,022	71,685	-82,249	-388,997	-145,025
0,187	474,316	333,162	88,574	-85,036	-384,703	-151,035
0,213	556,272	387,401	105,309	-87,984	-369,053	-154,34
0,237	633,855	437,318	121,699	89,707	-362,553	-163,929
0,263	705,874	483,005	137,208	88,908	-339,192	-156,87
0,288	771,585	524,711	151,196	89,692	-317,813	-148,701
0,312	830,702	562,666	163,212	-88,171	-295,703	-136,321
0,338	883,431	597,075	173,16	-85,54	-273,023	-125,546
0,363	930,406	628,165	181,269	-83,424	-263,025	-120,747
0,388	972,504	656,21	187,937	-82,531	-257,663	-118,89
0,413	1010,542	681,486	193,559	-82,653	-258,837	-121,283
0,437	1044,981	704,185	198,448	-83,487	-274,538	-139,378
0,463	1075,756	724,326	202,816	-84,278	-267,153	-142,241
0,488	1102,365	741,776	206,775	-84,483	-260,202	-152,747

In Table 4.28: Residual stress data for Laser Shock Peening, 5GW/cm2 at 75% coverage (2nd test) the captured results for residual stress of laser shock peening at 5GW/cm^2 can

be seen, this is a second test done to test repeatability, but in this test the strain gauge was orientated 90 degrees to the previous test setup.

Table 4.28: Residual stress data for Laser Shock Peening, 5GW/cm2 at 75% coverage (2nd test)

Depth [mm]	Strain (1) [1E 10^{-6}]	Strain (2) [1E 10^{-6}]	Strain (3) [1E 10^{-6}]	β Angle [°]	σ_{min} [N/mm^2]	σ_{max} [N/mm^2]
0,013	-1,016	5,454	13,932	3,827	-100,377	-9,071
0,038	6,707	30,798	50,821	-6,737	-247,106	-91,531
0,062	19,35	69,749	95,215	-19,163	-272,621	-96,315
0,088	34,573	115,126	142,317	-23,836	-266,376	-87,652
0,113	51,651	163,274	192,312	-23,191	-260,316	-94,952
0,138	70,614	213,146	246,116	-19,768	-267,603	-114,534
0,163	91,317	264,188	303,159	-16,282	-283,585	-137,371
0,187	112,964	314,995	361,051	-14,435	-293,835	-153,626
0,213	134,171	363,265	416,486	-13,795	-276,91	-151,383
0,237	153,451	406,641	466,577	-13,373	-249,304	-141,597
0,263	169,776	443,721	509,914	-12,058	-198,61	-111,425
0,288	182,951	474,618	546,88	-9,471	-158,297	-84,877
0,312	193,595	500,758	579,176	-6,481	-139,946	-70,51
0,338	202,76	524,074	608,84	-4,543	-147,912	-77,21
0,363	211,388	546,037	637,266	-4,137	-182,393	-104,327
0,388	219,887	567,064	664,697	-4,146	-214,923	-132,861
0,413	228,062	586,607	690,419	-3,404	-232,242	-150,802
0,437	235,435	603,836	713,5	-1,133	-229,094	-153,718
0,463	241,722	618,432	733,594	1,9	-196,001	-128,599
0,488	247,117	630,886	751,231	4,175	-198,187	-133,83

In Figure to Figure , the strain and stress curves for the successful results obtained from hole drill testing for residual stress can be seen for both shot peening and laser shock peening.

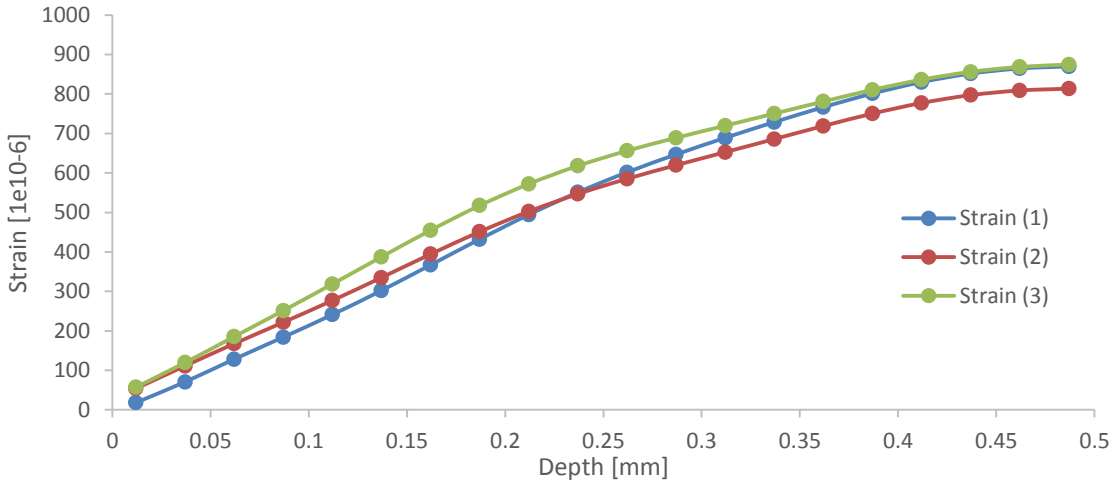

Figure 4.15: Stain data curve for Shot Peening at 60 Psi and 200% coverage

From Figure , for the strain curve of the 60Psi shot peened data, the strain is seen to act uniformly throughout the material as the 3 strain curves are in very close proximity to each other, thus indicating a uniform strain acts in all directions within the tested material.

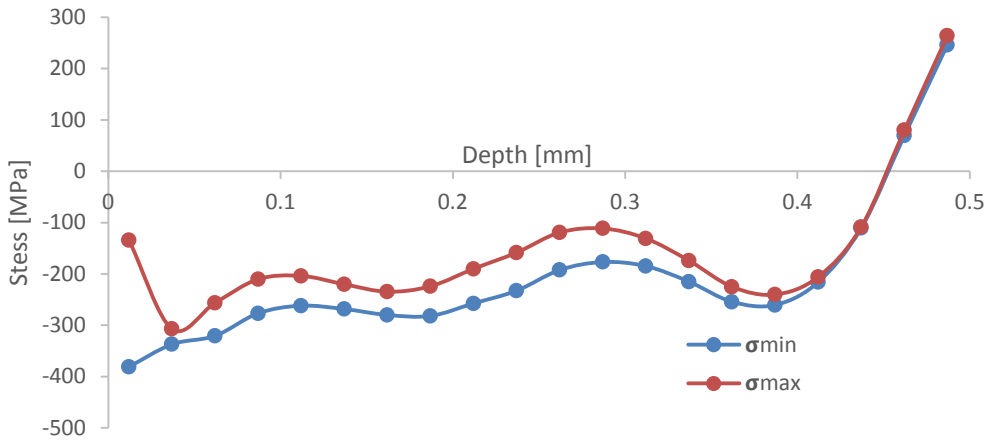

Figure 4.16: Stress data curve for Shot Peening at 60 Psi and 200% coverage

In Figure , the stress curves for the 60Psi shot peened data, the maximum and minimum stress curves are seen to follow a close trend to each other. The stresses are also seen to act in compression to around 0.45mm into the material thickness, and thereafter acting in tension.

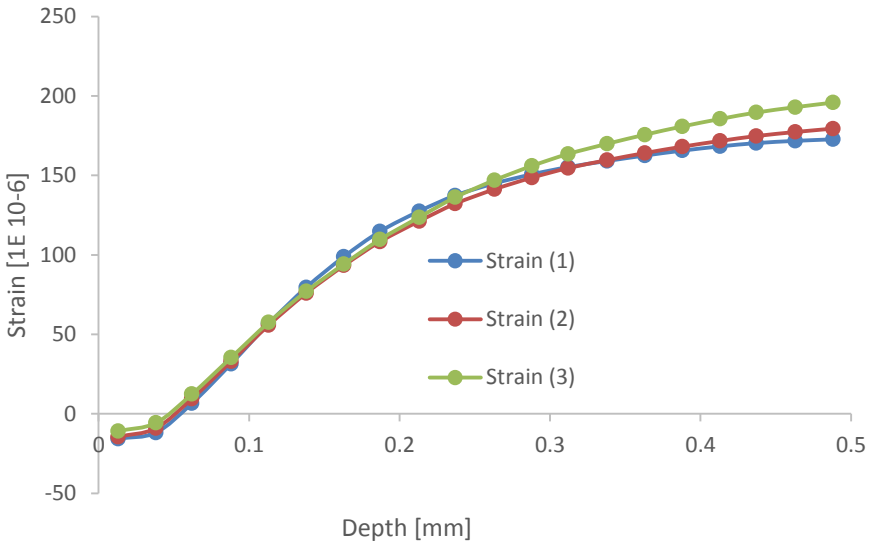

Figure 4.17: Stain data of Laser Shock Peening, 1GW/cm^2 at 75% coverage

In Figure , for the strain curve of the laser shock peening data of 1GW/cm^2 at 75% coverage, the strains are seen to follow in close proximity to each other, thus indicating a uniform strain acts in all directions within the tested material.

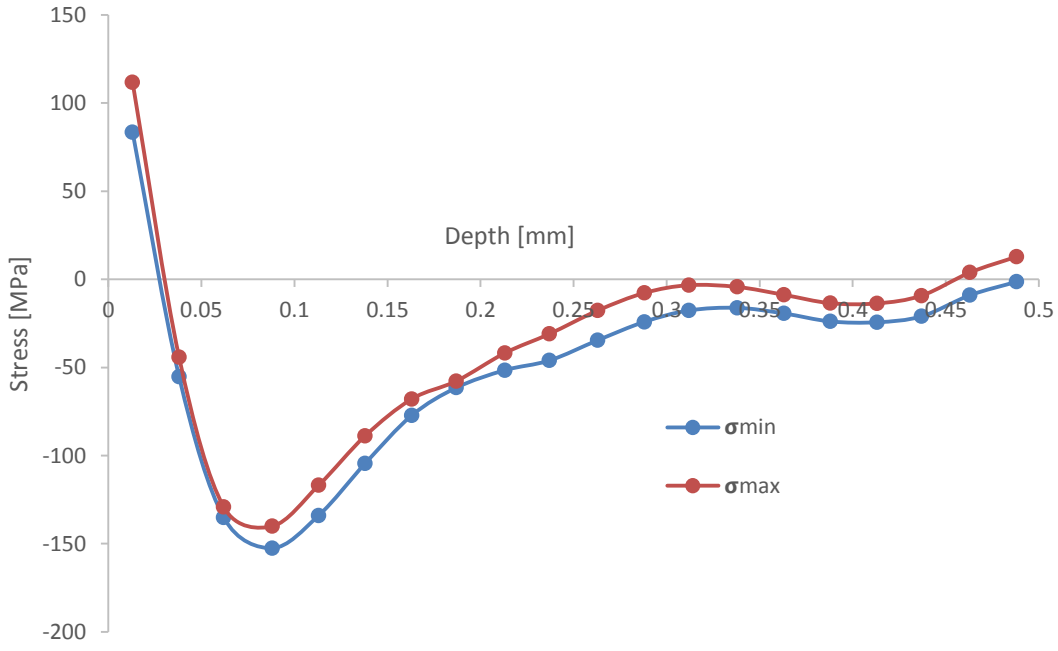

Figure 4.18: Stress data of Laser Shock Peening, 1GW/cm^2 at 75% coverage

In Figure , the stress curve of the laser shock peening data of 1GW/cm^2 at 75% coverage, shows the maximum and minimum stress curves are seen to follow a close trend to each other. The stresses are also seen to act in compression to around 0.5 mm into the material thickness.

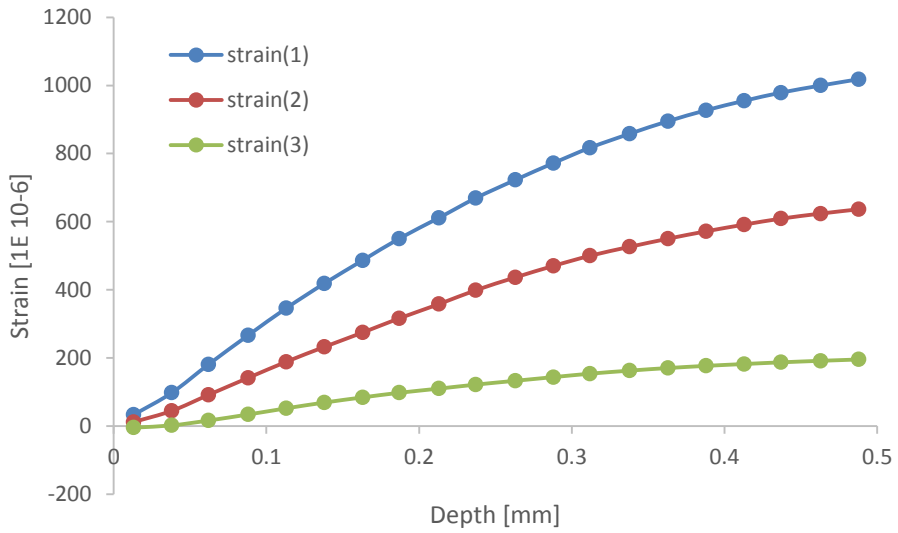

Figure 4.19: Strain data of Laser Shock Peening, 3GW/cm^2 at 75% coverage

In Figure , for the strain curve of the laser shock peening data of 3GW/cm^2 at 75% coverage, the strains are not seen to follow in close proximity to each other, thus indicating a non-uniform strain acts in the different directions within the tested material.

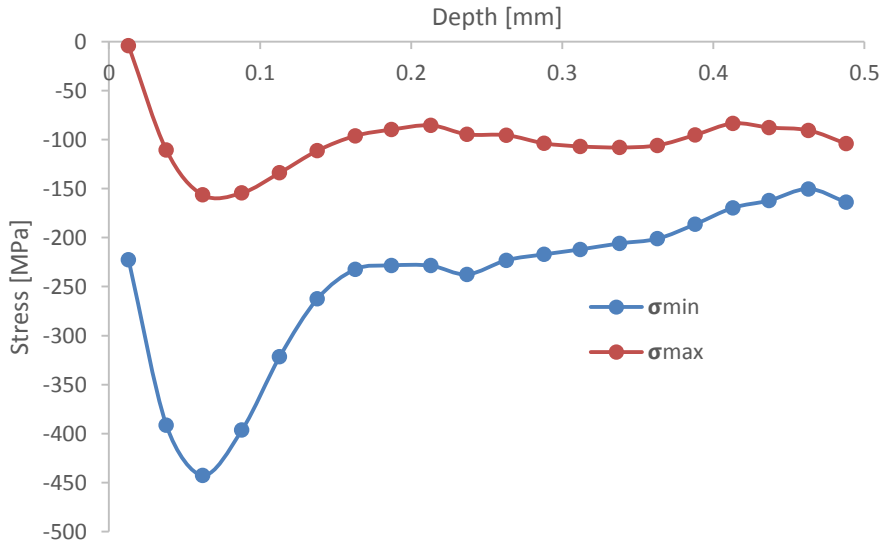

Figure 4.20: Stress data of Laser Shock Peening, 3GW/cm^2 at 75% coverage

In Figure , the stress curve of the laser shock peening data of 3GW/cm^2 at 75% coverage, shows the maximum and minimum stress curves are not seen to follow a close trend to each other as in the previous results for the 1GW/cm^2 data. The stresses are also seen to act in compression past 0.5 mm depth into the material thickness. Thus following expected trends in comparison to shot peening results, i.e. compressive residual stresses penetrating deeper in the material depth.

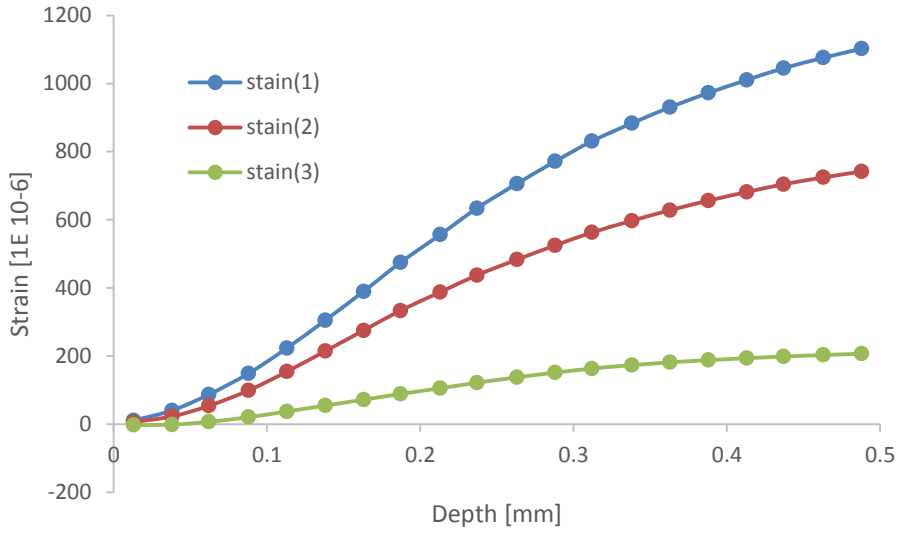

Figure 4.21: Strain data of Laser Shock Peening, 5GW/cm^2 at 75% coverage

In Figure , for the strain curve of the laser shock peening data of 5GW/cm^2 at 75% coverage, the strains are not seen to follow in close proximity to each other, thus indicating a non-uniform strain acts in the different directions within the tested material.

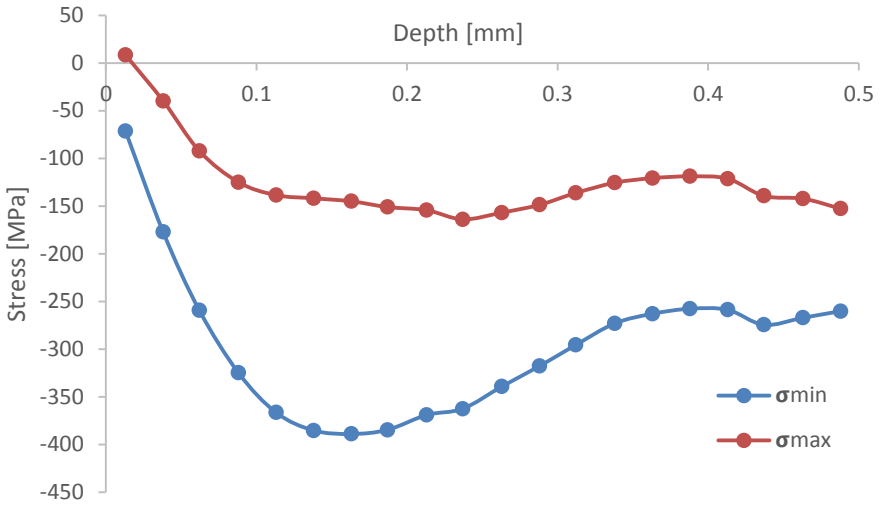

Figure 4.22: Stress data of Laser Shock Peening, 5GW/cm^2 at 75% coverage

In Figure , the stress curve of the laser shock peening data of 5GW/cm^2 at 75% coverage, shows the maximum and minimum stress curves are not seen to follow a close trend to each other as in the previous results for the 1GW/cm^2 data.

The stresses are also seen to act in compression past 0.5 mm depth into the material thickness. Thus following expected trends in comparison to shot peening results, i.e. compressive residual stresses penetrating deeper in the material depth.

In Figure and Figure , the strain and stress data for the second test done on the laser shock peening test piece of 5GW/cm^2 at 75% coverage can be seen respectively.

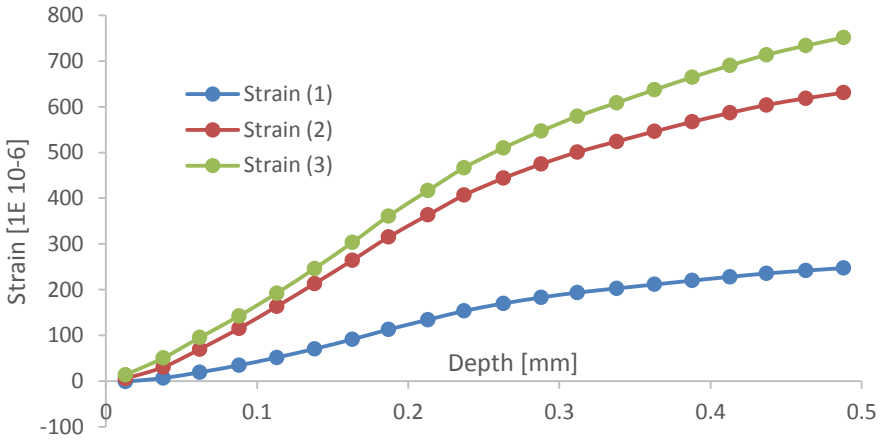

Figure 4.23: Strain data of Laser Shock Peening, 5GW/cm^2 at 75% coverage (2nd test)

In Figure , for the strain curve of the laser shock peening data of 5GW/cm^2 at 75% coverage, the strains are not seen to follow in close proximity to each other, thus indicating a non-uniform strain acts in the different directions within the tested material.

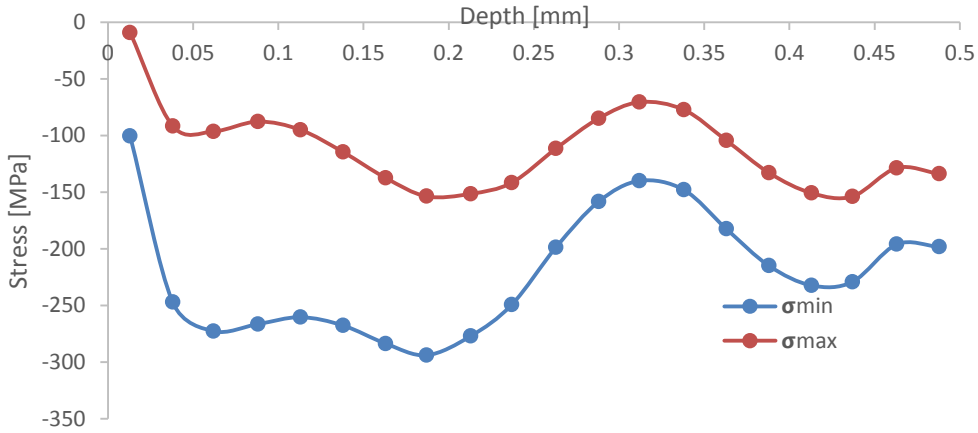

Figure 4.24: Stress data of Laser Shock Peening, 5GW/cm^2 at 75% coverage (2nd test)

In Figure , the stress curve of the laser shock peening data of 5GW/cm^2 at 75% coverage, shows the maximum and minimum stress curves are not seen to follow a close trend to each other as in the previous results for the 1GW/cm^2 data. The stresses are also seen to act in compression past 0.5 mm depth into the material thickness. Thus following expected trends in comparison to shot peening results, i.e. compressive residual stresses penetrating deeper in the material depth.

In Figure , the two graphs for the stress data of laser shock peening, for 5GW/cm^2 at 75% coverage are plotted together to establish repeatability.

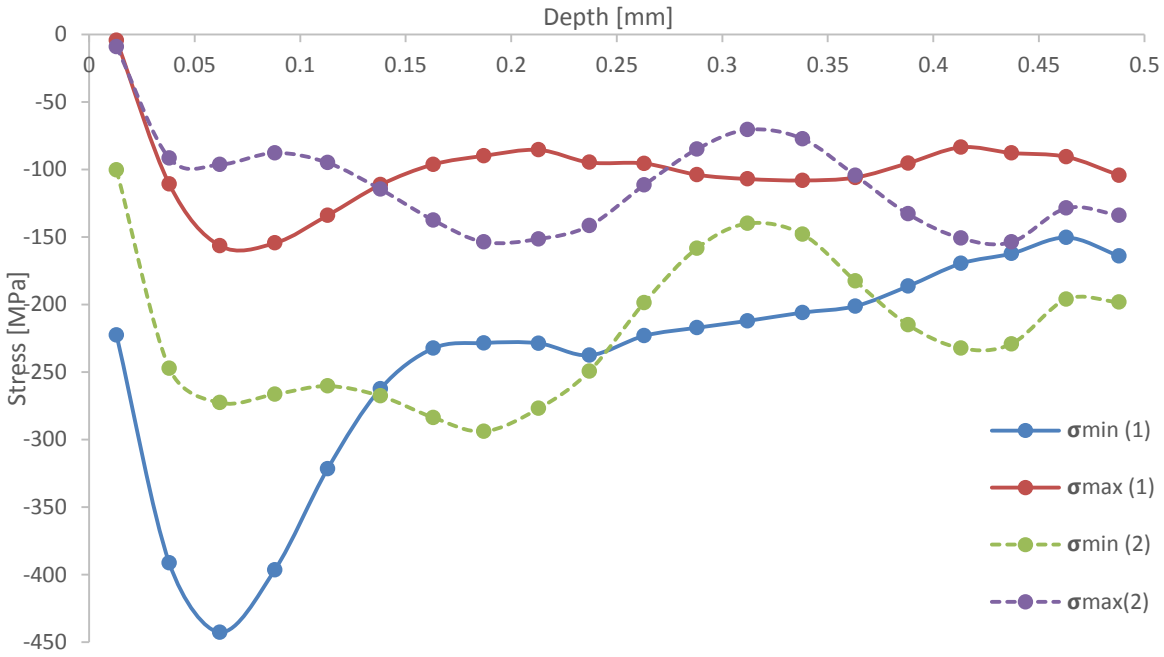

Figure 4.25: Stress data of Laser Shock Peening, 5GW/cm^2 at 75% coverage (1st and 2nd test)

In Figure 4.25, repeatability was not established, as both sets of data show no similarity in trend patterns. The only difference between the two test pieces was the orientation of the strain gauge. Further investigation would be required to establish if strain gauge orientation would affect data results.

4.5 Summary

In this chapter, the data and results for deflection, surface roughness, microhardness and residual stress was tabulated and analysed. The graphical data displayed comparisons between the shot peening and laser shock peening results for the material properties tested using the tabulated data. From the data laser shock peening showed higher deflection, a smoother surface finish, a deeper micro hardening penetration, and a deeper compressive residual stress penetration into the material in comparison to shot peening.

CHAPTER FIVE

5.0 Introduction

In this chapter, the conclusion of the results seen from chapter 4 is evaluated and summarised and further recommendations into advancing the experimentation process can be seen.

5.1 Conclusions

Shot peening process was accomplished at a significantly shorter time span in comparison to laser shock peening. All testing run for the deflection, surface roughness and micro-hardness were successfully accomplished. Test for hole drilling had encountered some problems and thus a limited range of data were achieved and evaluated.

In the deflection testing, laser shock peening results were seen to have a higher deflection in comparison to shot peening by a range of between 2.12 to 3, this is due to higher compressive residual stresses being subjected deeper into the test piece via the laser shock peening process. Deflection results also showed increase in curvature as "laser intensity" or "shot peening pressure" was increased. The highest curvature seen was along the travel direction (X) for all the samples, thus in line to research done by "*Daniel Glaser*" [48], [52]. The shot peening data also shows very small changes in deflection, as the coverage increased, in comparison to significant changes seen in the laser shock peening results. This indicates more energy is transferred to the work piece through laser shock peening and a higher compressive residual stress transferred to the material. Deflection results for shot peening between Almen 'A' strip and Aluminium alloy 6056-T4 was conducted to find if a relationship could exist between these materials. An average difference of 2.46 was found between the 60Psi and 80Psi data and a difference of 4.4 between the 60Psi and 100Psi data. Thus further research

would be required to find if a relationship between these materials does exist, across a range of pressures.

In surface roughness testing, shot peening results were seen to give a higher surface roughness value of around 5.7 times that for laser shock peening. This is due to the surface of the shot peened surface, being bombarded with a stream of shots, but with a randomly determine impact zone of each shot, whereas in laser shock peening the laser is shot within a designated sequence thus creating a more uniform impact zone, and with the aid of overlapping creating a much smoother finish. The surface roughness values had reached a value close to saturation from around the 100% coverage range. Visual inspecting and finger nail testing both validated the findings for the surface finish findings.

In microhardness testing, laser shot peening data are seen to follow in close proximity to each other over the laser intensity range. All results for laser shock peening show hardness is increased throughout the thickness of the material. Shot peening showed results for the higher pressures increase hardness to a certain depth into the material. When comparing the highest laser intensity and highest pressure used for the two peening procedures, laser shock peening is seen to propagate more than 3.8 times further into the material in comparison to shot peening. These results follow similar trends as seen in other material which underwent this type of testing procedure (seen in Figure 2.21 and Figure 2.23).

Residual stress testing showed a more uniform strain is created in the shot peening test piece and the lower intensity laser shock peening test piece. At the higher laser intensities strain is no longer seen to act uniformly within the material. The maximum and minimum principle residual stresses also show a close trend to each other for the shot peening result and the lower intensity laser shock peened material. Thereafter for the higher intensity test, maximum and minimum principle residual stresses no longer follow in close proximity to each other. Laser shock peening was

seen to create compressive residual stresses up to 442MPa and shot peening up to 380MPa.within the material.

Thus higher compressive stresses are created through laser shock peening processes. Shot peening result show compressive stresses penetrate the material up a depth of 0.45mm into the test piece and there after going into tension, whereas the compressive stresses for laser shock peening were seen to surpass the 0.5mm point. This corresponds to similar trends seen on other materials, which underwent this type of test comparison as was seen for Inconel 718, Aluminium 7375-T7351, Ti-6Al-4V and Ti-6Al-2Sn-4Zr-2Mo seen in Figure 2.16 to Figure 2.19. For crack tips at depth deeper than 0.45mm, shot peening would not be a sufficient process to prevent further crack propagation, and laser shock peening would serve as a better process as it penetrates deeper into the surface, thus further slowing down crack propagation. For repeatability two test of laser shock peening at

$5GW/cm^2$ were conducted, the results showed two very different graphs which would indicate repeatability was not achieved. The only difference seen in the two test pieces, was the orientation of the strain gauges, further investigation into this would be required to establish if strain gauge orientation would affect the results obtained during hole drill testing for residual stresses.

5.2 Summary

Laser Shock Peening process has been shown to give a higher deflection, smoother surface finish, deeper micro hardening, higher compressive residual stresses and deeper compressive residual stresses penetration in to the test material in comparison to the conventional shot peening process. Thus laser shock peening has shown significant material improvement, even with a slower application rate this would be the best process to select to be used on thin walled components within the aerospace industry. With the constant advancement in technology, this process would eventually improve and a faster process created and thus will be the superior process in all aspects.

5.3 Recommendations

- Further testing on Almen “A” test strips and AA6056-T4 can be conducted over a variety of shot peening pressures to establish if a deflection trend does exist between these materials.
- Further test to evaluate the Logarithmic saturation curve for deflection data between and GW/cm^2 -7GW/cm^2 for laser shock peening.
- Further test between the 50% to 100% coverage for surface finish, to evaluate the change in linearity of all the data captured.
- Further investigation into residual stress testing for different orientations of the strain gauge, to test if orientation would affect residual stress results.
- A design project can be develop to mount the hole drilling machine to create stability during testing, as the slightest of movements in the machinery could cause inaccurate results to incur. And to enable to machine to be used in different orientations (Vertically).

REFERENCES & BIBLIOGRAPHY

[1] Aging Aircraft Fleets: Structural and Other Subsystems Aspects, RTO LECTURE SERIES 218 bis, presented 13-16 November 2000 in Sofia, Bulgaria.

[2] Shot peening: http://www.metalimprovement.com/shot_peening.php [online] cited 21 July 2013

[3] Metal Improvement Co Inc, Newsbury, Uk, Peen-Forming-A Developing Technique, Peter O'Hara, 2002

[4] Lockheed Constellation Aircraft picture: http://luftwaffles.deviantart.com/art/Lockheed-Super-Constellation-73122649 [Cited 30 August 2013]

[5] History of Lasers: http://www.worldoflasers.com/laserhistory.htm [online] Cited 30 September 2013

[6] Metal Finish News, Vol. 10-March Issue-Year 2009, "A Historical Perspective on Laser Shock Peening", Dr. Allan H. Clauer

[7] Lasers: http://abyss.uoregon.edu/~js/glossary/laser.html [online], cited: 26 February 2013

[8] History of lasers: http://www.kigre.com/files/historylasers.pdf [online], cited January 2014

[9] Laser Shock Processing as a method of Surface Properties Modification of Metallic Materials, J.L.Ocana, M.Morales, C.Mopeceres, J.A.Porro; ETSIMLAS Dept. of Applied Physics (Polytechnic University of Madrid)

[10] How Lasers work: http://www.thefreedictionary.com/Light+amplification+by+stimulated+emission+of+radiation [online], cited: 28 February 2013

[11] Laser Process diagram: http://www.land-laser.com/laser.asp [online] Cited 23 January 2014

[12] Shot Peening Applications, Metal Improvement Co Inc, 2002

[13] Barret, C "Peen Forming" SME Handbook 1984

[14] Shot peening benefits: http://www.superiorshotpeening.com/treatments-shotpeening-tech.htm [online], cited: 20 August 2013

[15] "Physics and applications of laser-shock processing", R Fabbro, P Beyre, L. Berthe, X Scherpereel, Arcuel France : CLFA, 1998.

[16] Laser Shock peening: http://www.substech.com/dokuwiki/doku.php?id=laser_peening [online], cited: 26 February 2013

[17] Laser Shock peening: http://www.lsptechnologies.com/questions/ [online], cited: 20 March 2013

[18] "Taylor Impact Testing", House, J W., Florida : Air Force Armament Laboratory, September 1989.

[19] "Modelling and Parameter Design of a Laser Shock Peening Process". Gulshan Singha, Ramana V. Grandhia and David S. Stargelb. 5, s.l.: International Journal for Computational Methods in Engineering Science and Mechanics, 2011, Vol. 12.

[20] Surface Analysis of Laser Shock Peened Aluminium Alloys Without a Protective Coating, Madire, Matape.. Johannesburg : s.n., 2012.

[21] “Laser Shock Peening for Fatigue Resistance”, Clauer, Allan H., Dublin: s.n., 1996.

[22] Laser Shock Peening benefits: http://www.metalimprovement.com/shot_peen_forming.php [online], cited: 26 February 2013

[23] “Laser shock peening, performance and process simulation”, K Ding and L. Ye, Woodhead Publishing in Materials, Cambridge England

[24]Almen Strip: http://www.electronics-inc.com/uploads/StripTesting.pdf [online], cited: 16 May 2013

[25] Almen Strips: http://www.electronics-inc.com/typegrade.html [online] cited 17 July 2013

[26] Almen Gage: http://abrasivefinishingcompany.com/t-peen-forming.html [online], cited: 26 February 2013

[27] Shot peening process: http://www.pshotblast.com/shot-peening-increases-fatigue-life-of-auto-components-page-4.php [online] cited 26 February 2013

[28] “Surface Roughness Measurement”, Bulletin No.1984, Mitutoyo

[29] Hardness: http://www.hardnesstesters.com/Applications/Case-Depth-Testing.aspx [online] cited 22 September 2013

[30] Hardness: http://www.calce.umd.edu/TSFA/Hardness_ad_.htm [online] cited 22 September 2013

[31] Vickers Microhardness Testing: http://www.struers.com/default.asp?top_id=5&main_id=156&sub_id=220&doc_id=911 [online] Cited 24 September 2013

[32] “Vickers Microhardness Test”, Indentec Hardness Testing Machines Limited, West Midlands, DY9 8HX, Zwick/Roell

[33] Knoop Hardness Figure: http://www.ccsi-inc.com/t-rockwell2.htm [online] cited 29 September 2013

[34] Brinell Hardness Figure: http://www.instron.us/wa/applications/test_types/hardness/brinell.aspx?ref=https://www.google.co.za/ [online] cited 30 September 2013

[35] Rockwell Hardness Testing: http://www.instron.us/wa/applications/test_types/hardness/rockwell.aspx?ref=https://www.google.co.za/ [online] cited 02 October 2013

[36] Rockwell Hardness Figure: http://www.amesportablehardnesstesters.com/hardness-testing/what-is-rockwell-hardness/ [online] cited 02 October 2013

[37] “X-Ray Diffraction Residual Stress Measurement An Introduction” ISO/IEC 17025:2005, PROTO, Automated XRD Systems & Sevices Manufacturing

[38] “Handbook of Liquids-Assisted Laser Processing”, 1st Edition, Elsevier, Kruusing, A 2010,

[39] Residual Stress testing: http://www.vishaypg.com/doc?11053 [online], cited: 06 December 2013

[40] Aluminium Alloy properties: http://www.matweb.com/reference/aluminumtemper.aspx [online] cited 04 March 2013.

[41] Dif R., Bès B., Ehrström J.C., Sigli C., Warner T., Lassince P., Ribès H.: Master. Sci. Forum 331, 2000 1613–1618

[42] http://www.ctemag.com/aa_pages/2009/0908_PartsFinishing.html [online], cited: 03 April 2013

[43] Residual stress results: Laser shock processing of aluminium alloys. Application to high cycle fatigue behavior, P.Peyre, R.Fabbro, P.Merrien, H.P. Lieurade, 31 October 1995

[44] Residual stress results: http://www.sme.org/MEMagazine/Article.aspx?id=20229&taxid=3440 [online] cited 19 January 2014

[45] Hardness: http://www.emeraldinsight.com/journals.htm?articleid=1911988&show=html [online], cited:05 December 2013

[46] Laser shock processing of aluminium alloys. Application to high cycle fatigue behavior, P.Peyre, R.Fabbro, P.Merrien, H.P. Lieurade, 31 October 1995

[47] ND: Yag: http://www.slideshare.net/drfatmag/new-microsoft-word-document-2-30347413 [online], cited: 12 January 2014

[48] Glaser, D 2014, Laser Shock Peening for Integral Airframe Structures Applications. MSc. Dissertation (Unpublished), University of the Witwatersrand.

[49] Andrew Jackson, D 2013, Enhancement of Laser Beam Welded Joint Performance by Laser Shock Peening, BSc (Eng),Final Year research project, University of the Witwatersrand.

[50] ASTM E837-08, http://www.mts3000.com/gestione/docs/EVAL-Eng11.pdf [online] cited 21 January 2014.

[51] Principle stresses, http://www.efunda.com/formulae/solid_mechanics/mat_mechanics/plane_stress_principal.cfm [online] cited 21 March 2014

[52] An international patent,"PCT/IB2014/060814" has been filed in collaboration with Wits Enterprise in April 2014 to cover some of the cutting edge results obtained in this part of the activity.

[53] Dane, B., et al,"Laser Peening of Metals-Enabling Laser Technology

APPENDIX A: HISTORY OF LASER DEVELOPMENT

Outline History of the Development of the Laser		
Date	**Name**	**Achievement**
1900	Max Plank	Provided the understanding that light is a form of electromagnetic radiation
1916	Albert Einstein	Theory of light emission. Concept of stimulated emission.
1928	Rudolph W Landenburg	Confirmed existence of stimulated emission and negative absorption.
1940	Valentin A Fabrikant	Noted possibility of population inversion.
1947	Willis E Lamb R C Rutherford	Induced emission suspect in hydrogen spectra. First demonstration of stimulated emission.
1951	Charles H Townes	The inventor of the MASER (Microwave Amplification of Stimulated Emission of Radiation) at Columbia University - First device based on stimulated emission, awarded Nobel prize 1964.
1951	Charles H Townes Joseph Weber James P. Gordan	Inventors of MASER at University of Maryland.
1951	Alexander M. Prokhorov Nikolai G. Basov	Independent inventors of MASER at Lebedev Institute of Physics, Moscow. Awarded Nobel prize 1964.
1954	Robert H. Dicke	"Optical Bomb" patent. Based on pulsed population inversion for superradiance and separately Fabry-Perot resonant chamber for "Molecular Amplification and Generation system".
1956	Nicolas Bloembergan	First proposal for a three-level solid state MASER at Harvard University.
1957	Charles H Townes	Sketches an early optical MASER in his lab book.
1957	Gordon Gould	First document defining a LASER; notarized by a candy store owner. Credited with patent rights in the 1970s.
1958	Arthur L Schawlow Charles H Townes	First detailed paper describing "Optical MASER". Credited with invention of LASER. from Columbia University.
1959	Gordon Gould	Applies for LASER related patents
1959	John D. Myers	First stroboscopic X-Ray system at Pennsylvania State University. Precursor to X-ray LASER.
1960	Arthur L Schawlow Charles H Townes	LASER patent No. 2,929,922.
1960	Theodore Maiman	Invented first working LASER based on Ruby. May 16th 1960, Hughes Research Laboratories.
1960	Peter P Sorokin Mirek Stevenson	First Uranium LASER - Second LASER overall. Nov. 1960 IBM Labs.

1960	Ali Javan, William Bennett Donald Herriot	First helium-neon LASER at Bell Labs Dec. 1960, First gas laser and first CW laser.
1961	Lloyd G. Cross	First commercial laser company, Trion Instruments was founded in March, First spinning prism Q-switched Ruby LASER. Third Ruby LASER, Trion became Lear-Siegler, Laser Systems Center in 1962.
1961	Robert Rempel	Co-founded Spectra-Physics, which became the 2nd company to make LASERS.
1961	A G Fox and T Li	Theoretical analysis of optical resonators at Bell Labs.
1961	Elias Snitzer	First glass LASER and clad laser rods at American Optical.
1961	Leo F. Johnson, K. Nassau	First neodymium crystal LASER at Bell Labs
1961	Ralph R. Soden Scotch Plains Le Grand (Larry) G. Van Uitert	First continuous wave operation of rare earth doped crystal LASER at Bell Labs. Patent No. 3,177,155.
1961	John D. Myers	Fourth Ruby LASER at Cornell Aeronautical Laboratory.
1962	Fred J. McClung	First electro-optic Kerr cell Q-switch.
1962	Robert Hall Nick Holonyak	Invention of semi-conductor LASER at General Electric Labs.
1962	Alan White Dane Rigden	First helium neon (HeNe) visible CW LASER at Bell Labs.
1962	Fred Brech Lloyd G. Cross	First LASER Induced Breakdown Spectroscopy (LIBS) chemical analysis system at Jarrell-Ash & Trion Instruments.
1963	Robert Keyes Theodore Quist	First diode pumped solid state LASER, uranium doped calcium fluoride at MIT Lincoln Labs.
1963	Logan E Hargrove Richard L Fork M. A. Pollack	First mode locked acousto-optic Q-switch.
1964	John D. Myers	First Gigawatt LASER (Ruby) oscillator/amplifier system at Cornell Aeronautical Laboratory.
1964	Emmett Leith Juris Upatnieks	First display of LASER holograms of 3D objects. April 3, at Spectra-Physics.
1964	John D. Myers	First field demonstration of a Ruby LASER rangefinder/ceilometer at Cornell Aeronautical Laboratory.
1964	Elias Snitzer	First fiber LASER & first fiber LASER amplifier at American Optical.
1964	John D. Myers	First demonstration of LASER propulsion. Lear-Siegler, Laser Systems Center
1964	Joeseph E Geusic Richard G. Smith H M Markos L G Van Uiteit Bob Thomas Leo Johnson	Inventor of first working Nd:YAG LASER at Bell Labs.
1964	Kumar N Patel	Inventor of CO_2 LASER at Bell Labs.
1964	William Bridges	Invention of Argon Ion LASER at Hughes Labs.
1965	J.P. Chernoch	Invention of the solid-state Disk LASER at General Electric. US Patent 3,466,569 (1969)
1965	John D. Myers	First dual frequency LASER ceilometer at Lear Siegler Laser System Center.
1965	George Pimentel J V V Kasper	First chemical LASER at University of California, Berkley.
1965	John D. Myers	First frequency-doubled LASER rangefinder at Lear Siegler Laser System Center.

1966	Ed Gerry Arthur Kantrowitz	First 10+ Kilowatt CO2 LASER at Avco Everett Research Lab.
1966	James Hobart	Founded first commercial CO2 LASER company Coherent Radiation (now Coherent Inc.) Hobart was an employee of Trion Instruments the first commercial laser company founded by Lloyd G. Cross in 1961.
1966	William Silfvast Grant Fowles and Hopkins	First metal vapour LASER - Zn/Cd - at University of Utah
1966	John D. Myers	First plane position indicating LASER radar at Lear Siegler Laser System Center.
1966	Peter Sorokin John Lankard	First dye LASER action demonstrated at IBM Labs.
1966	Mary L. Spaeth	First tunable dye LASER at Hughes Research Labs
1967	John D. Myers	First commercial Nd:Glass LASER rod at Owens-Illinois.
1967	Bernard Soffer B. B. McFarland	First wavelength tunable dye LASER at Korad.
1967	John D. Myers	First Gigawatt Nd:Glass LASER oscillator/amplifier system at Owens-Illinois.
1968	Dr. Bhaum	First CO_2 LASER application for refractive eye surgery.
1969	Keeve M. Siegel	First commercial fusion LASER research program at KMS Industries.
1969	G M Delco	First industrial installation of three LASERS for automobile application.
1969	John D. Myers* Luther C. Salter** Tom Crow***	Invention of samarium filters for Nd:YAG LASER at *Owens-Illinois, **Hughes Aircraft & ***Martin Marietta.
1970	Nikolai Basov Yu M. Popov	First Excimer LASER at Lebedev Labs, Moscow based on Xenon (Xe) only.
1970	Alferov' Group Mort Panish Izuo Hayashi	First CW semiconductor LASER at Ioffe Physico-Technical Inst. & Bell Labs
1972	Charles H, Henry	First quantum well LASER
1973	ManiLal Bhaumik	First eximer LASER application for refractive eye surgery.
1973	Lloyd Cross	First commercial LASER hologram company at Multiplex Company
1974	J. J. Ewing and Charles Brau	First rare gas halide excimer LASER at Avco Everet Labs.
1976	Jim Hsieh	First InGaAsP diode LASER at MIT Lincoln Labs.
1976	John M J Madey's Group	First free electron LASER at Stanford University.
1980	Geoffrey Pert's Group	First report of X-ray LASER action, Hull University, UK.
1981	Arthur Schawlow Nicolas Bloembergen	Awarded Nobel Physics Prize for work in non-linear optics and spectroscopy.
1982	Peter F. Moulton	First titanium sapphire LASER at MIT Lincoln Labs
1984	Dennis Matthew's Group	First reported demonstration of a "laboratory" X-ray LASER from Lawrence Livermore Labs.
1985	John D. Myers	First commercial LASER eye surgery device and method, US patent No. 4,525,942 and UK patent No. GB 2 157 483 A at Kigre, Inc.
1987	David Payne	First erbium fiber LASER amplifier

1994	Jerome Faist Federico Capasso Deborah L. Sivco Carlo Sirtori Albert Hutchinson Alfred Y. Cho	First quantum cascade multiple wavelength LASER at Bell Labs
1994	Nikolai Ledentsov	First quantum dot LASER at Ioffe Physico-Technical Institute.
1996	Wolfgang Keterle	First pulsed atom LASER at MIT
1996		First Petawatt LASER at Lawrence Livermore National Labs.
1997	Wolfgang Ketterle	First atom LASER at MIT Lincoln Labs.
2004	Ozdal Boyraz Bahrom Jalali	First silicon Raman LASER at the University of California, Los Angeles
2006	John Bowers	First silicon LASER
2007	John Bowers Brian Koch	First mode-locked silicon evanescent LASER
2010		First 10 Petawatt LASER at Lawrence Livermore National Labs.

APPENDIX B: DRILLING MACHINE SPECIFICATIONS

Technical specifications of the MTS3000 system: alignment-drilling tool

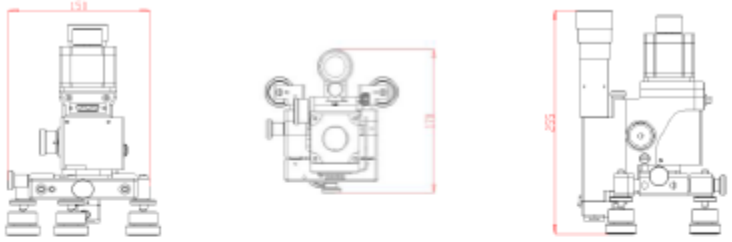

Dimensions (height, width and length) without dial gages	mm	270 x160x175
Weight	kg	4.6
Maximum turbine speed	RPM	400,000
Acoustic emission (at 1 meter)	dBA	76
Max turbine feed pressure	bar	5
Drilling resolution	µm	5
Drilling speed range	mm/min	0.03 to 1
Vertical lift (fast/manual)	mm	60
Vertical lift (slow with motor)	mm	6
Horizontal movement (x,y)	mm	7 -10
Height adjustment of feet	mm	60

Technical specifications of the MTS3000 system: electronic control system

Dimensions (height, width and length)	mm	140 x 245 x 220
Weight	kg	5.4
Grid power supply	Vac	90 - 264 (50 - 60Hz)
Compressed air max. input pressure	bar	6

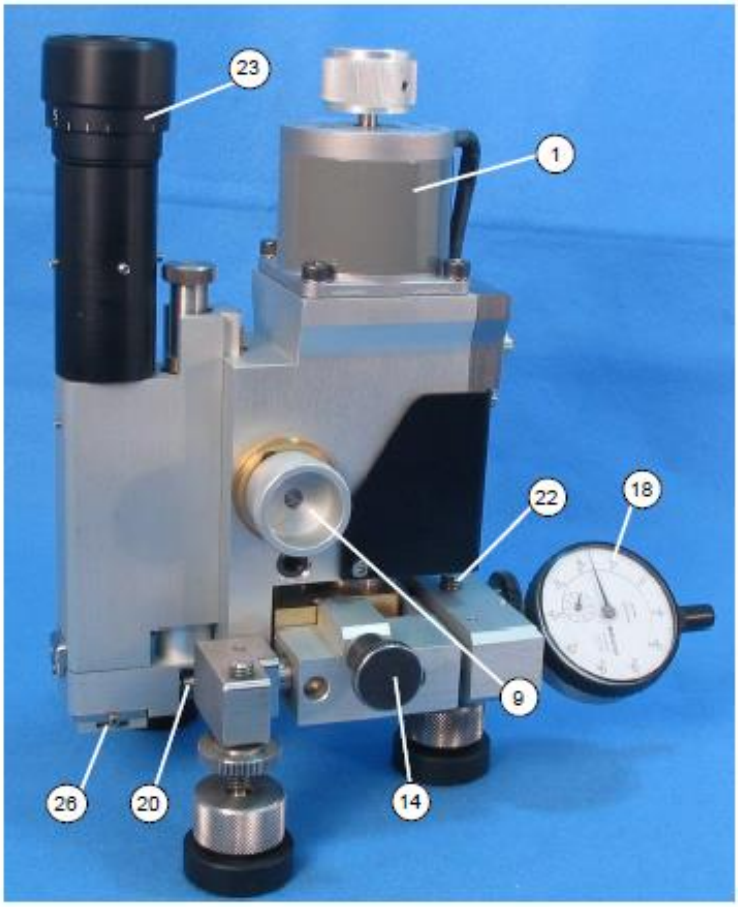

Fig. 1.3 - Mechanical-Optical System

1 – Stepping motor
9 – Vertical adjustment
14 – Horizontal adjustment, X-axis
18 – Y-axis dial gauge
20 – Compressed air connection
22 – Socket head screw for fixing the Y-axis dial gauge in position
23 – Eyepiece
26 – Screw for alligator clip (zero setting)

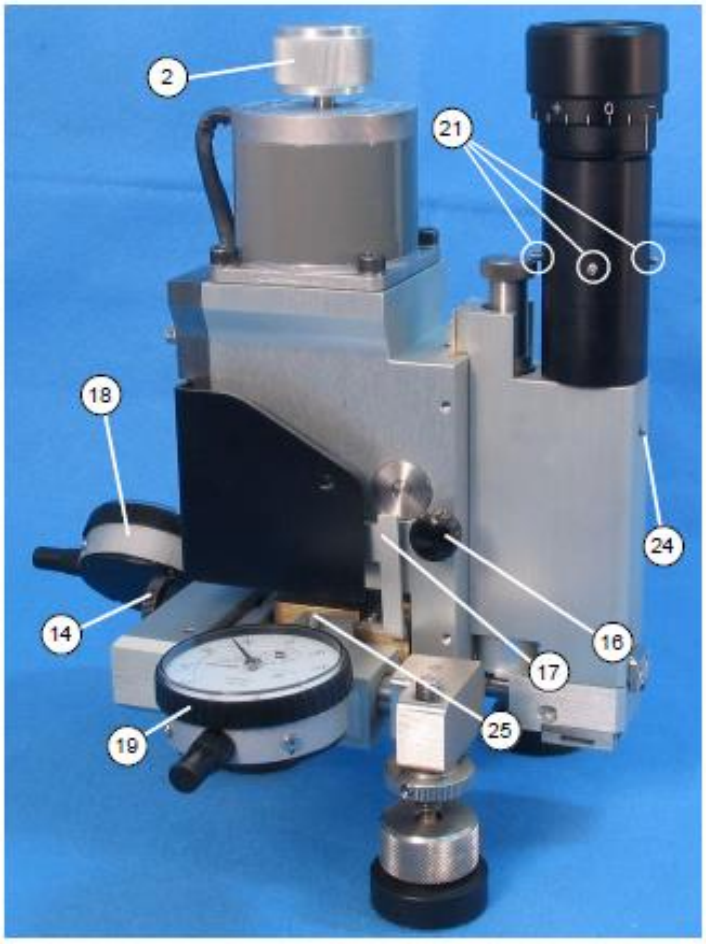

Fig. 1.2 - Mechanical-Optical System

2 – Slow manual feed control

14 – Horizontal adjustment, Y-axis

16 – Vertical slide lock

17 – Limit switch

18 – Y-axis dial gauge

19 – X-axis dial gauge

21 – Socket head screws for aligning the microscope during calibration.

24 – Socket head screw for fixing the microscope in position

25 – Socket head screw for locking the X-axis dial gauge

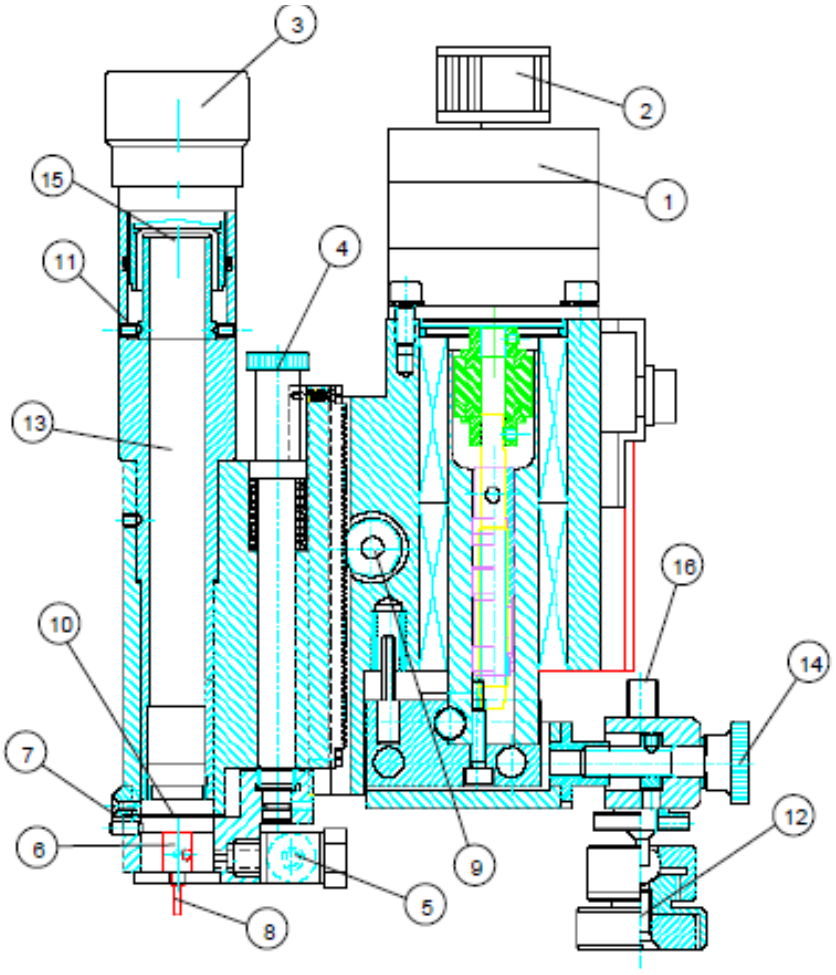

Fig. 1.4 - Mechanical-Optical Device – Cross Section

1 - Stepping motor for automatic fine speed control
2 - Knob for manual operation of the stepping motor
3 - Eyepiece
4 - Turbine release
5 - Compressed air connection
6 - Air turbine
7 - Spindle
8 - End mill
9 - Knob for fast vertical feed
10 -Back cap for closing the turbine
11 -Socket-head screws for calibrating the optical device
12 -Support of the feet
13 -Microscope
14 -Horizontal adjustment knob
15 -Eyepiece target
16 -Vertical adjustment threaded pin